Performance of all dielectric self- supporting fibre optic cable in high voltage environments

Mohamed Fayaz Khan

Submitted in fulfillment of the academic requirements of the Master of Engineering Degree in the School of Electrical, Electronic and Computer Engineering, University of Natal, Durban, South Africa. September 15, 2003.

ABSTRACT

Power utilities around the world are now in the practice of installing fiber optic cables on their high voltage transmission networks. These high-speed communication channels can, not only transmit data needed for utility operation, but the unused fiber capacity may also be rented to others for communication. All-dielectric self-supporting (ADSS) fiber optic cable appears to be the fiber optic cable most frequently installed by power utilities as it is more economical, has a larger fiber capacity and may be installed on a transmission line without de-energization. When installed however, ADSS fiber optic cable does undergo some degree of degradation caused either by armor rod corona at the towers or dry-band arcing. A comprehensive literature survey regarding both phenomena is presented in this study, as well as current mitigation techniques.

Different models that describe the process of dry-band arcing are discussed, including those where an equivalent circuit is used to represent a polluted fiber optic cable in a high voltage environment. An implementation of this model on a MATLAB® based computer program is used to evaluate parameters such as leakage current magnitude, which may be used to predict the possibility of dry-band arcing. This leakage current is also compared to simulated results that were generated using a power system analysis program called Alternate Transients Program (ATP).

A finite element package, FEMLAB®, was used to model the experimental system, prior to construction. A single-phase transmission line with an accompanying fiber optic cable was constructed. The leakage current magnitude obtained from this experiment was subsequently compared to those obtained from the simulations. These leakage current comparisons are discussed and explained in view of limitations with the theoretical models and refinements in the experimental techniques employed.

The results clearly indicate that physical parameters like pollution severity, system voltage, length of span and the point of attachment of the ADSS fiber optic cable in the tower play a significant role in the determination of leakage currents induced on

the outer sheath of the cable. These induced currents result in the formation of 'dry bands', due to joule heating, and this could result in arcing activity that erodes the fiber optic cable.

Declaration

The research work discussed in this thesis was performed by Mr. Mohamed Fayaz Khan, under the supervision of Dr. D.A. Hoch, in the School of Electrical and Electronic Engineering at the University of Natal, Durban, South Africa. This work was partially sponsored by Eskom, as part of their "Masters Degree Programme for Black Engineers".

Parts of this dissertation has been presented by the student at the SAUPEC `2001 conference in Vanderbijlpark, South Africa and the IEEE AFRICON `2001 in George, South Africa.

The entire dissertation unless otherwise indicated, is the student's own original work and has not been submitted in part, or in whole to any other University for degree purposes.

M F Khan

4 December 2003

Acknowledgements

First and foremost thanks goes to the Almighty, to whom all thanks are due.

Secondly an enormous thanks to Dr. Derek Hoch for his help, encouragement and enthusiasm during my period of study. His constructive criticism and patience are greatly appreciated and I hope to develop the same passion for research that he displays.

Thanks are due to my father, mother and sister who have been an enormous pillar of support for me over the years. They have always encouraged me in whatever challenge I have taken up in my life, and for this, I will be eternally grateful.

Thanks are owed to ESKOM for their much appreciated and enjoyed financial support during my studies at University. Special mention must be made of Mrs. Kate Paterson and Mrs. Krishnie Govender from the Training and Development Department, Eastern Region, ESKOM Distribution.

Thanks are also owed to my two best friends, Miss Themesha Murugas and Mr Yuvaan Gugrajah for my making this study period, the most enjoyable period of my life.

Finally I would like to thank my postgraduate colleagues for their help and friendship and for providing many hours of entertainment and thought provoking discussions, which helped create a most enjoyable working environment.

Table of Contents

List of Figures / Tables

Chapter 2

Chapter 3

Chapter 4

Chapter 5

Chapter 6

Chapter 7

Chapter 8

CHAPTER ONE

INTRODUCTION

1.1 Motivation

Power utilities throughout the world are now in the practice of installing fibre optic cables on overhead transmission lines. This has been driven both by the need for effective internal utility communications and the desire for revenue from unused fibre capacity. There are currently three types of fibre optic cables that are commercially available for installation on high voltage networks. The first is optical ground wires (OPGW) in which the fibres are installed at the center of shield wires that are normally used for lightning protection. The disadvantage of an OPGW installation on an existing power network is that it requires the removal of the currently installed shield wire before it can be installed. This would prove both time consuming and relatively expensive. However OPGW should be considered a viable option on a new route or if the route is being restrung for another reason. An alternative technique is to wrap an optical cable around an existing earth or phase conductor (WRAP). The common disadvantage in both these methods is that they physically link the communication and power networks. Separation of the communication and power transmission lines would assist in maintenance work, as work on one would not affect the other. This would be a considerable advantage.

The third is all-dielectric self-supporting (ADSS) fibre optic cable, which is mounted below the phase conductors and is attached to the tower by means of grounded clamps. This technique does separate the power and communication networks and ADSS fibre optic cable is therefore much easier to install and maintain on energized circuits. This in addition to their smaller material cost and higher fibre count, makes this option the preferred option amongst power utilities throughout the world. This dissertation specifically investigates and reports on the ageing mechanisms of ADSS fibre optic cable.

1.2 Ageing Mechanisms of ADSS Fibre Optic Cables

A primary disadvantage of the use of ADSS fibre optic cable is the reported cable jacket deterioration that occurs near the grounded armor rod assemblies installed on the transmission towers. Field observations and laboratory tests have identified two likely causes for this ageing mechanism. The first phenomenon has a higher probability of occurring along the coast or near industrialized areas due to the increased pollution level.

In service, the cable will experience an induced voltage over most of its suspended length and this voltage is induced be means of capacitive coupling with the energized conductors. When the polluted fibre optic cable jacket is lightly wetted by fog, dew or light drizzle, a milliampere sized current is known to flow on the cable jacket from midspan outwards to the earthed suspension points [Brewer et al, 1992]; [Rowland, 1992]. The heating effect (ohmic) of this current may dry the jacket preferentially, forming 'dry bands' which no longer conduct. Preferential drying of the pollution layer results in an increase in sheath resistance across these 'dry bands'. The voltage across the dry band now increases, as the large resistance of the dry band is in series with the small resistance of the wet cable. If the induced voltage across the dry band exceeds the withstand level, an arc may result.

Deterioration of the cable jacket in this case is determined by the duration and energy dissipation of a resulting arc. Continued arcing activity on the cable jacket would affect the long-term integrity of the cable. The phenomenon of dry-band arcing occurs in other avenues of high voltage engineering quite frequently. Other subject material e.g. Composite Insulator Flashover, needed to therefore also be thoroughly investigated.

The second ageing mechanism is as a result of a corona discharge. This may be described as a localized low energy discharge occurring at the tips of the armor rods

and initiated by high electric fields and attachment hardware that have a small radii of curvature. Laboratory tests [Karady et al, 1999a] have shown that this phenomenon first causes discoloration of the cable jacket, followed by surface erosion that may puncture the protective jacket of the fibre optic cable thereby compromising both the structural and communication capability of the cable. There is also a third phenomenon. Microsparking on water droplets may be the cause of some of the cable jacket degradation found in the field. Droplet geometry has been observed, in the laboratory, to sometimes enhance the surface electric fields and initiate a discharge [Karady et al, 1999a]. Further simulation and experimentation is still, however, required to determine whether microsparking contains enough energy to cause cable deterioration on the ADSS cable jacket.

1.3 Scope of Research

The primary focus of this dissertation was to develop models to predict the magnitude of the leakage currents induced on the ADSS fibre optic cable as this parameter may be used to determine the probability of dry-band arcing. The effect of parameters like system voltage, pollution severity etc. on the leakage current induced was also investigated. Laboratory experiments were then conducted to ascertain the degree of correlation between the simulated and experimental results.

1.4 Dissertation Outline

This dissertation consists of nine chapters. Chapter 1 has introduced the area of interest and also discussed the different types of fibre optic cable that are commercially available for installation on high voltage power transmission networks. The key outline of this study was then stated along with a description of the two most prominent ageing mechanisms related to ADSS fibre optic cable.

Chapter 2 provides the context of this research effort and begins by outlying the theory of dry-band arcing on an insulated surface due to pollution. The flashover mechanism of silicone rubber insulators is more adequately investigated and was researched to obtain a better understanding of the phenomenon of dry-band arcing. Both associated ageing mechanisms are also succinctly explained in this chapter. The chapter concludes with research on contamination methods, pollution testing and an investigation into the thermal analysis of sheathing materials used on fibre optic cables.

In Chapter 3, models representing the phenomenon of dry-band arcing on fibre optic cables are introduced and developed. The chapter begins with an overview of an earlier mathematical model [Carter, Waldron, 1992] and then develops the model postulated by Karady et al [1999b]. This model is then modified to represent a polluted fibre optic cable in a single-phase high voltage environment. This model was used to predict the leakage current that would be induced during the laboratory experiments conducted in this study.

The model developed in Chapter 3 was then simulated on MATLAB®, a dynamic mathematical software package. The results of this simulation are included in Chapter 4 of this dissertation. The algorithm was used to investigate the effects of pollution, increased system voltage, span length and other associated parameters on the induced leakage currents.

Chapter 5 develops and analyses the results of a simulation conducted in ATP (Alternative Transients Program). The chapter begins by outlining relevant ATP theory and then discusses the development of the model. The simulation results are then presented and compared against the MATLAB® simulation.

FEMLAB® is a powerful modeling tool whose basic mathematical structure is a system of partial differential equations that are solved using finite element modeling techniques. The software was used in this study to investigate component parameters for the laboratory experiment and investigate the consequence of incorrect

installation in the field and a possible mitigation technique. It was also used as an alternative method of calculating the phase to fibre optic cable capacitance used by the MATLAB® simulation. This is the focus of Chapter 6.

Chapter 7 describes and details the results of the experimental investigations conducted as part of this study. Specific emphasis was placed on the design of the towers and measurement circuit.

An in-depth discussion of these results is contained in Chapter 8. In Chapter 8, all the results, both simulated and measured, are collated and the correlation between the simulated current predictions and the experimental data is investigated in this chapter. The chapter concludes with an analysis of dry-band formation (aided with experimentally obtained leakage current waveforms). Finally, Chapter 9 concludes this dissertation.

CHAPTER TWO

CONTEXT OF RESEARCH

This chapter begins by describing the background theory of dry band arcing on an insulated surface due to pollution. Numerous researchers throughout the world have investigated the effect of dry band arcing on outdoor composite insulators and these experiments and models are also reported on in this chapter. These experiments were performed to help obtain a better understanding of this damage mechanism and the factors that influence it. It was initially assumed that fibre optic cables, when installed in a high voltage environment, would be immune to electromagnetic interference, but recent studies have shown that under polluted conditions, sheath damage has been known to occur due to the mechanism of dry band arcing [Carter, 1993]. Both the models and the experimental investigations describing this process are discussed in this chapter together with another possible damage mechanism; corona discharge at the armour rod assembly on the tower. Contamination methods and pollution testing were also extensively researched during this study. The chapter concludes with an investigation into the thermal analysis of sheathing materials used on fibre optic cables.

2.1 Discharges on polluted insulation

The flashover of outdoor insulation (both glass and non- ceramic) due to pollution was, and still is, one of the foremost challenges in high voltage engineering. It has been reported that during the years 1951 to 1955, the number of insulator flashovers due to pollution on the 132 kV British grid was second only to those caused by lightning [Alston, Zoledziowski, 1963]. A prelude to pollution-induced insulator flashover is the mechanism of "dry band arcing", which is briefly explained below.

The dry pollution that settles on outdoor insulation does not itself affect the performance of the insulation significantly. It is when this pollution layer is wetted (either by dew, fog or drizzle) and begins to conduct that flashover becomes possible. The milliampere-sized currents that flow on the insulator surface distorts the electric

field along the insulation and also causes localised drying which results in the formation of small dry bands amongst the water droplets and filaments. Water filaments are formed when neighbouring droplets coalesce due to the small distances between them. Sparking occurs when the intensified stress between droplets or filaments locally exceeds the electric strength of air. These discharges are randomly distributed along the surface of the insulation. These discharges are known to elongate and may result in a flashover, but it should be remembered that not all discharges result in a flashover as many sparks are extinguished after having spanned only a fraction of the insulator surface.

There are numerous papers that postulate flashover models for both ceramic and silicone rubber outdoor insulators. The complexity of arcing phenomena necessitates that many simplifying assumptions have to be made in order to make mathematical modeling feasible. A common feature of these models, however, is a simplified representation of a propagating arc consisting of a partial arc in series with the resistance of the non-bridged section of the polluted layer. One of the first quantitative analyses of arcs on contaminated surfaces was made by Obenaus [Obenaus, 1958]. This approach (illustrated in Figure 2.1.1 and Figure 2.1.2) models the flashover process as a discharge in series with a resistance representing the non-bridged portion of the insulator and was derived for DC energization.

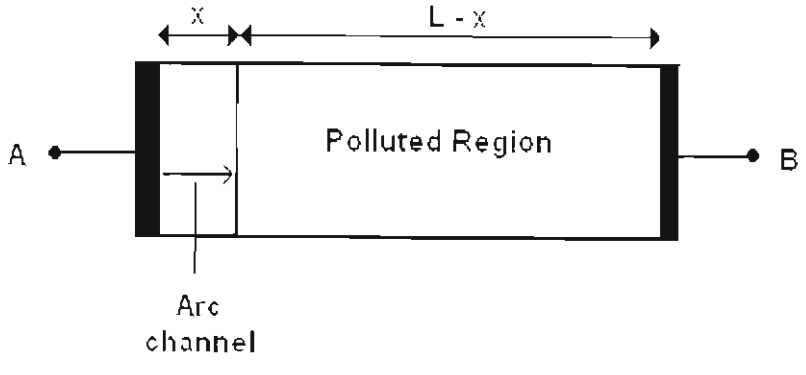

Figure 2.1.1: Simplified representation of the Obenaus model [Alston, Zoledziowski, 1963]

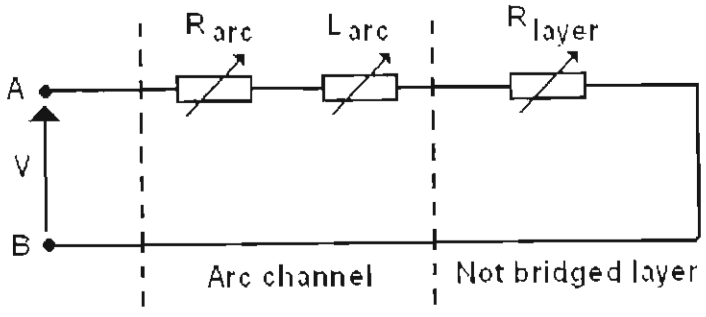

Where V – represents the voltage drop at the electrodes

R_{arc} – represents the arc resistance

L_{arc} – represents the arc inductance

R_{layer} – represents the un-bridged pollution resistance (Ω/m)

Figure 2.1.2: Equivalent electrical representation of Obenaus model

The voltage equation for the complete Obenaus model is therefore,

$$V = V_{arc} + R_{layer}.(L - x).I_{leakage} \quad ...(2.1.1)$$

In the equation above, all factors vary with distance (x) and the resistance of the layer is dependent on the resistivity of the pollution and the size and shape of the insulator. The following assumptions were made in this model. It was assumed that the discharge current is constant along the length of the discharge and the resistivity of the pollution layer was taken as a constant. The anode and cathode voltage drops on the electrolyte and the metal have also been ignored in this model but the sum of these models is estimated to be in the order of 400 V [Alston, Zoledziowski, 1963]. This voltage drop is justifiably ignored if the voltage applied to the insulator exceeds a few kilovolts [Alston, Zoledziowski, 1963]. The arc in the Obenaus model (V_{arc}) is represented by a voltage – current characteristic with the following equation,

$$V_{arc} = A.x.I^{-a} \quad ...(2.1.2)$$

where: V_{arc} represents the arc voltage

A, a represents the arc constants, and

x represents the length of the dry band

This model was then analysed by Alston [Alston, 1963] who experimentally derived the arc constants (A = 63: a = 0.76) and defined the following relationship for the critical electric stress E_c that may lead to flashover,

$$E_c = A^{1/a+1} . R_{layer}^{a/a+1} \ldots (2.1.3)$$

When the basic arc constants, as determined by Alston are used, the critical stress in V/cm are given by,

$$E_c = 10{,}5 . R_{layer}^{0{,}43} \ldots (2.1.4)$$

Another development in DC arc propagation theory was proposed by Hampton [Hampton, 1964], who postulated that a necessary condition for arc propagation is that the voltage gradient in the pollution layer ($dV/dx_{pollution}$) should exceed that in the arc (dV/dx_{arc}). Another model was also developed by researchers at the University of Manchester [Wilkins, Al-Baghdadi, 1971] that may be termed "discharge elongation by ionisation and successive root formation". This new theory involved the continuous transfer of current to new ionised paths ahead of the discharge tip. The probability of ionisation immediately ahead of the discharge root is high in this region as it is characterized by both a high voltage gradient and high temperatures. The total current during a discharge is therefore,

$$i = i_p + i_d \ldots (2.1.5)$$

where i represents the total current

i_p represents the current that flows through the pollution layer, and

i_d represents the current that flows through the ionisation path

Although Obenaus's model was derived for DC energization it has been applied to AC. Earlier researchers however found that when the basic DC values (as determined by Alston) were used to determine the flashover stresses, they were lower than the measured results. A higher value for the arc constant "A", often resulted in more acceptable AC predictions [Rizk, 1981]. Rizk [1981, 1988] also developed the AC mathematical model for pollution flashover. His model is also comprised of arcs and the surface resistance connected in series and bears a strong resemblance to the model proposed by Obenaus. The arc re-ignition voltage is calculated by:

$$V_{ignition} = 700 L_{arc} I_{leakage}^{-0.5} \quad ...(2.1.6)$$

During an arc free period, the leakage current on the surface of the insulator is simply calculated by:

$$I_{leakage}(t) = V(t) / R_L \quad ...(2.1.7)$$

where, V(t) represents the sinusoidal line to neutral voltage, and

R_L represents the surface resistance

Using Rizk's model, the leakage current expression during arcing is given by:

$$I_{leakage}(t) = \left[\frac{V(t) - V_a - V_c}{R_{L-L_{arc}} + R_{arc}} \right] \quad ...(2.1.8)$$

where, V_a is the arc anode voltage drop

V_c is the cathode voltage drop

V_{arc} is the arc voltage

R_{arc} represents the arc resistance, and

L_{arc} represents the arc length

The arc resistance in equation 2.1.8 is obtained dynamically using numerical differentiation and $R_{L\text{-}Larc}$ represents the arc free surface resistance of the insulator. The definition of the arc parameters for AC systems remains a challenge as they vary depending on different experimental methodologies or mathematical derivations. Researchers are now considering using arithmetic optimisation methods that use generic algorithms to determine these constants [Gonos et al, 2002].

2.2 Flashover mechanism of silicon rubber insulators

Experiments with regard to dry band arcing and flashover of silicone rubber insulators are more numerous and well developed, mainly due to the fact that the introduction of ADSS in a high voltage environment is relatively recent. Some of the more important concepts are the diffusion of LMW polymer chains and the wetting of the silicone rubber surface.

2.2.1 Introducing silicone rubber insulators

The use of silicone rubber insulators has increased significantly in the last 20 years, as they display a superior performance (higher flashover voltage) in contaminated environments as opposed to glass or porcelain insulators. Although aging reduces the flashover voltage of the contaminated composite insulator, their overall performance is good [Karady et al 1999c]. Other advantages of composite insulators are their lightness in weight and a reduction in the damage caused by vandalism [Liang et al, 1992].

Surface hydrophibicity, a quality of silicone rubber, ensures that water drops bead up and do not wet the surface completely. Nearby droplets are known to sometimes join, to form longer water filaments. This is the main reason for the superior performance of silicone rubber, since it is known to reduce leakage current and the probability of dry band formation, which leads to a higher flashover voltage. It is however known that heavy pollution and simultaneous wetting produce surface arcing, which destroys surface hydrophobicity and increases leakage current.

The surface may recover hydrophobicity after 10 – 12 hours of a dry and arc free period [Karady, Shah, Brown, 1995]. This is due to the diffusion of mobile low molecular weight polymer chains (LMW) from the bulk to the surface. It is during this recovery period that the insulator surface remains hydrophilic and flashover remains unlikely. The pollution withstand characteristics of silicone rubber insulators is known to deteriorate due to a combined effect of UV degradation and surface arcing [Karady, Shah, Brown, 1995].

2.2.2 Silicone rubber insulator contamination

There are mainly two types of contamination viz. sea pollution and inland pollution. Sea pollution consists mainly of wind-driven salt from the ocean, whereby dust, tar and industrial pollution are the main constituents of inland pollution. When dew, fog or light rain interacts with the pollutants, it generates a conducting surface layer. Both ESDD (equivalent salt deposit density) and NSDD (non-soluble deposit density) testing can be used to evaluate the contamination build-up on insulators. Figure 2.2.1 below shows the pollution collecting areas of an insulator that has alternate shed diameters along its length.

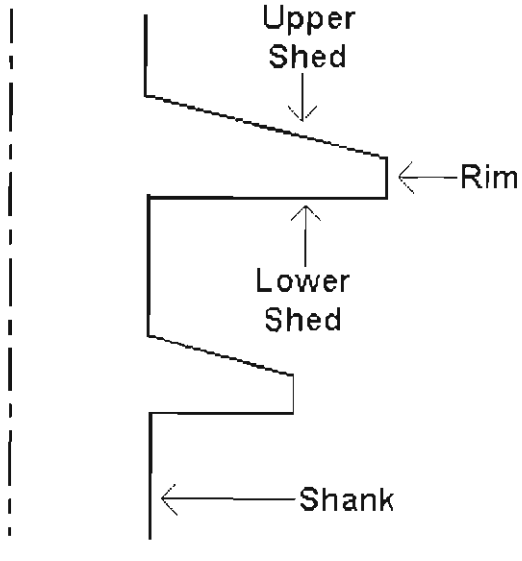

Figure 2.2.1: Pollution collecting areas on a silicone rubber insulator [Karady et al, 1999c]

NSDD testing performed on composite insulators at Arizona State University [Karady, 1999] has shown that pollution deposition is maximum at the ends of the insulator and that smaller sheds collect less pollution than the larger ones. It was also found that more pollution accumulates on the lower shed than the upper shed of the insulator but the maximum pollution was however found on the rim of the shed. The pollution level of the shank was found to be comparable with the lower surface of the nearby shed.

2.2.3 Flashover of silicone rubber insulators

To better understand the flashover mechanism of silicone rubber insulators, experiments were performed on insulators with one skirt that were contaminated and tested with a constant voltage [Karady et al 1999c]. In these experiments, filamentation and spot discharges were observed for nearly all of the withstand cases. It is the spot discharges that destroy the hydrophobicity of the neighbouring surface which lead to filamentation and the formation of irregularly shaped wet regions. This results in an increase in the local electric field strength.

When these wet regions short the insulator surface, an arc may result, as the current-limiting resistance decreases considerably [Danikas, Karafyllidis, 1998]. The arc travels above the wet layer and this may result either in the extinction of the arc or a flashover. Continuous arcing activity on the surface of the insulator is known to reduce the hydrophobicity of the insulator.

2.3 Dry band arcing on ADSS fibre optic cable

When ADSS fibre optic cables were first installed on 110 kV overhead power lines in 1979 [Carlton et al, 1993], no reports of sheath degradation were received. None were expected as ADSS fibre optic cables are non-conductive and thus thought to be immune to electromagnetic interference [Phillips, 1987]. However, when ADSS fibre optic cables were installed on higher voltage transmission lines, sheath degradations were reported that could result in cable dropping [Carlton et al, 1993]. It was postulated by high voltage researchers that this degradation was a result of dry band

arcing as experienced previously on outdoor insulators [Carter, Waldron, 1992]. This phenomenon is described below [Rowland, 1992].

Capacitive coupling between the ADSS cable and the phase conductors induces a voltage on the surface of the cable. The combined effect of pollution and natural precipitation creates a conductive layer on the outer sheath of the ADSS cable. The cable is earthed at its suspension points on the tower and an earth leakage current will therefore flow axially from mid-span towards the tower. The Joule heating effect of this current may dry the layer in spots forming "dry bands" which no longer conduct, resulting in a localised increase in sheath resistance. Since this large resistance is in series with the small resistance of the wet cable, the voltage across the dry band, and hence the electric field within it, rises. It is when this induced voltage that develops across the dry band exceeds the withstand level that an arc results. The heat given off by this arc is commonly assumed to cause degradation of the sheathing material. The mechanism described is illustrated in Figure 2.3.1 below.

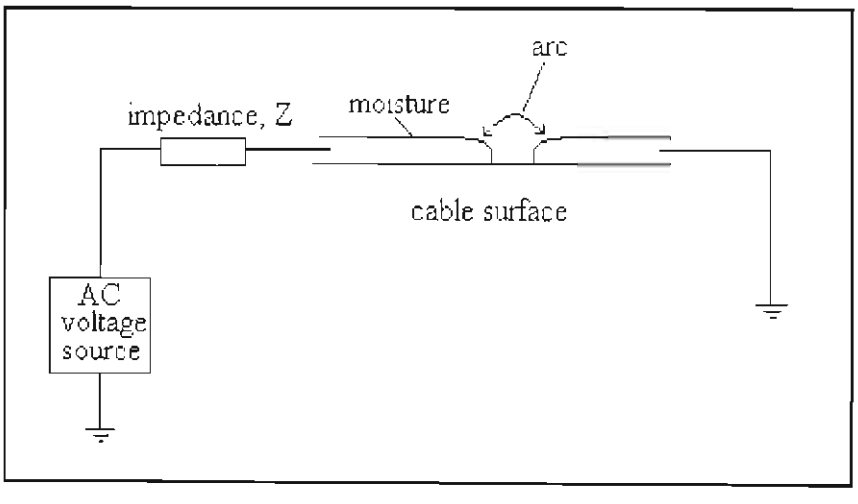

Figure 2.3.1: Schematic of a dry band arc

The leakage current found on the surface of the ADSS cable is of vital importance to any investigation regarding dry-band arcing. Carter and Waldron [1992] were amongst the first researchers to develop a mathematical model for the determination of leakage current on polluted fibre optic cables. This model was subsequently

revised and improved by Karady, Devarajan and Tuominen [1999]. The development of this mathematical model is re-visited in Chapter 3.

Another researcher, Olsen was however concurrently working on another model that described the phenomenon of dry band arcing on ADSS fibre optic cables installed near high voltage power lines [Olsen, 1999(a), 1999(b)]. He used a single-phase conductor (that represented the total 3 phase contribution in a network) to pass through the centre of two grounded tower windows that were electrically connected to a length of ADSS fibre optic cable. The tower windows were modelled as torroids that were concentric with the phase conductor and the advantage of this model was that it explicitly took into account the effect of the tower windows on the induced electric fields.

2.3.1 Experimental investigations

When dry band arcing was identified as being the primary cause for sheath degradation on installed ADSS fibre optic cables, laboratory tests were quickly set-up to reproduce this degradation mechanism in the laboratory for investigative purposes. Some researchers simulated the voltage induced by capacitive coupling by connecting a length of ADSS cable between earth and a high voltage transformer [Brewer et al, 1992]. These researchers investigated the development of a dry band through a wet/ dry test cycle. The ADSS sample in this experiment is sprayed with water to simulate natural precipitation.

It was found that large currents (>80 mA) occurred on the surface of the test sample at the beginning of each spray cycle. Stable arcs that caused serious damage were observed for up to several seconds. After saturation of the surface with water, the current profile was found to revert to a pure sine wave of between 80 120 mA that resulted in rapid drying. It was observed that the sample dried out more rapidly at the top of the sample than at the bottom. This observation has been attributed to the effect of gravity. The final stage in the development of the dry band was the creation of a "vee-shaped" dry region that rapidly opens out to form a parallel dry band approximately 7 mm wide. Dry band arcing was found to occur during this stage and

continued for up to 90 seconds before which activity ceased [Brewer et al, 1992]. These researchers also suggested that sheath damage is caused by radiated and convected heat from the body of the arc as opposed to thermal energy released at the arc root. The absence of a current-limiting resistor in this experiment resulted in the high leakage currents observed during this experiment.

Other experiments have therefore been known to vary the type of coupling. In [Rowland, 1992], each sample was connected to the HV supply secondary coil, either directly, through a HV resistor or through a capacitance. The performance of cable sheathing under surface arcing conditions generated in a salt fog chamber is then monitored and the resulting voltage and current waveforms for the various coupling methods were observed.

It was found that the observations made for the "directly coupled" case were similar to that obtained by Brewer et al [1992] (discussed above). When the sample was capacitively coupled to the transformer, bursts of brief activity were observed on the sample surface, but these bursts of activity were considerably more violent than the directly coupled case. A current pulse of 120 mA was observed for a duration of 1 ms during arcing. It has been suggested that the arc sounds more violent because higher currents are discharged for a shorter time as opposed to the directly coupled case. In the resistively coupled case, the arc appeared visually different than in the previous two cases, as the dry band arc length was very precisely defined. Once arcing began, it was continuous rather than occurring in bursts.

Researchers Peacock and Wheeler [1992] have also proposed a test procedure to ascertain the viability of installing certain ADSS fibre optic cables in high voltage environments. This procedure incorporates ultraviolet preconditioning followed by a salt fog test under combined high voltage and tension. Ultraviolet radiation, incident on the earth's surface, affects the hydrophobicity of installed ADSS cables [Peacock, Wheeler, 1992] and it is therefore an important factor to consider in any ADSS accelerated ageing test.

2.3.2 Dry band arc compression

Previously it was thought that all ageing on ADSS fibre optic cables was due to the gradual effect of long-term low current magnitude arcing. However, it has been observed that in conditions under which Hampton's criterion is not met (i.e. when an arc is confined in length), arc compression can occur. In these circumstances, a dry band is reduced in length and an existing arc is continually shortened until it is extinguished. Moisture running along the cable is one way in which arc compression can occur. Such an event may be rare, but only one occurrence may be required for significant damage to be inflicted upon the cable. The mechanism of arc compression is based on the net flow of water on the surface of the cable. This could be caused by wind blowing water up the cable, towards the earthed clamp at the tower. A dry band arc that forms would then be compressed against the clamp.

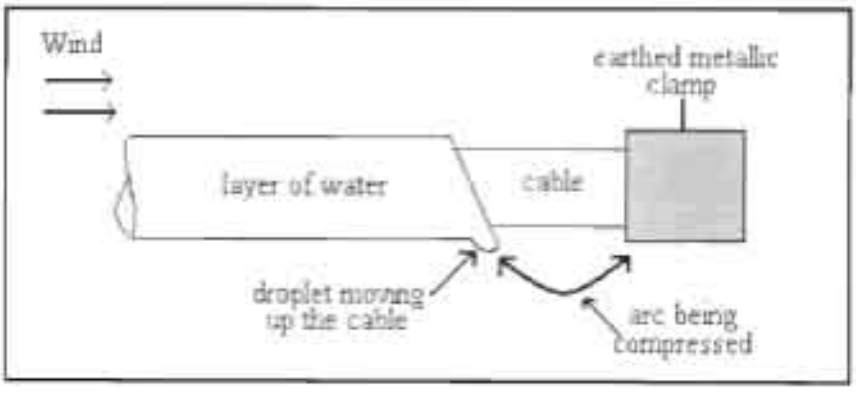

Figure 2.3.2: Dry band arc being compressed against a metallic clamp

Another way that arc compression may occur on the cable is when moisture flows down an incline. The higher droplet would move down the cable to the dry band edge with the lower arc root fixed against a large, immobile droplet. Continued movement of this droplet, due to gravity, would cause arc compression. This is illustrated in the diagram below.

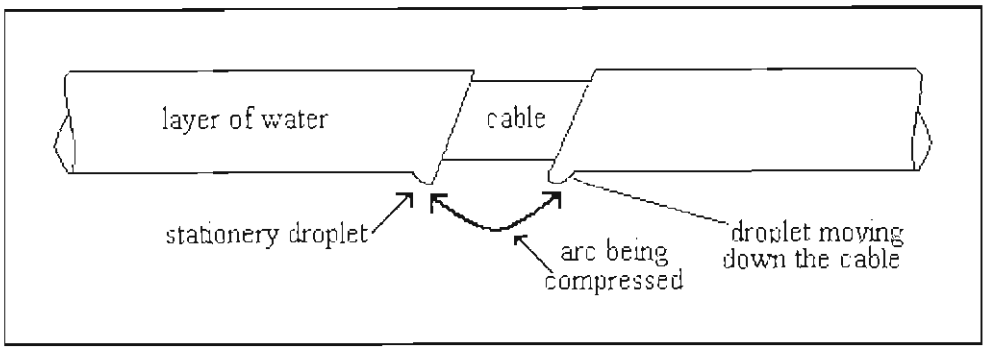

Figure 2.3.3: Dry band arc being compressed against an immobile droplet

The phenomenon of arc compression was experimentally investigated to determine whether dry-band arc compression always leads to sheath failure and whether unstable arcs are able to damage the cable surface [Rowland, Nichols, 1996]. In this experiment, two electrode arrangements were employed and these are shown below. The first configuration was used to investigate fixed arc lengths, whereas the second configuration was used to investigate arc compression. To reproduce arc compression events, a copper wire was fixed to a rod so that it could be pushed along the surface of the cable until it touched the other foil electrode. A ballast high voltage resistor is used in both configurations to limit the current.

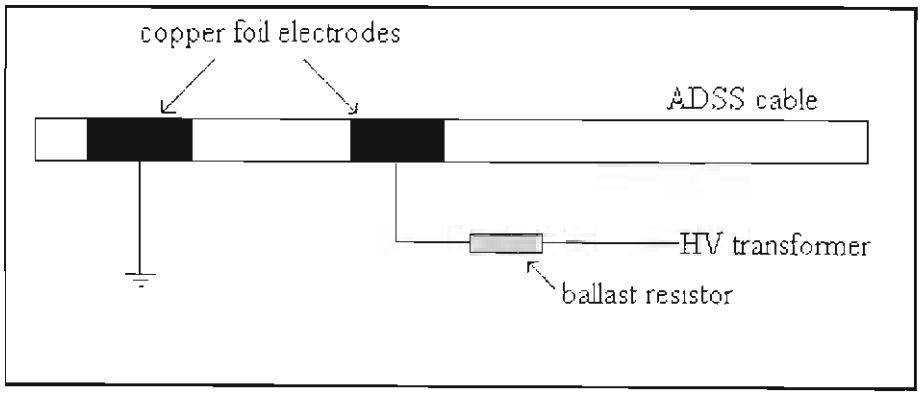

Figure 2.3.4: Electrode arrangement for arcing experiments: Stationery electrodes. Redrawn from [Rowland, Nichols, 1996]

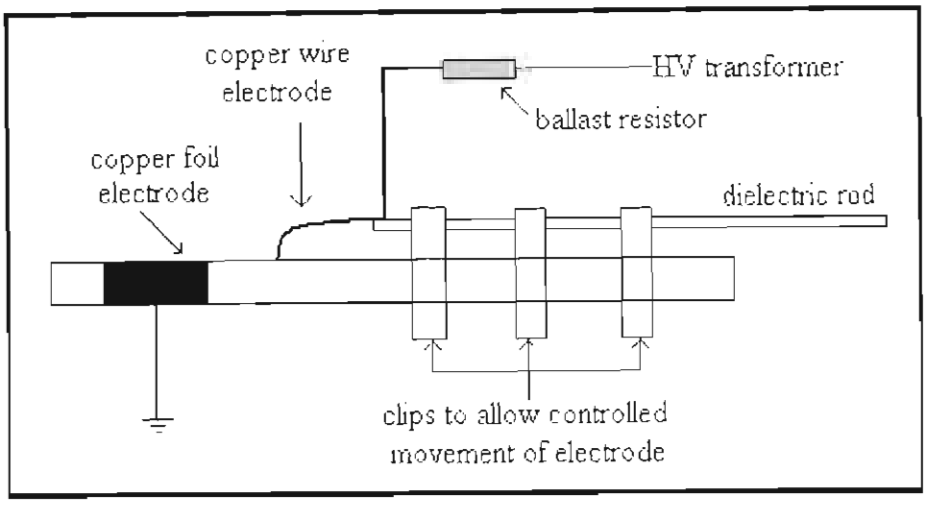

Figure. 2.3.5: Electrode arrangement for arcing experiments: Arc compression Redrawn from [Rowland, Nichols, 1996]

The results of the experiments conducted in [Rowland, Nichols, 1996] have found that as long as sufficient voltage was available to break down the gap, the magnitude of the voltage had no direct influence on the rate of aging. It was rather the current that determined the effect of an arc and was therefore proposed that ADSS cables should not be defined by system voltage, but by the maximum current that may be seen in service.

For the stationary electrode arrangement, varying the resistance of the ballast resistor varied the current on the arc surface. It was found that currents less than 2mA caused little or no damage to the cable sheath, but currents that ranged between 2mA and 3mA was found to cause deep localized erosion. The use of higher currents was found to slow the ageing process down as opposed to accelerating it. It was found that arc compression resulted in severe damage even at lower currents. During compression, it was observed that even unstable arcing resulted in damage to the cable sheath. Arc instability occurs when there is insufficient voltage available to drive the arc current.

2.3.3 Mitigation techniques

The most common way of reducing the risk of ADSS mechanical failure when installed on high voltage lines is a combination of calculating the stringing position,

which will best reduce induced currents, and the use of degradation resistant sheathing materials. There are, however, telecommunication networks that have already been installed on power networks. These networks need to be retrofitted with devices that limit the sheath degradation. Many devices and techniques have been proposed and some of these would be discussed in this section. Some of these methods may appear impractical or too expensive, but have been included to simulate discussion and understanding of this problem. The feasibility of most of these devices has been tabulated in [Carter, 1993].

a) A rain shield [Carter, 1993]

Leakage current tends to flow on the outer sheath of the cable only after wetting since this lowers the resistance of the surface. The concept of a rain shield operates on the principle that a short length of dry cable would reduce the leakage current to an acceptable level. A simple rain shield is shown in Figure 2.3.6 below.

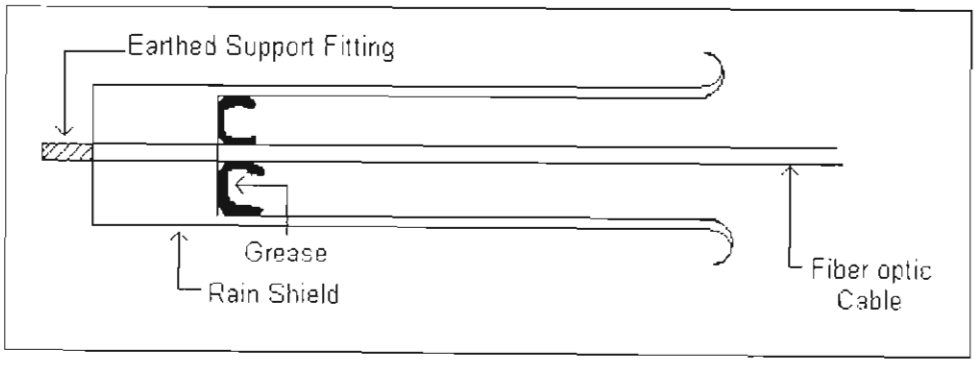

Figure 2.3.6: A simple rain shield.
Redrawn from [Carter, 1993]

Great care should be taken to insure that the clearance between the rain shield and the cable is large enough to prevent arcing and the open end of the shield should be radiused (as illustrated in Figure 2.3.6) to minimize stress enhancements. Disadvantages of this method include cost, size of the device and hardships encountered during installation. Another improvisation of this method is to allow

controlled arcing at the open end of the rain guard. This would considerably reduce the size of the rain guard.

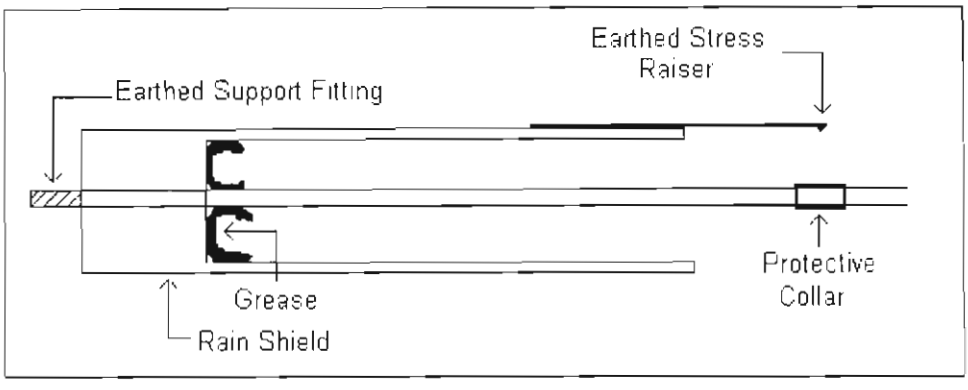

Figure 2.3.7: Smaller rain shield incorporating a spark gap
Redrawn from [Carter, 1993]

As illustrated in Figure 2.3.7 above, it was proposed that controlled arcing be achieved by placing an earthed stress raiser at the mouth of the shield and a protective collar on the cable beneath it. A serious disadvantage to this proposed method is the fragility of the earthed stress raiser.

b) Alter the electrical coupling at the fitting [Carter 1993]

Since arcing damage is most severe adjacent to the fitting (arcs are less mobile), damage could be prevented by re-arranging the electrical coupling so that arcing is encouraged to take place away from the fitting. This can be achieved by allowing some of the leakage current to flow to earth capacitively, well before the fitting is reached. This would move the position of maximum current away from the fitting. It has therefore been proposed that an earthed torroid be attached to the ADSS support fitting as shown in Figure 2.3.8.

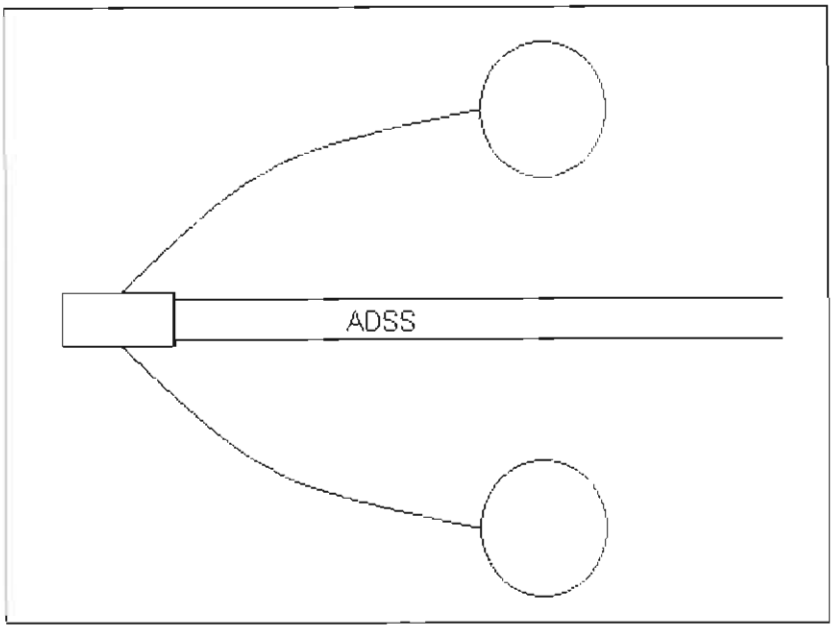

Figure 2.3.8: An earthed torroid
Redrawn from [Carter, 1993]

One way to do this is to place an earthed torroid around the cable but not touching it. It would be required to couple capacitively with the wet pollution on the cable sheath, at a position having enough voltage to drain about 10% of the earth leakage current, and yet have sufficient clearance between the cable and the torroid to avoid electrical breakdown. This device is intended to increase the mobility of the arc roots, thereby reducing cable degradation but is as yet unproven in the laboratory.

c) Use of composite insulators at tower support [Karady et al, 2000]

A proposed mitigation method was recently introduced by researchers at Arizona State University [Karady et al, 2000] that involved supporting the armour rod assemblies at the tower with silicone rubber composite insulators. These assemblies are normally installed directly onto the earthed tower as shown below.

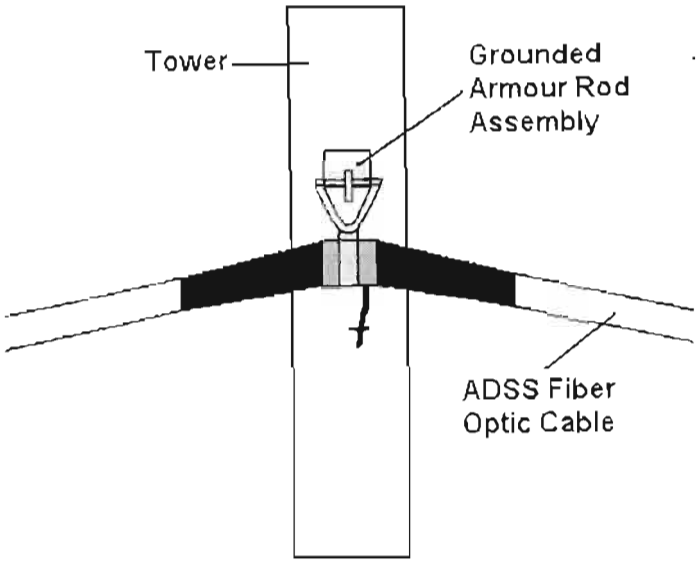

Figure 2.3.9: Grounded armour rod assembly supporting fibre optic cable at tower. Redrawn from [Karady et al, 2000]

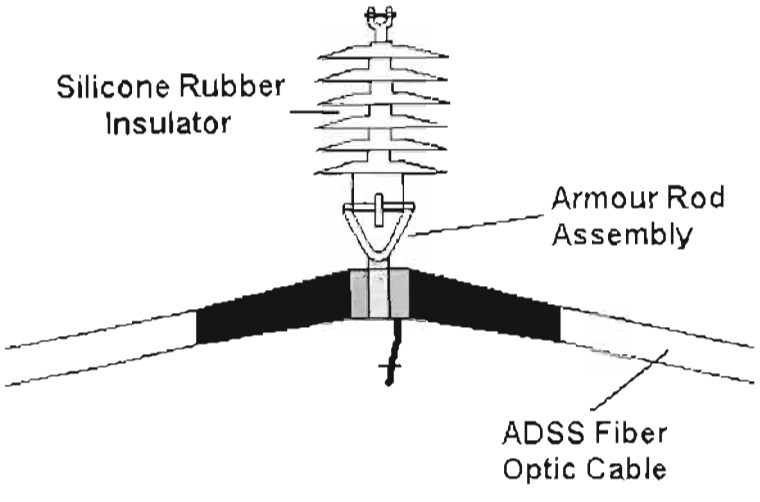

Figure 2.3.10: Proposed mitigation method
Redrawn from [Karady et al, 2000]

A series of experiments were performed to determine the feasibility of this proposed method. It was found that a 69 kV silicone rubber insulator was effective up to an open circuit voltage of 20 kV. This technique is considered to be economical when

compared to the cost of a fibre optic cable outage, as the price of silicone rubber insulators is low. It was also suggested that this method only be used in heavily polluted areas.

d) Real-time leakage current monitoring [Karady et al, 2001b]

Another mitigation technique would be a preventative one. If the current that flows on the outer sheath of the cable were monitored, then it would be possible to determine the pollution status of the ADSS sheath. When the currents increase to dangerous levels, an alarm could be sent to the utility and cable washing could be scheduled. Different current sensors were investigated for this method [Karady et al, 2001b]. These included a simple shunt resistor, an active Rogowski coil and a double core sensor. The shunt resistor was chosen as the current sensor as this provided the best accuracy, frequency response and temperature performance of the three sensors investigated. It was also the most cost-effective sensor investigated.

A complete, self-contained current monitoring system was designed and consisted of the sensor, a solar panel (for power), data acquisition system and cellular communications. The complete system was tested and found to operate reliably in an outdoor environment.

2.4 Corona caused deterioration

The other main degradation mechanism found when ADSS fibre optic cables are installed in high voltage environments is cable surface erosion due to armour rod corona. Corona discharge, which may be described as a continuous, localised, low energy discharge, occurs at the tip of the metallic armour rods, which surrounds the cable and attaches it to the tower. The existence of armour rod corona has been observed, both in the field and during laboratory tests [Karady et al, 1999e]. Corona discharge is initiated by the high electric fields that are created when the sharp edges of the armour rod assembly intensify the generated electric field. It has been reported that a local electric field of about 20 kV/cm will generate a corona discharge [Karady et al, 1999e] and that unmitigated corona may firstly cause a discolouration of the

cable sheath, followed by surface erosion. This compromises both the mechanical integrity and communication capability of the cable.

2.4.1 Electric field calculations

When investigating corona related deterioration, electric field studies are pivotal. The electric field needs to be accurately modelled since it is these measurements that determine the probability of discharges occurring. It is therefore advisable to employ a three-dimensional simulation method, over the classical two-dimensional method, when determining the space potential that exists for a particular tower configuration. The 2-dimensional model assumes that the field only has radial components and does not take the grounding of the armour rod assembly and tower into account. Researchers, [Karady et al, 1999e] using a 3-dimensional electric field program (developed by Olsen (1981)) have proved that longitudinal electric fields exist in this environment, by showing how the electric field increases as the grounded hardware is approached. Their model included both the tower and grounded armour rod assembly. A worst case scenario was also investigated. In this model, one rod was simulated to protrude 2.5 cm past all the others and this resulted in surface gradients on the tips, which exceeded 20 kV/cm on a 230 kV power network.

2.4.2 Experimental Investigation

The Electrical Engineering Department at Arizona State University have conducted experiments with regards to the corona caused deterioration of ADSS fibre optic cables when installed in a high voltage environment [Karady et al, 1999e]. An interesting result was obtained when three fibre optic cables (A, B and C) were placed at different locations in an electric field generated by a tubular 75 kV electrode. Each fibre optic cable was fitted with three armour rods that were each exposed to the same electric field to increase confidence in the results obtained. Figure 2.4.1 below shows the simplified electrical connection for Cable A. The electrical connections for cables B and C would be similar to Figure 2.4.1 below. The cables were positioned such that cable A would experience heavy corona generation, whilst cables B and C would experience only moderate to light corona generation.

This information was obtained using the same three-dimensional electric field simulation program used earlier to prove the existence of longitudinal electric fields.

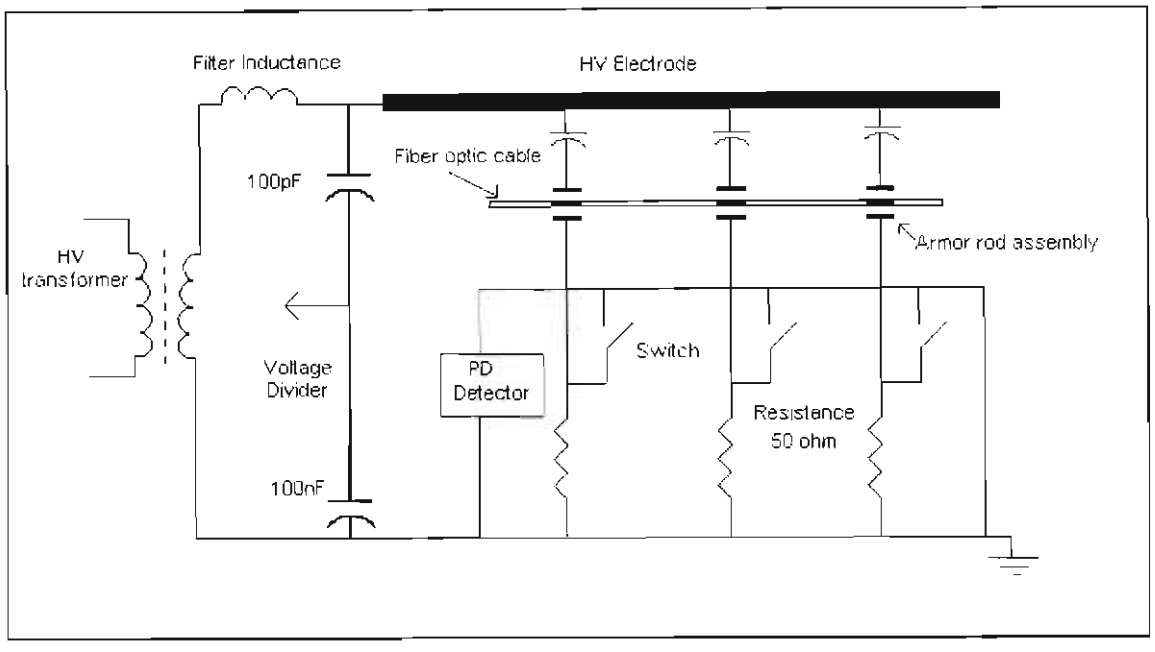

Figure 2.4.1: Simplified Electrical connection for Cable A
[Karady et al, 1999e]

In this experiment, round-ended brass rods were used in place of the actual armour rod assembly. This was done so that the worst-case scenario (where one rod protrudes 2.5 cm past all the others) could be properly investigated. This experiment was continuously conducted for over nine months. During this period, the corona discharge intensity (in nC) was measured about once a day and the system was also periodically de-energised to allow for photographs of the surface erosion to be obtained. The measured values of corona discharge intensity showed significant scatter when plotted against time but the trends observed suggested that the partial discharge level increased with exposure time.

The photographs that were periodically taken during the experiment were used to observe the progression of surface deterioration on the cable jacket. The corona-induced degradation on the cable sheath began with a greyish-white discolouration on the cable jacket. This was followed by small surface erosion, which may lead to

the development of an erosion spot (hole). The eroded area was divided into two regions,

- A core area (Ac) that was identified by a slight depression (if applicable). This indicated material loss
- The surrounding area (Af)

A photograph of the degraded area was scanned and the areas specified above were determined using image processing software that measures dimensions from an analysed digital image. It was found that the erosion was, as expected, larger for cable A as opposed to cable B. The erosion found on cable C was negligible as there was only a discolouration found on the cable surface. This result proved that cable surface erosion caused by corona increases with field strength. The depth of the core area is very significant to this experiment as it is directly related to cable damage. The depths of the depression for this experiment were measured and are represented below in Table 2.4.1.

Cable	1	2	3
A	>25.4	127	101.6
B	0	>25.4	50.8
C	0	0	0

Table 2.4.1: Depth of corona depression in micrometers after 5500 hours [Karady et al, 1999e]

Using these findings and assuming linear degradation, it has been proposed [Karady et al, 1999e] that unmitigated corona would puncture the cable jacket after 8 – 15 years. This would destroy the communication capabilities of the cable and also jeopardise the mechanical integrity of the fibre optic cable. In other experiments by the same researchers it was found that rain and high humidity also mitigated the corona inception voltage.

Deterioration on ADSS fibre optic cables, caused by corona, has been observed by power utilities in the field [Karady et al, 1999a]. Manufacturers of fibre optic cables need to therefore design cables that are more resistant to the corona-induced degradation. [Karady et al, 1999a] have therefore proposed a new method to the IEEE for the evaluation of corona caused aging on ADSS fibre optic cables. Five different cables were tested for 3052 hours to illustrate the feasibility of this method by determining their resistance to corona discharge.

As in earlier experiments [Karady et al, 1999e], the armour rod assembly was replaced with brass rods that surrounded the fibre optic cable and one rod protruded 2.5 cm farther than the others. This was done to accelerate jacket deterioration. It was found that the discharge intensity during the experiment did not correlate well with the cable jacket deterioration.

It was suggested by these authors [Karady et al, 1999a] that a cable's resistance to corona degradation should be evaluated using optical microscopic measurement techniques. The cables were ranked on two criteria namely, the area of the surface degradation and the depth of localised erosion. Since some cables experienced a small area of degradation with deep erosion and vice versa, the overall ranking of the tested cables were obtained by multiplying the area of the surface degradation with the maximum depth of erosion.

2.4.3 Mitigation techniques

There are currently many proposed mitigation techniques to reduce corona-induced degradation on ADSS fibre optic cables. Almost all of these proposed and existing methods involve significantly reducing the rod tip surface gradients to well below 20 kV/cm. Great care should be taken when installing ADSS fibre optic cables onto high voltage towers as they should be exposed to as low a space potential as possible. If the cable is already installed then the ADSS may be relocated to an area of lower electric field activity. In the case of a double circuit line, re-phasing can be quite effective in reducing the space potential in which the cable is installed.

Researchers have suggested that the metallic armour rod be replaced with a fibreglass rod assembly [Karady et al, 1999e]. Although this would reduce the rod tip gradient significantly, it would not prove to be economically viable. A plastic corona coil may also be used to effectively shield the armour rod assembly as laboratory tests have shown that this device can reduce rod tip gradients by a factor of about six [Karady et al, 1999e].

2.5 Pollution Testing

Under outdoor conditions, electrolytic conductive layers are known to form on the surface of cable insulation. These layers are generated mainly due to the presence of pollution and moisture. When the term "polluted" is used to describe the cable insulator surface, it should be acknowledged that it is not in reference to its appearance or contamination severity but rather to the presence of soluble electrolytes. The most significant contamination with regards to dry-band arcing on fibre optic cables are marine pollution, road-salt from salt flats and desert dust storms, and industrial pollution from the petrochemical industry. These deposits require water to become conductive and fog, dew and drizzle are therefore highly significant deposits as well. There are also pollutants like carbon and some metallic oxides that are electrically conductive even in the absence of water but cable degradation caused by this contamination is rare.

2.5.1 Processes of Contamination

Pollutants are transported onto the surface of the cable by processes like gravity, electrostatic attraction, evaporation of solutions or suspensions and aerodynamic catch. Aerodynamic catch is the predominant contamination process of all those listed above.

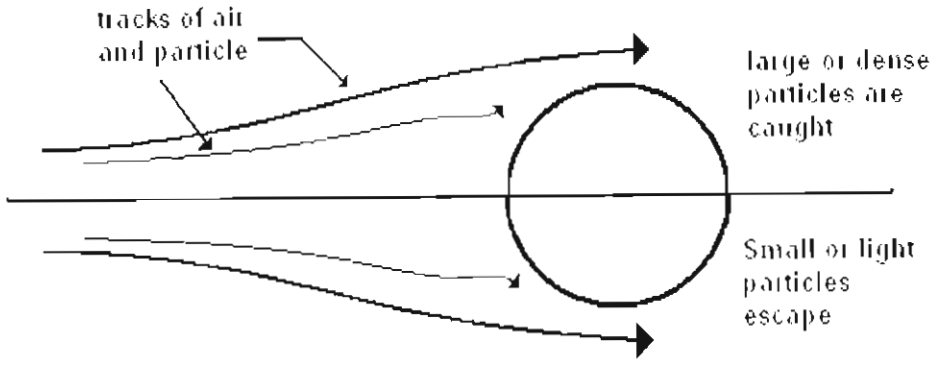

Figure 2.5.1: Process of aerodynamic catch [Looms, 1988]

Wind is the primary pollutant transport mechanism in the process of aerodynamic catch. As illustrated by Figure 2.5.1 above, the efficiency of the cable to "catch" a particle is dependant on both the size and density of the pollutant particle and the speed of the airflow that carries it. The simplest case of particle catch occurs when a relatively large particle is deposited at a point of stagnation. The point of stagnation is created when the cable forces the airflow to divide around it, thus creating a region where the air is at rest. The simple design of the cable insures that the effects of rotating-flow and vortex generation, as experienced by insulators in the field, are of minimal importance to this investigation.

The pollution layer that forms on the cable surface require water before they can become conductive. However, it may be assumed that heavy rainfall would remove most types of pollution from the cable surface, as is the case with high voltage insulators. This purging process is largely attributed to droplet size and the high impact speed involved. A recent study investigated the affect of rainfall on the pollution performance of insulators on four island networks [Tsanakas et al, 1999]. In this study, the number of pollution flashovers per month was correlated with the measured rainfall for that month and it was found that the fault numbers were highest during the rainless period. This suggests that rainfall contributes greatly in cleaning the insulators of its pollution layer.

2.5.2 Pollution severity measurement

In any given power network there would be areas of varying pollution severities ranging from high pollution areas to low pollution areas. Power utilities need to be aware of the pollution severity in an area so that the proper precautions may be exercised to avoid damage to the installed fibre optic cable. These precautions could range from cable washing to the fitment of various retrofit devices that are known to mitigate dry-band arcing.

The current most common method of determining pollution severity on field insulators is the ESDD (equivalent salt deposit density) method and these results are generally obtained in accordance with regulation IEC 507. The pollution severity on ADSS fibre optic cables may also be monitored using the ESDD method. This method is however labour intensive and therefore not very cost effective. Power utilities would therefore welcome alternatives to the traditional method of determining ESDD.

One of these alternatives is the directional deposit gauge (DDG). After extensive investigations researchers at the University of New Orleans found the DDG to be a very cost effective method of monitoring pollution severity [Lannes et al, 1997]. These devices are easy to install and are equivalent to ESDD measurements. They require minimal maintenance and also provide the direction from which the pollutants came.

Researchers at Washington State University have also in recent times designed a portable ADSS surface contamination meter [Edwards et al, 1999]. This device was designed to measure the amount of contamination on an in-service ADSS cable so that the induced leakage current could be more accurately determined. The contamination meter designed was comprised of three sub-units that are listed below:

1) Coaxial electrode structure
2) The meter cabinet for measurement, and
3) A computer for data storage

The measurement device took the appearance of a coaxial cable where the contamination layer represents the inner conductor. The internal DC measurement was shielded from the high voltage induced fields by the Faraday cage design of the outer shell. Compressible conducting pads made of stainless steel wool provide the electrical contact to the contamination layer. The device uses a centre tap configuration and one lead of the ohmmeter is connected to this centre node while the other node of the ohmmeter is connected to the outer shell of the electrode structure. This is represented in Figure 2.5.2.

To eliminate the effect of capacitive coupling, the outer shell of the electrode structure was shunted to ground to eliminate any capacitance current from entering the meter. Preliminary testing [Edwards et al, 1999] has led to the belief that this device may be used to measure the contamination level of the ADSS cable in the field. The measurements obtained could be used to determine when or whether cable washing is required to mitigate dry band arcing.

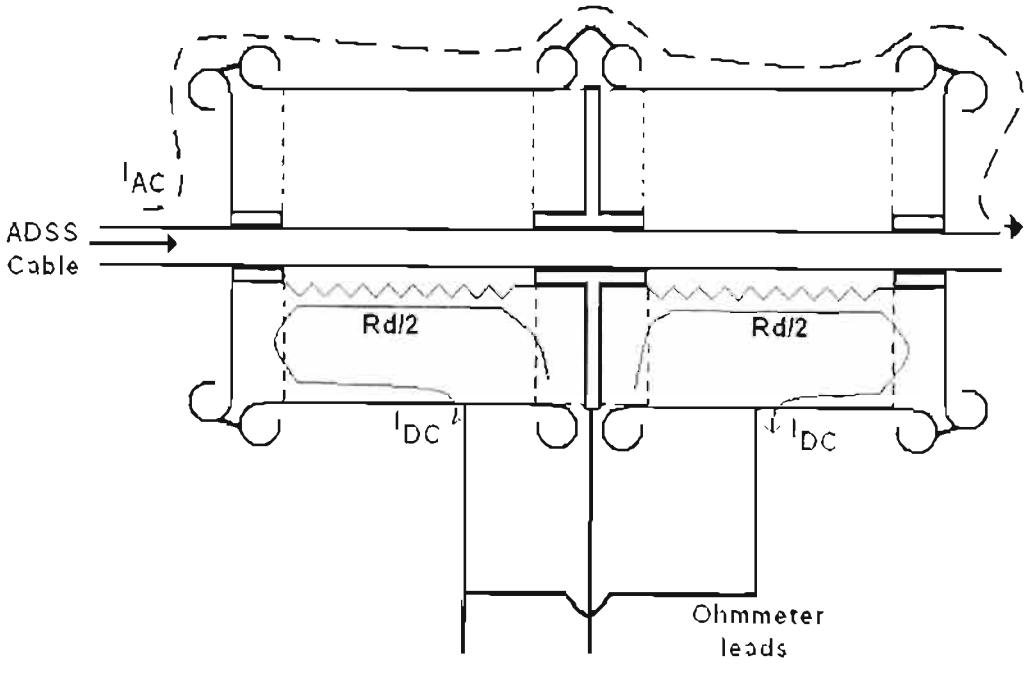

Figure 2.5.2: Circuitry of electrode structure [Edwards et al, 1999]

2.5.3 Methods of accelerated pollution testing

Laboratory testing of the tracking performance of ADSS fibre optic cables are very significant when either designing or selecting a cable to be installed on a high voltage transmission network [Gorur et al, 1987]. The problem with laboratory tests of this nature is that they require an acceleration factor to avoid long time-consuming tests. This acceleration factor involves the application of much higher electrical fields and more severe artificial test conditions than the existing ones found under real service conditions. These tests are not meant to simulate real service conditions but rather, to test the tracking and erosion performance of the cable. The results obtained from artificial aging tests should therefore always be regarded critically.

When deriving tests that would be appropriate to measure the pollution performance of ADSS cable, a lot of information may be obtained from the pollution testing of composite insulators. This is merely because the pollution performance of composite insulators has had a longer time to be researched. The reason as to why the research is relevant is that both display the same failure mechanism, namely dry band arcing.

The 1000-hour salt-fog test is one of the harshest accelerated aging tests to evaluate the performance of composite insulators, because it does not give silicone the opportunity to recover lost hydrophobicity. As shown in the Salt-fog experiment of [Barsch et al, 1997], if the silicon is given a 70h break to recover lost hydrophobicity after a 1000-hour test, it would be found that the flashover voltage would be much higher than that measured immediately after the test. The main reason for this is that a break of 70 hours was sufficient for the penetration of low molecular silicone components through the layer consisting of salt and degradation deposits.

The salt fog test is a 'component' test, as opposed to being a 'material' test. The performance of an insulator in a power system, with regards to surface leakage currents, hydrophobicities etc. are influenced by both the shed material itself and the shed shape, creepage distance, etc. It is therefore desirable in this instance to perform a component test over a material test since a component test is more realistic than a

material test. The major drawback of component testing is that it is much more time consuming.

A continuous changing of dry and wet periods is much more realistic as it is a more accurate simulation of outdoor conditions and would allow the silicon sufficient time to recover its hydrophobicity [Kim et al, 1990]. Researchers in India have also modified the salt fog test to simulate the actual conditions of the pollution layer being wetted with slight rain or drizzle by performing the wetting action with tap water instead of steam [Devendranath et al, 1999]. This method is referred to as the Rain Fog Method and in this method the insulator was coated with a pollution layer and then wetted with tap water to simulate light rain as opposed to being wetted with a 'salt-fog'.

The pre-treatment of the insulator surface in most salt-fog tests has however been questioned in recent times [IEEE Standard Techniques for High Voltage Testing, 1995]. These researchers believe that the pre-treatment of the insulator surface using detergents and other abrasive techniques seriously alters the hydrophobicity of the sample thereby raising questions regarding the validity of these tests. Researchers in China [Xidong et al, 1999] have therefore developed a pre-treatment procedure that aims to maintain the original hydrophobicity of the test sample. Dry kieselguhr is gently and uniformly applied to the sample surface using a soft tampon or brush. Any excess kieselguhr is then blown off, resulting in a very thin pollution layer on the original hydrophobic surface that may then be wetted to obtain a target pollution level.

The Swedish Transmission Research Institute (STRI) have recently developed a novel pollution test method called the Dust Cycle Method (DCM) [Eklund, Hartings, 1997]. This method is best illustrated in Table 2.5.1.

Voltage								
Dust								
Fog		40 min						
Rain				1 min				
Wet					15 min			
Drying								

Table 2.5.1: One cycle of the Dust Cycle Method pollution test [Eklund, Hartings, 1997]

This method imitates the natural pollution transport mechanism as the pollution (kaolin and salt) is applied by wind in consecutive cycles. Each cycle includes pollution application, wetting (both rain and fog), and drying and the duration of the test is usually two hours. A contamination method that better simulates natural pollution accumulation can be achieved by using a specially designed mixing nozzle that is illustrated below in Figure 2.5.3 [Besztercey, Karady, 2000].

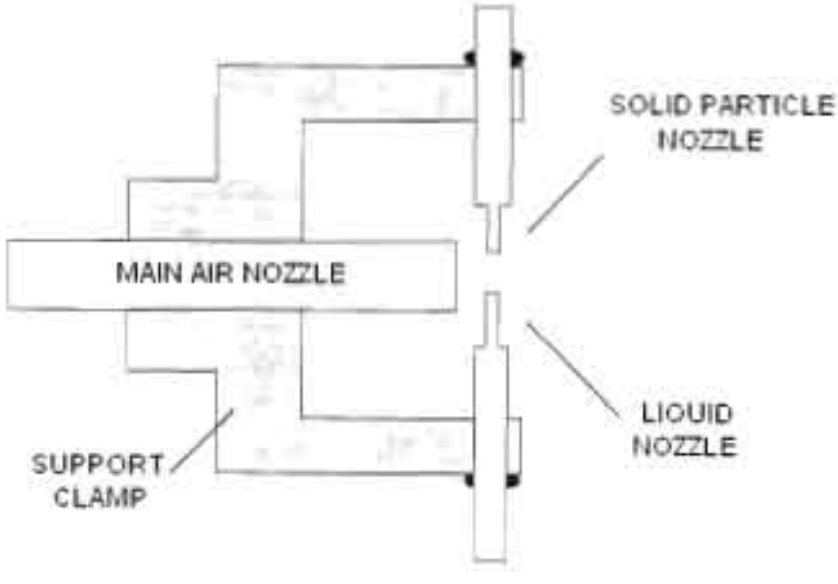

Figure 2.5.3: Cross section of dry mixing nozzle [Besztercey, Karady, 2000]

This nozzle pollutes the surface of the insulator (or ADSS fibre optic sample) with a mixture of dry contamination particles and an atomised salt solution. A significant

advantage of this novel method is that both the ESDD and NSDD of the artificial pollution can be accurately controlled. This form of pollution application also renders the time-consuming process of surface pre-treatment unnecessary, thereby maintaining the original hydrophobicity of the insulator surface.

2.6 Thermal Analysis

Dry Band Arcing is a localized surface discharge phenomenon that is one of the primary causes of sheath degradation on ADSS fibre optic cables. Other known causes of sheath degradation are microsparking and corona discharge on the tip of the armor rods initiated by high electric fields. Electrical activity on the surface of a material will cause degradation both thermally and because of active chemical species formed in the discharge. The thermal component of this electrical activity is vital in terms of both designing and choosing an application specific fibre optic cable.

The University of Reading in the UK has performed a study of thermal effects for a range of different polymer based composite systems that have been proposed for use as sheathing materials [Vaughan, Swingler, 1993]. The three material types considered were, a thermoplastic, a filled organic elastomer and a filled silicone rubber. The aim of these experiments were to gauge how these different materials would perform at the elevated temperatures that occur as a result of arcing activity. Before explaining the experiment and its findings however, one needs an understanding of the thermal tests performed for the results make sense. The two thermal tests performed during this experiment was Differential scanning calorimetry (DSC) and Thermogravimetric analysis (TGA).

2.6.1 Differential scanning calorimetry

Differential scanning calorimetry is a laboratory technique used to study the thermal transitions that a polymer undergoes when heated. The melting of a crystalline polymer is one example of a thermal transition. The fundamental design and basic operation of a DSC thermal analysis system is quite elementary and is best described using the figure below.

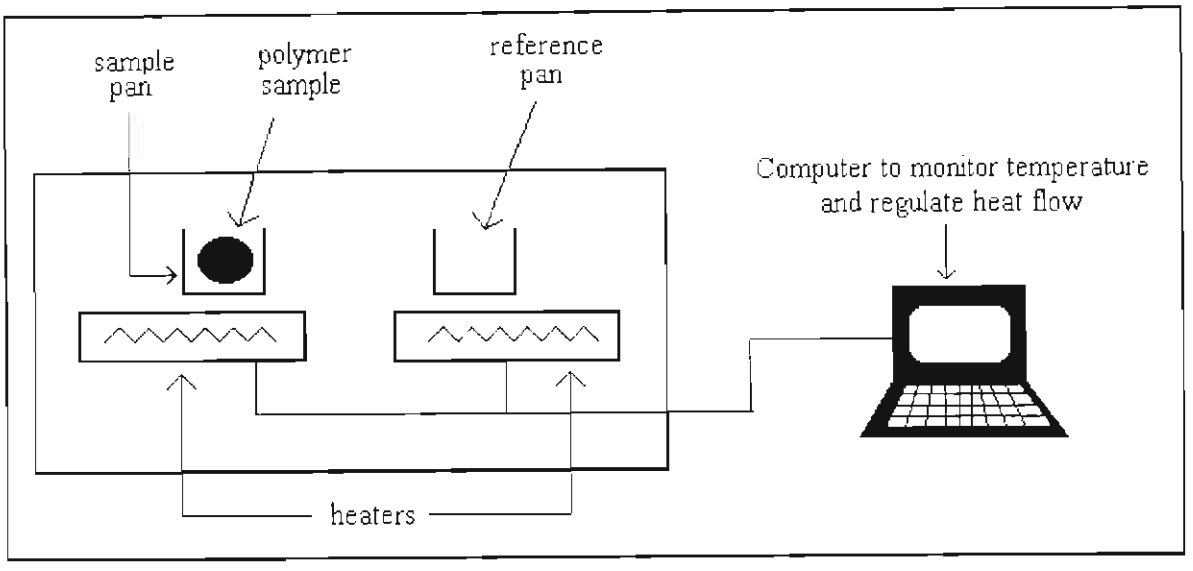

Figure 2.6.1: DSC experimental set-up

[J F Rabek, 1980]

There are two pans on a DSC device and the sample to be investigated is placed in one pan (sample pan) whilst the other pan is left empty (reference pan). Each pan sits atop a heater, which is digitally controlled to heat both the pans at a specific programmable rate e.g. 20°C per minute.

A computer is often used to control these heating rates, as it is extremely important that the heating rates of both pans are identical throughout the experiment. The two pans would obviously not heat at the same rate as the polymer sample represents extra material in the sample pan. The sample pan would therefore require more heat to ensure that temperature of both the sample and reference pan increase at the same rate. A DSC experiment essentially measures how much more heat is applied to the sample pan as the temperature is increased. The plot obtained would resemble Figure 2.6.2 below. On the x-axis, we plot the temperature and on the y-axis, we plot the difference in heat output of the two heaters at a given temperature.

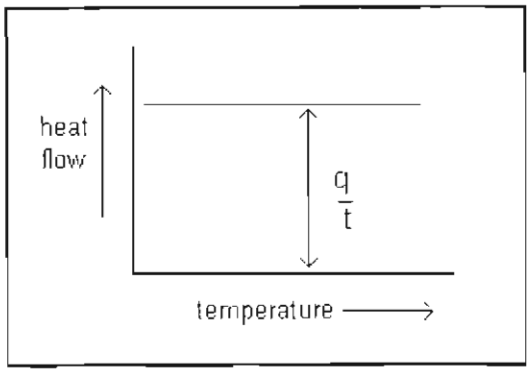

Figure 2.6.2: Typical DSC plot [J F Rabek, 1980]

At higher temperatures, polymers are known to sometimes undergo crystallisation as they would have obtained enough energy to move into more ordered arrangements. Since this process is exothermic, it would appear as a dip on a DSC plot. A DSC plot may be used to determine whether crystallisation did in fact occur, the crystallisation temperature and the latent energy of crystallisation for the polymer.

When a polymer is heated past its crystallisation temperature, another thermal transition called melting may be attained. At this temperature, the polymer crystals begin to fall apart and the chains come out of their ordered arrangements and begin to move around more freely. As this is an endothermic transition, it is also observable on a DSC plot as a peak. The temperature at the top of this peak is known as the polymer melting temperature whilst the area of this peak is used to determine the latent heat of melting. The DSC plot may also be used to determine the polymer crystallinity percentage, which is an indication of the fraction of the polymer that was crystalline.

2.6.2 Thermogravimetric analysis

Thermogravimetric analysis (TGA) is a qualitative technique, which investigates a materials mass loss with increasing temperature. It is valuable if used in conjunction with methods such as differential scanning calorimetry (DSC) and differential thermal analysis (DTA) in order not only to investigate a weight loss due to degradation or decomposition upon thermal changes, but also to distinguish what chemical structures are given off.

Depicted below is a TGA scan of a proprietary block copolymer. It can clearly be seen that the sample mass decreases with rising temperature as its chemical structure is being degraded at higher temperatures. When one analyses the decomposition data obtained from a TGA, one usually records the temperature at which the mass loss initiated and the temperature that corresponds to both 1% and 10% mass loss.

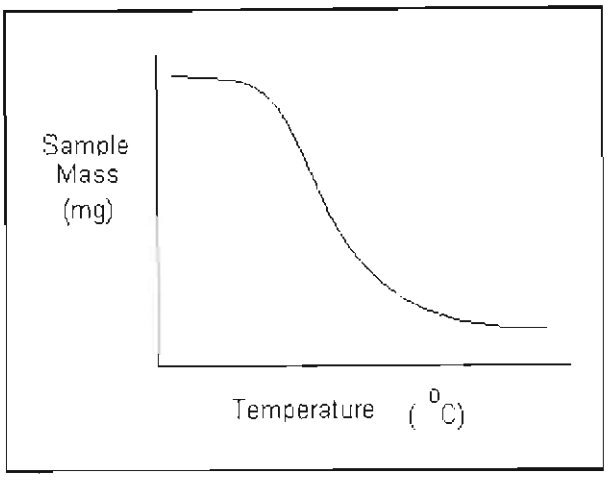

Figure 2.6.3: Typical TGA plot for a polymer

[Blaedel, Meloche, 1966]

2.6.3 Experimental Procedure [Vaughan, Swingler, 1993]

A DSC and TGA analysis in atmospheres of air and oxygen free nitrogen was initially performed on the three sample materials mentioned above, so that their thermal properties could be ascertained. The small samples used were heated at a rate of 20 K/min over a temperature range 100°C to 800°C for the TGA. The DSC experiment then investigated the enthalpy changes from 25°C to an upper limit that was determined by the results of the TGA. All samples, after being cooled to 25°C, were rescanned such that the reversibility of any transition could be determined. An electronically controlled laser was then used to produce local thermal erosion on the sample materials being investigated such that they may be ranked.

2.6.4 Experimental results [Vaughan, Swingler, 1993]

The tables that follow summarize the thermal analysis experiments conducted.

Material	Peak Melting	Melting Enthalpy (Jg^{-1})	Polymer Crystallinity
Thermoplastic	128	125.8	43%
Organic Elastomer	83	17.5	14%
Silicone Rubber	-	-	0%

Table 2.6.1: Summary of DSC results [Vaughan, Swingler, 1993]

Material	Temperature (°C)		
	1% Mass Loss	10% Mass Loss	Onset
Thermoplastic	320	431	282
Organic Elastomer	249	367	212
Silicone Rubber	275	488	381

Table 2.6.2: Decomposition data from the TGA scans in nitrogen [Vaughan, Swingler, 1993]

Material	Temperature (°C)		
	1% Mass Loss	10% Mass Loss	Onset
Thermoplastic	284	351	275
Organic Elastomer	244	306	191
Silicone Rubber	254	462	364

Table 2.6.3: Decomposition data from the TGA scans in air [Vaughan, Swingler, 1993]

It should be stated that this study did not determine the suitability of a sheathing material based on its ability to prevent dry band arcing, which is important, but rather on its ability to withstand a surface discharge. A weighted combination of both these factors and cost would be the ideal determining factor. There are two changes that are fundamentally important when investigating the ability of a sheathing material to

withstand a surface discharge. The first is with regards to its phase transition temperatures and the second is its decomposition behaviour.

These experiments showed that the sheath integrity of the thermoplastic was compromised due to melt flow at a low temperature of about 150°C. A cross-linked system is known to add a degree of dimensional stability at higher temperatures and should therefore be a prerequisite for any sheathing material considered. Because the thermoplastic does not have a cross-linked structure, it follows that both elastomers considered would initially outperform the thermoplastic.

The decomposition behaviour of the sheathing material plays a considerable role in determining suitability. Of the three samples under investigation, both the organic elastomer and silicone rubber are carbon based polymers based on the ethylene monomer. They therefore decompose in a similar manner and temperature range (400°C - 500°C). At higher temperatures failure occurs by erosion rather than by tracking and the presence of fillers play an important role in this decomposition process.

The presence of aluminium hydroxide (ATH) filler in the organic elastomer shows this. When ATH decomposes into alumina and water, it slows down the decomposition process as the water generated would affect the discharge activity and the reaction is endothermic, thereby reducing the energy available for degradation. The disadvantage of this filler is that it can only play an active role in the decomposition process once, since the reaction is irreversible. However, continuous decomposition reactions would result in an inert inorganic surface layer that may prevent further degradation in the underlying layers.

There is no qualitative difference in the manner in which the silicone rubber decomposes when compared to the ATH-filled organic elastomer mentioned above. The thermal experiments conducted in this study did however find a quantitative difference, as it was found that the mass loss experienced by the silicone rubber sheathing was considerably smaller than that of the organic elastomer. This is due

largely to the fact that silicone rubber decomposition results in both a volatile organic species together with a large inorganic residue, as opposed to most other linear organic polymers that produce only volatile decomposition products. The 5% carbon black that was included as a filler in the thermoplastic does not play a major role in the decomposition process. It was included as a UV stabilizer.

The sheathing materials considered in this study may be easily ranked on localized thermal performance using the results obtained thus far. The thermoplastic would be the least likely choice as it undergoes melt flow at the relatively low temperature of 150°C due to its poor dimensional stability. The thermal performance of both elastomers were far superior to that of the thermoplastic, but the silicone rubber would be more suitable as it would provide greater erosion resistance and possess greater mechanical integrity. Laser ablation tests were then conducted and these conclusions were confirmed. This would suggest that laser irradiation is a convenient way of simulating a local heating process to investigate the erosion processes of a sheathing material.

This chapter began with a brief history of the research undertaken to both understand and prevent electrical discharges on polluted insulation. The research "began" with the Obenaus model (Figure 2.1.1) in 1958 and remains one of the foremost challenges in high voltage engineering. The flashover mechanism of silicon rubber insulators was also thoroughly researched by the author as experiments and publications on this subject matter were more numerous and explained a similar electrical phenomenon to the one being investigated. Subsequently, an in-depth study is presented on the degradation mechanism of dry band arcing and armour rod corona associated with the installation of ADSS fibre optic cables in high voltage environments. Possible mitigation techniques were also investigated and assessed. Modern methods of pollution testing and measurement were then discussed along with methods of accelerated pollution testing. Finally the thermal effect of dry band arcing on the cable sheath was presented. This criterion for selection of ADSS fibre optic cable is an emerging technology that will prove to be fundamental in terms of choosing an application specific cable in the future.

CHAPTER THREE

EQUIVALENT MODEL REPRESENTING DRY-BAND ARCING ON ADSS FIBRE OPTIC CABLES

The phenomenon of dry band arcing on silicone rubber insulators is well researched and documented and mathematical models describing this phenomenon on silicone rubber insulators are more numerous and well developed. This is due largely to the fact that the introduction of ADSS in a high voltage environment is relatively recent. It was believed by most researchers that the leakage currents induced on the outer jacket of the fibre optic cable was of paramount importance in the prediction of dry band arcing. Carter and Waldron [Carter, Waldron, 1992] were amongst the first researchers to postulate a mathematical model to determine the leakage currents induced on the outer sheath of a fibre optic cable installed in a high voltage environment.

3.1 Overview of an early mathematical model [Carter, Waldron, 1992]

3.1.1 The concept of *'Active Length'*

A concise description of dry band arc formation was presented in the previous chapter. Carter and Waldron developed this concept further, whereby they introduced the concept of an *'active length' (δ)* of cable adjacent to the armour rod assembly at the tower. *'Active length'* refers to a length of span on the fibre optic cable (measured from the tower), wherein all residing charge contributes to the earth leakage current. Any charge residing further out on the span, *"cannot contribute to the earth leakage current, because the time taken to drain it is longer than the interval between polarity inversions."* (Carter, Waldron, 1992, pg. 187). The *'active length'* is determined by

$$\delta^2 = \frac{2}{\omega R(C_1 + C_2)} \quad \text{... (3.1)}$$

where

- ω is the angular frequency
- R represents the resistance per unit length of wet polluted cable
- C_1 represents the capacitance per unit length of the optical cable to line voltage
- C_2 represents the capacitance per unit length of the optical cable to ground

3.1.2 Mathematical determination of the current distribution

This system was devised to accurately calculate the current magnitudes at specific points on the cable. It was proposed that knowledge of the leakage current induced would be used to predict dry band arcing in fibre optic cables. Thevenin's theorem was firstly used to simplify the problem by replacing all the phase conductors with an equivalent conductor, at potential V_S, relative to ground. An infinitesimal element of the cable (length dx) was considered and it was assumed that C_1, C_2 and R are constants that are independent of position. Since the element considered has a potential, V, relative to ground and carries a current, I, the current continuity gives

$$dI = j\omega C_1 V_S dx - j\omega V(C_1 + C_2)dx \quad \ldots (3.2)$$

and the voltage drop along the fibre optic cable as a result of the resistive pollution layer is

$$dV = -IRdx \ldots (3.3)$$

Using common algebraic techniques and given boundary conditions, these equations are solved analytically to yield the magnitude of the leakage current on the cable jacket at the support tower. This is given by

$$I_1 = V_S \omega C_1 \delta \quad \ldots (3.4)$$

The complete derivation of this equation is included in Appendix A. The implication of this result is that the maximum leakage current found at the support tower is independent of both span length and fibre optic cable to ground capacitance.

3.2 Equivalent model development

Karady and Devarajan [2001a] have subsequently presented an algorithm that improves upon the method discussed above. In their calculation of leakage current, Carter and Waldron [1992], made the assumptions that the line voltage to fibre optic cable capacitance, the fibre optic cable to ground capacitance and the resistance of the wetted pollution layer were constant along the length of the span. This was an over-simplification as it is common practice for the sag on the fibre optic cable to be smaller than that of the phase conductors thereby altering both the phase to fibre optic cable capacitance and the fibre optic cable to ground capacitance along the span. Also, the assumption that the resistance of the pollution layer is constant throughout the entire length of the cable is not very realistic. Whether windborne coastal pollution or industrial soot, pollution does not settle uniformly on the ADSS cable. The algorithm presented by [Karady et al, 2001a] can include both the effect of sag and the effect of non-uniform pollution. They have developed an equivalent circuit to represent the polluted fibre optic cable in a high voltage environment.

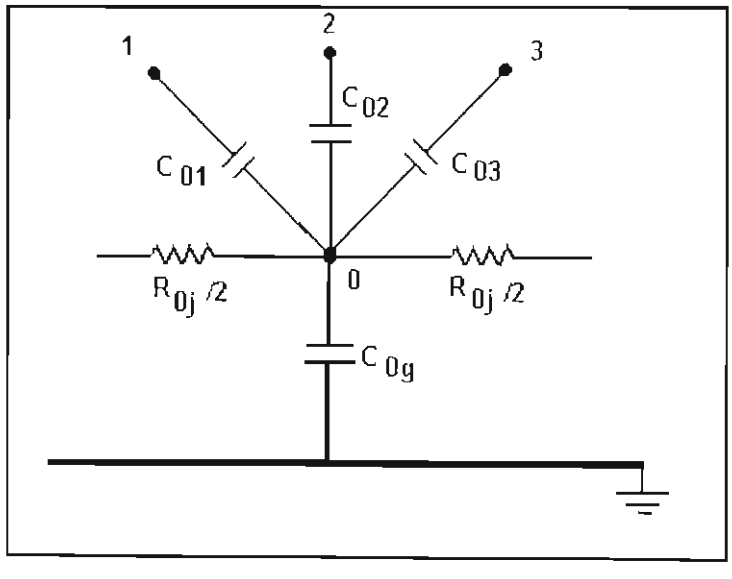

Figure 3.1: Equivalent circuit of polluted fibre optic cable [Karady et al, 2001a]

Figure 3.1 is a diagrammatic representation of the equivalent circuit at a given point along the span. The numbers 1, 2, and 3 represent the phase conductors (assumption of a single circuit three phase transmission line) and 0 represents the ADSS fibre

optic cable. C_{01}, C_{02} and C_{03} are the respective phase to fibre optic cable capacitance and C_{0g} represents the fibre optic cable to ground capacitance. R_{0j} represents the wetted pollution layer on the outer sheath of the cable. A finite number of these sections in series, approximates the distributed nature of the circuit such that numerical analysis would yield the leakage current induced on the cable sheath.

3.3 Algorithm development for the three-phase system

3.3.1 Spatial determination

This is a three dimensional problem and the z-dimension is defined along the span of the fibre optic cable and the conductors. The point of origin was taken to be at mid-span, on the ground at the middle of two transmission towers. This resulted in the x-dimension representing lateral displacement from the reference point and the y-dimension representing the height of either the conductor or fibre optic cable from the ground. To take into account the effect of sag, the height of the cable and conductors were assumed to be a hyperbolic cosine function along the span [Karady et al, 2001a]. The height of the conductors and fibre optic cable are required to calculate the capacitance values along the length of the span.

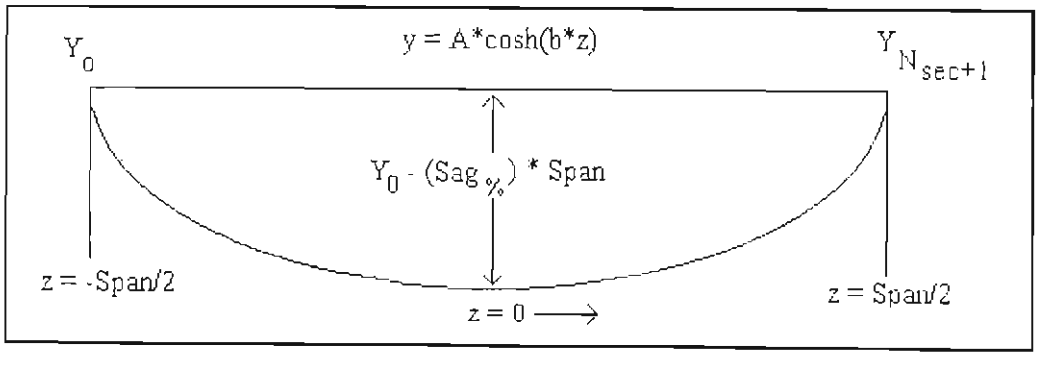

Figure 3.2: Sag calculation model [Karady et al, 2001a]

The sag is specified as a percentage of the span length at mid-span as depicted in Figure 3.2 above. In the field, the sag of the line conductors is usually greater than the sag of the fibre optic cable. Using this method of height determination, allows for the algorithm to take this factor of differing sag into account. The height of the phase conductors and fibre optic cable is given by

$$Y = A.\cosh(b.z) \quad \ldots \quad (3.5)$$

where

Y represents the height of the relevant cable

z represents the distance from the tower, and

A, b are constants

The constants A and b, used in the above equation are dependent on the sag, span length and the initial height of the cable on the tower. They are derived using the boundary conditions at the tower and mid-span and are given by

$$A = Y_0 - (Sag_{\%} * Span) \quad ...(3.6)$$

$$b = \frac{2}{Span} \cosh^{-1}\left(\frac{Y_0}{A}\right) \quad ...(3.7)$$

Using these constants and the knowledge that the span is to be divided into multiple sections, the height of the conductor or fibre optic cable at section N is determined by

$$Y_N = A * \cosh\left(b * \frac{span}{2}\left(\frac{2N}{N_{sec}+1} - 1\right)\right) \quad ...(3.8)$$

where N_{sec} represents the total number of sections. Using this method of spatial determination, one may also take the effect of strong crosswinds into account.

3.3.2 Capacitance calculations

The capacitance values required in this algorithm were determined using the method of Maxwell's potential coefficients (EPRI, 1987). Earlier researchers (Olsen, 1999b) used a simplified expression for the capacitance obtained by ignoring the phase conductor to fibre optic cable capacitance. This result did not take the effect of sag into account and depended only on the height and radius of the fibre optic cable. The method of Maxwell's potential coefficients is commonly employed when parallel conductors are separated from each other and ground by relatively large distances. If one assumes that the line charge in this case is located at the centre of the conductor, then

$$[V] = [P][Q]$$

where

[V] = conductor line to ground voltage

[Q] = linear charge densities, (coulomb metre)

[P] = Maxwell's coefficients, (metre/farad)

Determination of the capacitance matrix at each section therefore requires inversion of the Maxwell's coefficient matrix. The size of Maxwell's coefficient matrix, [P], is dependent on the number of conductors found within the system and is determined by

$$P_{ii} = \frac{1}{2\Pi\varepsilon} \ln\left(\frac{2h}{r}\right) \quad ...(3.9)$$

$$P_{ij} = \frac{1}{2\Pi\varepsilon} \ln\left(\frac{l_{ij'}}{l_{ij}}\right) \quad ...(3.10)$$

with

i, j = represents conductors or fibres found within the system

h = conductor or fibre height

r = conductor or fibre radius

$l_{ij'}$ = direct distance from conductor i to the image of conductor j across the ground plane

l_{ij} = direct distance from conductor i to conductor j

Upon the determination of the three phase to fibre optic cable capacitances (assuming a three phase system) using the method specified above, a Thevenin equivalent capacitance is used to replace these three capacitances at each node. This is given by

$$C_{th\,N} = C_{01\,N} + C_{02\,N} + C_{03\,N} \quad ... \ (3.11)$$

The three phase voltage are also replaced by their Thevenin equivalent by

$$Vth_N = V * \frac{C_{01\,N} + a^2 C_{02\,N} + a C_{03\,N}}{C_{01\,N} + C_{02\,N} + C_{03\,N}} \quad ... \ (3.12)$$

3.3.3 Node equations

The diagram below is a representation of the span divided into 3 sections. The first and last sections are grounded to represent the armour rod assembly at the tower.

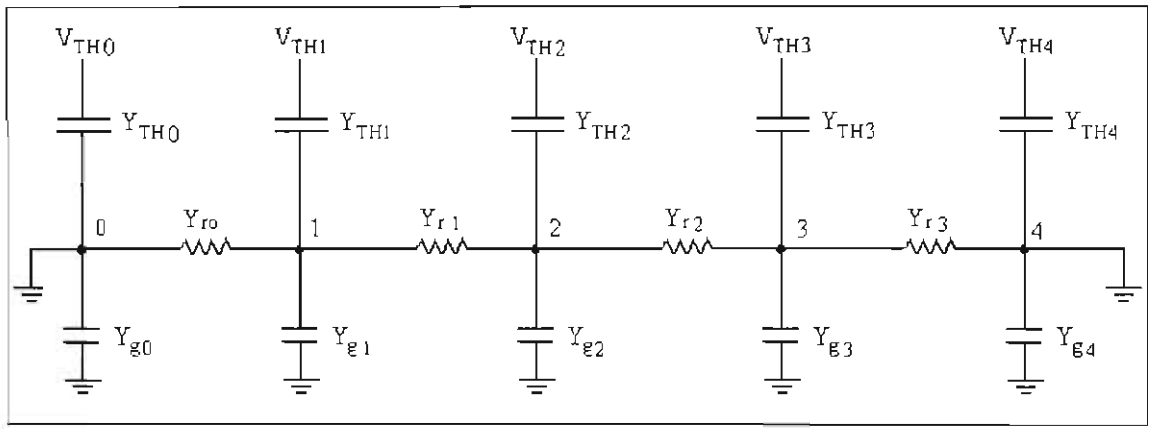

Figure 3.3: Circuit representing span divided into 3 sections [$N_{sec} = 3$]

Node equations may now be written for each node in the circuit using Kirchoff's current law (KCL). At node 1,

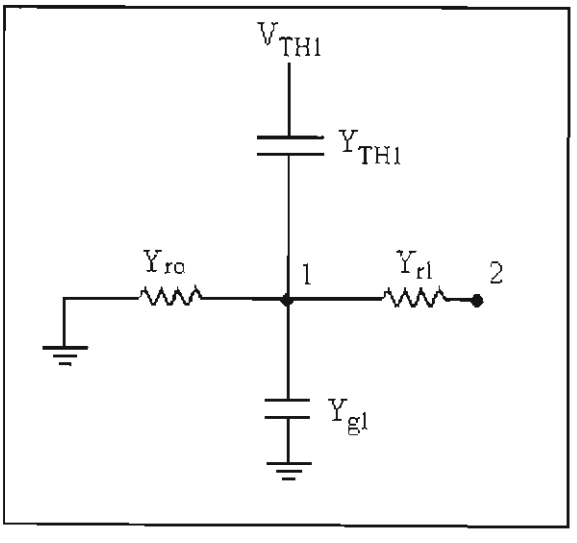

Figure 3.4: Node 1 of Figure 3.3

$$(V_{TH1} - V_1)\, Y_{TH1} = V_1 Y_{r0} + V_1 Y_{g1} + (V_1 - V_2)\, Y_{r1}$$

$$V_{TH1}\, Y_{TH1} = V_1 (Y_{ro} + Y_{r1} + Y_{TH1} + Y_{g1}) - V_2 Y_{r1}$$

$$= V_1 Y_{R0} + V_1 Y_{R1} + V_1 Y_{TH1} + V_1 Y_{g1} - V_2 Y_{r1}$$

$$\Rightarrow \mathbf{I_{TH1}} = \mathbf{V_1 Y_{n1} - V_2 Y_{r1}} \quad \ldots (3.13)$$

where

$$Y_{nN} = Y_{r\,N-1} + Y_{rN} + Y_{THN} + Y_{gN}$$
$$1 \le N \le N_{scc}$$

Similarly at Node 2,

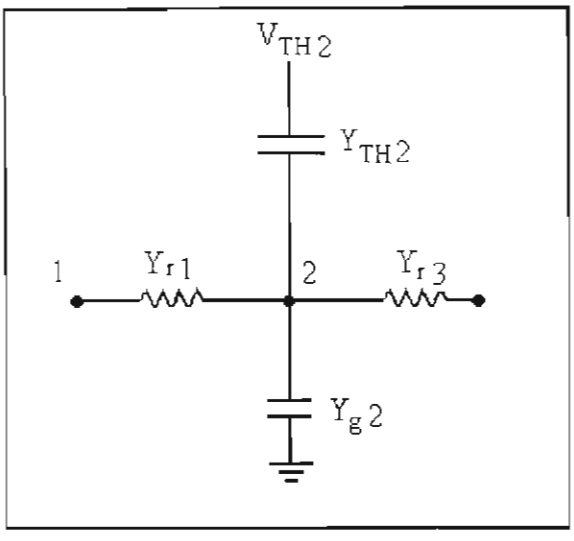

Fig. 3.5: Node 2 of Figure 3.3

$$(V_{TH2} - V_2)\,Y_{TH2} = (V_2 - V1)\,Y_{r1} + V_2 Y_{g2} + (V_2 - V_3)\,Y_{r2}$$

$$V_{TH2}\,Y_{TH2} = V_2\,(Y_{r1} + Y_{r2} + Y_{TH2} + Y_{g2}) - V_1 Y_{r1} - V_3 Y_{r2}$$

$$\Rightarrow \mathbf{I_{TH2}} = \mathbf{V_2 Y_{n2} - V_1 Y_{r1} - V_3 Y_{r2}} \quad \ldots \quad (3.14)$$

All the nodes in the circuit may be solved in similar fashion. Using a method of forward elimination to eliminate V_1 from equations (3.13) and (3.14), one obtains

$$V_2 Y_{new(2)} - V_3 Y_{r2} = I_{new(2)} \ldots (3.15)$$

where

$$Y_{new(N)} = \begin{cases} Y_{n(1)} & N = 1 \\ Y_{n(N)} - \dfrac{Y_{r^2(N-1)}}{Y_{new(N-1)}} & 2 \le N \le N_{scc} \end{cases} \quad \ldots \quad (3.16)$$

and

$$I_{new(N)} = \begin{cases} I_{TH(1)} & N = 1 \\ I_{TH(N)} + \dfrac{I_{new(N-1)} Y_{r(N-1)}}{Y_{new(N-1)}} & 2 \le N \le N_{scc} \end{cases} \quad \ldots \quad (3.17)$$

Now using the backward substitution of node voltages, all the node voltages may be calculated since it is known that the voltage on either tower is 0 Volts. These nodal voltages are given by

$$V_{(N)} = \frac{I_{new(N)} + Y_{r(N)} V_{(N+1)}}{Y_{new(N)}}, \qquad (N_{sec} - 1) \geq N \geq 1 \quad \text{... (3.18)}$$

The current induced in the wetted pollution layer may now simply be determined by

$$I_{(N)} = \left(V_{(N+1)} - V_{(N)}\right) Y_{r(N)}, \qquad (N_{sec} - 1) \geq N \geq 1 \text{...(3.19)}$$

MATLAB®, a mathematical software program, was used to implement the algorithm presented above. The results of this simulation will be presented in the next chapter.

3.3 Algorithm development for the single-phase system

An experiment was designed to validate the proposed algorithm above, but due to both economic and physical constraints, a single-phase system was employed for the experiment. This, however, involved a modification to the model presented above. This modified model represents a polluted fibre optic cable in a single-phase high voltage environment.

The only difference between this model and the three-phase model is in terms of the three phase to fibre optic cable capacitances. The three phases (represented by numbers 1, 2, and 3 in Figure 3.1) is replaced in this model by a single phase, represented by "1" in Figure 3.6. The Thevenin voltage used in the model now represents the single-phase system voltage and the equivalent Thevenin capacitance is now simply given as

$$C_{th\,N} = C_{01\,N} \text{...(3.20)}$$

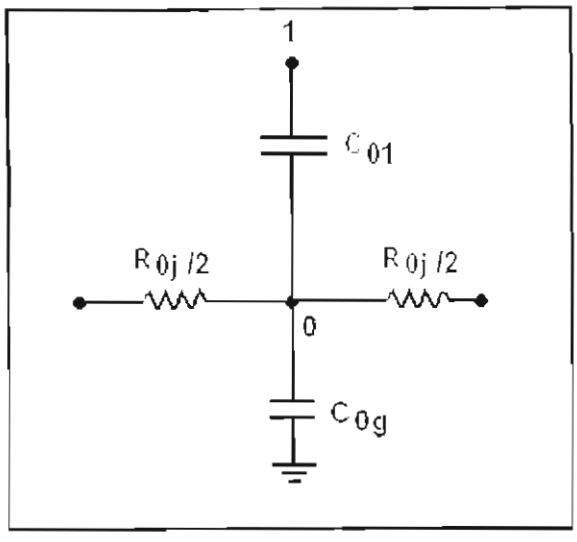

Figure 3.6: Equivalent circuit representing a polluted fibre optic cable in a single-phase, high voltage environment

The phase to fibre optic cable capacitance for the single-phase model was also calculated using the method of Maxwell's potential coefficients as described earlier for the three-phase model. However, finite element techniques were also employed to determine these capacitances for the single-phase model. The system was modelled on a finite element package called FEMLAB®. These results would be discussed in later chapters relating to both the single-phase simulation results and experimental work. It is there that, the relative accuracy of both capacitance calculating techniques would be assessed.

This chapter highlighted the development of both the mathematical and electrical model used to represent dry band arcing on ADSS fibre optic cables. It began with a description of the model postulated by Carter and Waldron [1992] that could be solved analytically to yield the magnitude of the leakage current on the cable jacket. This model was then improved upon by [Karady et al, 2001a]. One of the ways in which they improved the model was that they took the effect of differing cable and conductor sags into account. This algorithm was then modified to represent a polluted fibre optic cable in a single phase high voltage environment, which enabled the author to compare the results obtained using this model with those obtained experimentally.

CHAPTER FOUR

SIMULATION RESULTS

The numerical algorithm that was developed in the preceding chapter was implemented on MATLAB®, a dynamic mathematical software package. The algorithm was used to investigate the effects of pollution, increased system voltage, span length, sag and uneven pollution deposition on the induced leakage currents that flow on the outer sheath of the fibre optic cable.

4.1 Simulation parameters

The positioning of the fibre optic cable and phase conductors on the tower for these simulations is best illustrated in Figure 4.1 below.

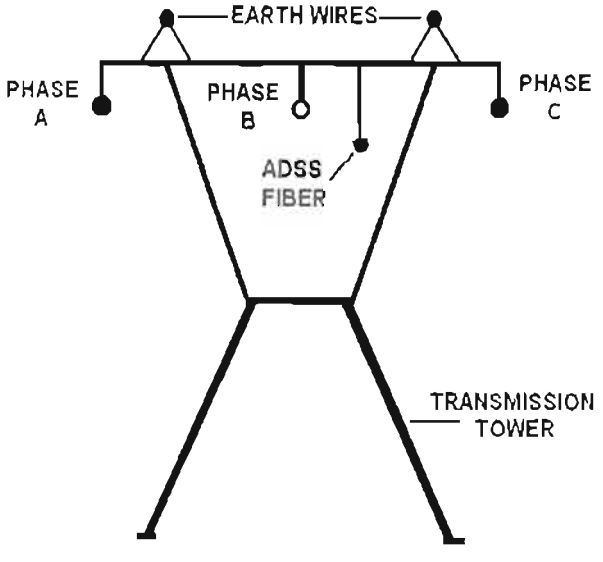

Figure 4.1: Two-dimensional diagram of tower, highlighting position of ADSS fibre

Figure 4.1 is only one example of the many tower configurations found throughout the country. In fact, a lot of towers in the field today, are known to carry two circuits, one on either side of the supports. All of these towers may be analysed using this algorithm. Two tower geometries were investigated in this study and they corresponded to two different system voltages, namely the 132kV and 275 kV system voltages.

Table 4.1 illustrates the geometry of the fibre optic cable and phase conductors on the tower window. These dimensions are with respect to a reference point located on the ground, at the centre of the tower.

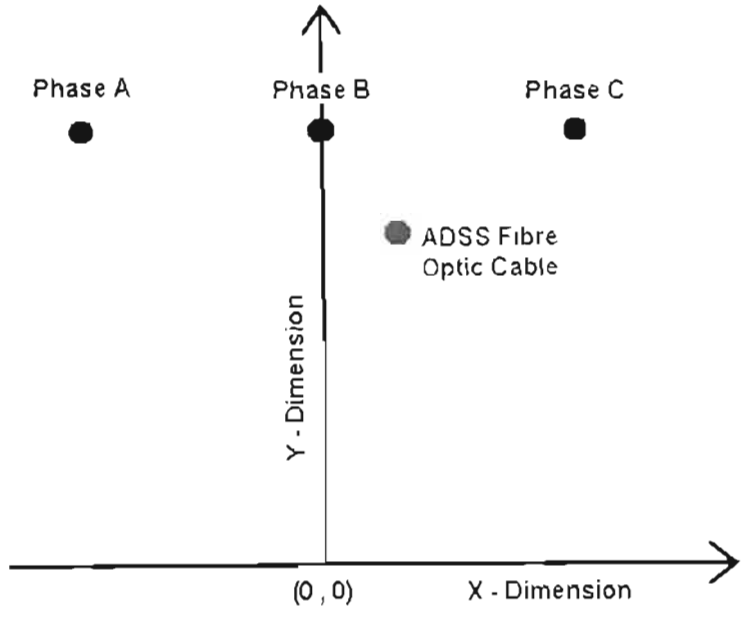

Figure 4.2: Geometry of tower configuration with chosen reference point

Tower	Fibre		Phase A		Phase B		Phase C	
	X (m)	Y (m)	X (m)	Y (m)	X (m)	Y (m)	X (m)	Y (m)
132kv	17.875	2.88	-6.72	17.875	0.00	17.875	6.72	17.875
275 kV	18.766	2.88	-8.60	18.766	0.00	18.766	8.60	18.766

Table 4.1: Spatial positions of the fibre optic cable and phase conductors on the tower window

The tower geometries given above were obtained from Eskom (Bologna, 2002) and represent tower geometries that exist in the field. ADSS fibre optic cable installations exist on the 132 kV installation as illustrated in Table 4.1 above, however no current knowledge existed of a similar installation on a 275 kV system in the South African grid. The positioning of the fibre optic cable on the 275 kV tower was chosen to be the same as found on the 132 kV tower such that the effect of system voltage on

leakage current could be adequately determined. It was also known that this position did not represent the ideal attachment position on the 275 kV tower. A suitable attachment position for the 275 kV tower window was determined using the numerical algorithm described in the preceding chapter. This result is discussed later in this chapter.

In most investigations, a test span of 300m was assumed for both system voltages. This span was generally divided into 600 sections when performing the numerical algorithm. Increasing the number of nodes along the span was found to increase the accuracy of the simulation but any further increase in the number of nodes was found to not change the result beyond any acceptable level. Both systems were simulated at U_{MAX}.

4.2 Effects of pollution on leakage current

In the equivalent model of the polluted fibre optic cable in a high voltage environment, the pollution layer is represented as a resistance (Figure 3.1). This resistance is only applicable after the thin conductive pollution layer has been lightly wetted by light rain, fog or drizzle. As described earlier, pollution severity is difficult to categorize in absolute terms, as it is highly dependent on both the type of pollutant and the amount of moisture present. Three pollution levels that represent varying levels of conductivity have been considered and investigated in this study as defined by Karady and Devarajan [2001]. These are

10^5 Ω/m	-	Heavy pollution
10^6 Ω/m	-	Medium pollution
10^7 Ω/m	-	Light pollution

The 132 kV system was investigated first and as observed in Figure 4.3 below, the voltage distribution was found to be symmetrical with respect to the centre of the span.

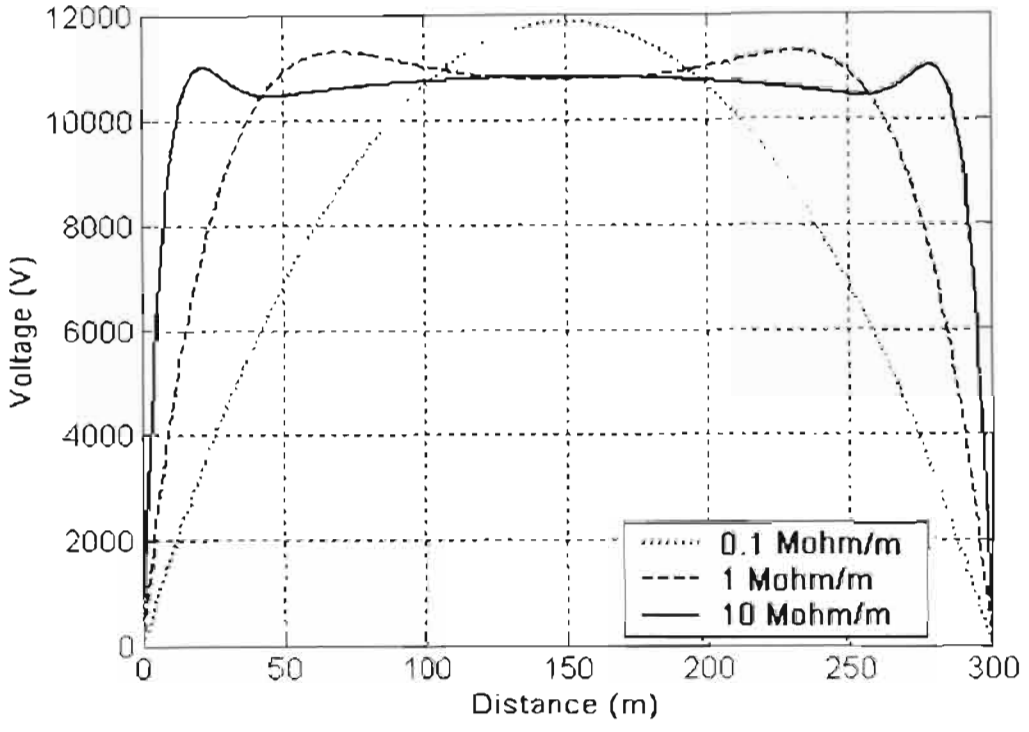

Figure 4.3: The effect of pollution on voltage distribution – 132 kV installation

These results correlate well with those obtained by Karady and Devarajan [2001a]. The calculated space potential for this system ranges from 9.45 kV at mid-span to 10.15 kV at the tower. It is determined by evaluating the Thevenin open circuit voltage of the system. The space potential is exceeded at mid-span for all levels of pollution as illustrated by Figure 4.3. For the light pollution condition, the space potential is reached at less than 20 meters from the tower. Incidentally, Karady et al [2001a] report that at low pollution conditions cable deterioration is most likely caused by corona rather than by dry band arcing.

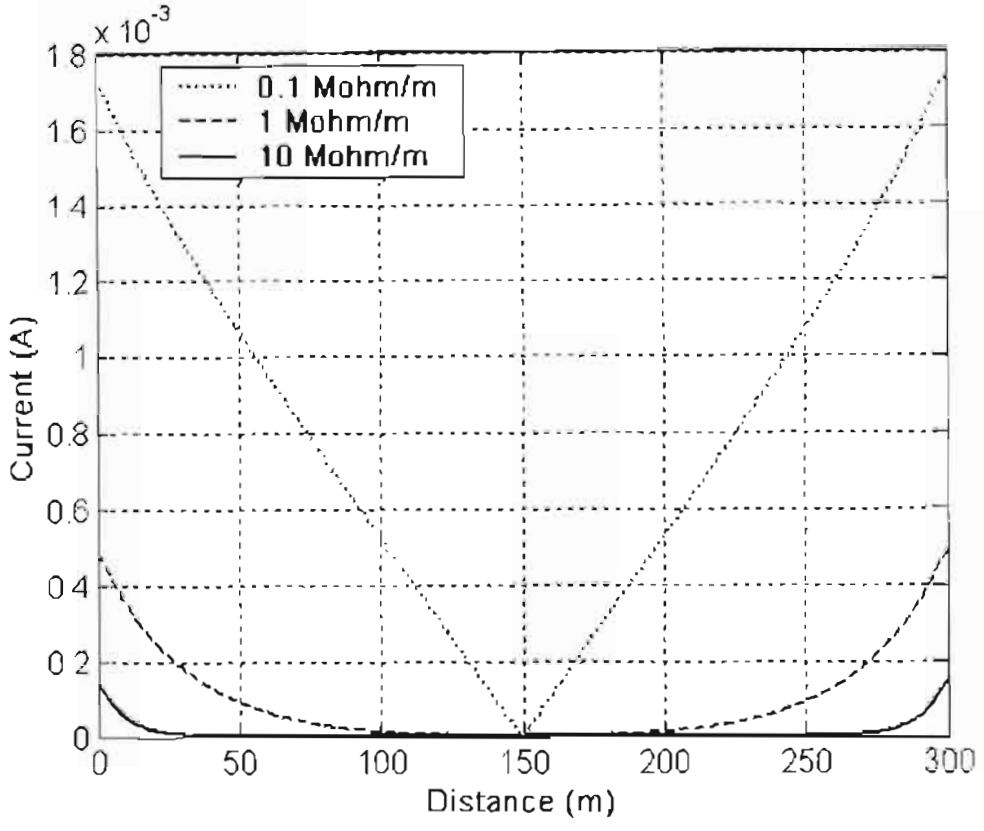

Figure 4.4: The effect of pollution on current distribution – 132 kV installation

The effect of pollution on the leakage currents induced is illustrated above in Figure 4.4. The current distribution is also symmetric to the centre of the span where the current reduces to zero. The peak current magnitude is observed to occur at the towers and this concurs with field experience as the majority of dry band arcing is reported to occur close to the grounded armour rod assemblies at the towers, [Brewer et al, 1992], [Rowland, 1992]. The peak current at the tower for a heavily polluted cable, found in the 132 kV system, is approximately 1.7 mA. This indicates a high probability of dry band activity as it has been reported that currents greater than 1 mA have a higher probability of causing dry band arcing, [Karady, Devarajan, Tuominen, 1999b]. Figure 4.5 shows the current distribution for pollution severities that will be re-visited in Chapter 7. These pollution severities correspond to those used when performing the experimental investigation. One should bear in mind, however, that this simulation was performed for a three phase system whereas the experimental arrangement is single phase.

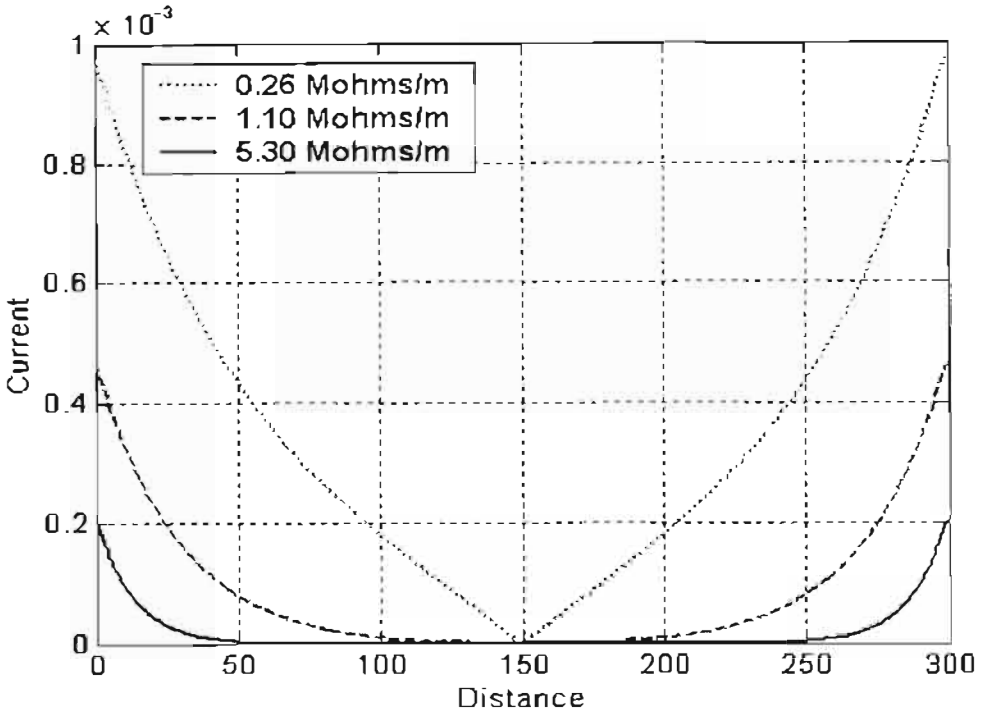

Figure 4.5: The effect of pollution on current distribution – 132 kV installation (using pollution values that were used in the experimental investigation)

Figure 4.6 shows the longitudinal field distribution along the fibre optic cable. Since this too is symmetric to the centre of the span, only half the span length is shown.

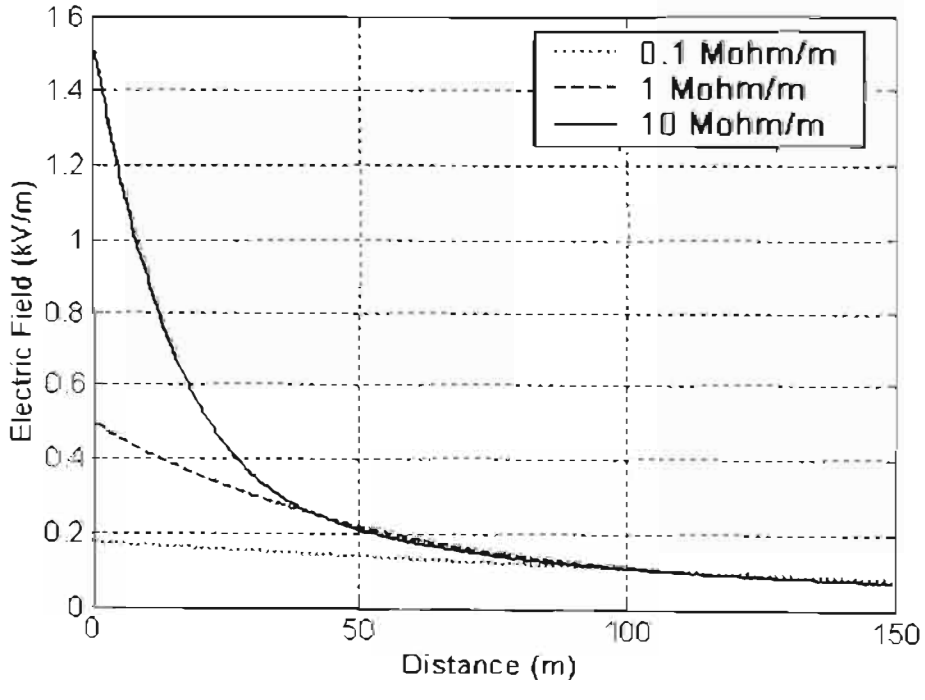

Figure 4.6: Longitudinal field distribution along ADSS fibre optic cable

The longitudinal electric field is observed to decrease exponentially from the towers. The maximum induced electric field occurs at the earthed suspension point on the tower, as the space potential is known to decrease rapidly when in close proximity to these fittings. It is this rate of decrease, in terms of kV per mm of air, which can cause the air around the fitting to break down. However, figure 4.6 clearly suggests that the longitudinal electric field found on the ADSS fibre optic cable is not high enough to initiate a corona discharge on its own.

The electric field is highest when the pollution layer on the cable is low. Corona inception may be intensified by the sharp edges of the armour wires that tend to concentrate the electric force field.

4.3 Effects of system voltage on leakage current

The effects of system voltage on the induced leakage currents were investigated by simulating the 275 kV tower arrangement with varying pollution levels. These results were then compared to those obtained from the 132 kV installation. Larger current and voltage magnitudes were basically observed on the 275 kV line. It should also be noted that other effects such as armour rod corona need to be carefully considered when considering ADSS fibre optic cable installation at a higher system voltage. Figure 4.7 below illustrates the effect of pollution severity on the current distribution of the 275 kV system.

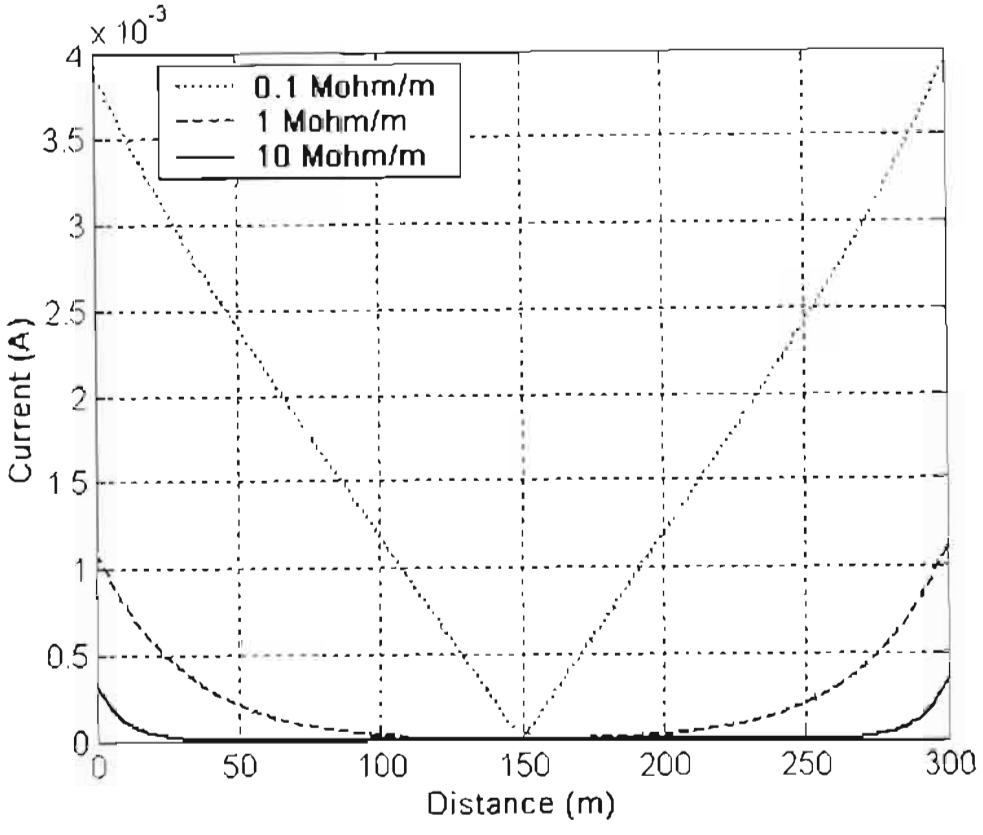

Figure 4.7: The effect of pollution on current distribution – 275 kV installation (fibre positioned as for 132kV geometry)

The result above suggests that the installation of ADSS fibre optic cable on a 275 kV line requires important consideration, especially with regards to the correct positioning of the fibre on the tower. For the above geometry, the critical current of 1mA is exceeded even at medium pollution conditions. Note that the position of the fibre optic cable in the above geometry was chosen to be laterally the same as that of the 132 kV installation, and did not necessarily represent the best placement position for the fibre optic cable on the 275 kV tower window. The algorithm may be utilized to determine a better position for the fibre optic cable installation on the 275 kV tower window. Varying the spatial position of the fibre optic cable around the tower window, and selecting the position that yielded the smallest relative current magnitude achieved this. The ranges of positions considered in this investigation are limited by both the tower geometry and the minimum ground clearance allowed. This resulted in a spatial position of (X, Y) = (-3, 14) as defined in Table 4.1 above. The current distribution for this given geometry is shown below in Figure 4.8.

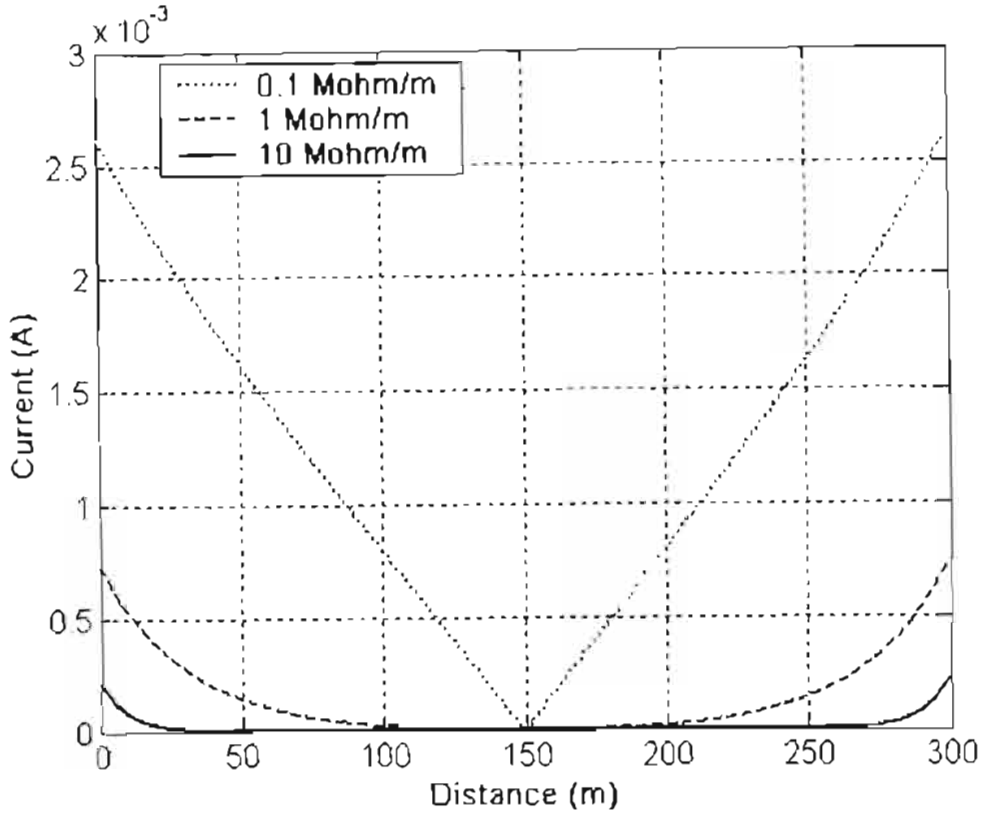

Figure 4.8: The effect of pollution on current distribution –275 kV installation - (fibre optimally positioned as determined by algorithm)

As expected the currents induced for this fibre optic cable location is much smaller than those simulated earlier in Figure 4.7. The current magnitude for the medium pollution condition is observed to have been reduced by approximately 31 percent. This result highlights the importance of correct positioning of the fibre optic cable on the tower window.

4.4 Effect of height above ground on leakage current

An initial investigation into the effect of height above ground level on leakage current induced, involved varying the height of the entire configuration, above and below their normal position on the tower window. This meant varying the heights of both the phase conductors and fibre optic cable in relation to the ground. It was correspondingly found that the differences in leakage currents during this investigation were negligible at both system voltages. This result suggests that the height of the entire configuration above ground level is of little consequence to the leakage currents formed on the ADSS cable. This implies that the fibre optic cable to

ground capacitance is not dominant in the determination of the leakage currents induced.

It was then decided to vary only the position of the fibre optic cable in the tower window with respect to its normal position. A significant change in leakage currents was now observed as the position of the fibre optic cable was varied from 1m below its normal position to 1m above. The results for both system voltages are displayed in Table 4.2 below.

Cable position	Leakage current (mA)	
	132 kV	275 kV
1m lower	0.76	1.50
Normal height	0.91	1.78
1m higher	1.05	2.10

Table 4.2: Peak current magnitudes simulated at varying cable heights

This investigation assumed a pollution resistance value of 0.3 MΩ/m. This value was chosen to highlight the importance of proper placement of the fibre optic cable on the tower. It was discussed earlier that some authors consider a current of 1 mA to be a critical current for tracking or erosion, dependant on the track resistance of the sheath material [Wetzer, 1998], [Karady, Devarajan, Tuominen, 1999]. As illustrated in Table 4.2, the current magnitude at this pollution level is exceeded on the 132 kV system when the fibre optic cable is moved 1metre higher with respect to its normal position.

4.5 Effect of Span Length on Leakage Current

The distances between high voltage transmission towers in the field are rarely equidistant apart. Their positioning is largely dependant on their geographical location and the terrain and vegetation found therein. It was therefore decided to investigate the effect, if any, of span length on the leakage currents induced. Figure 4.8 below depicts the result of this investigation, for both system voltages.

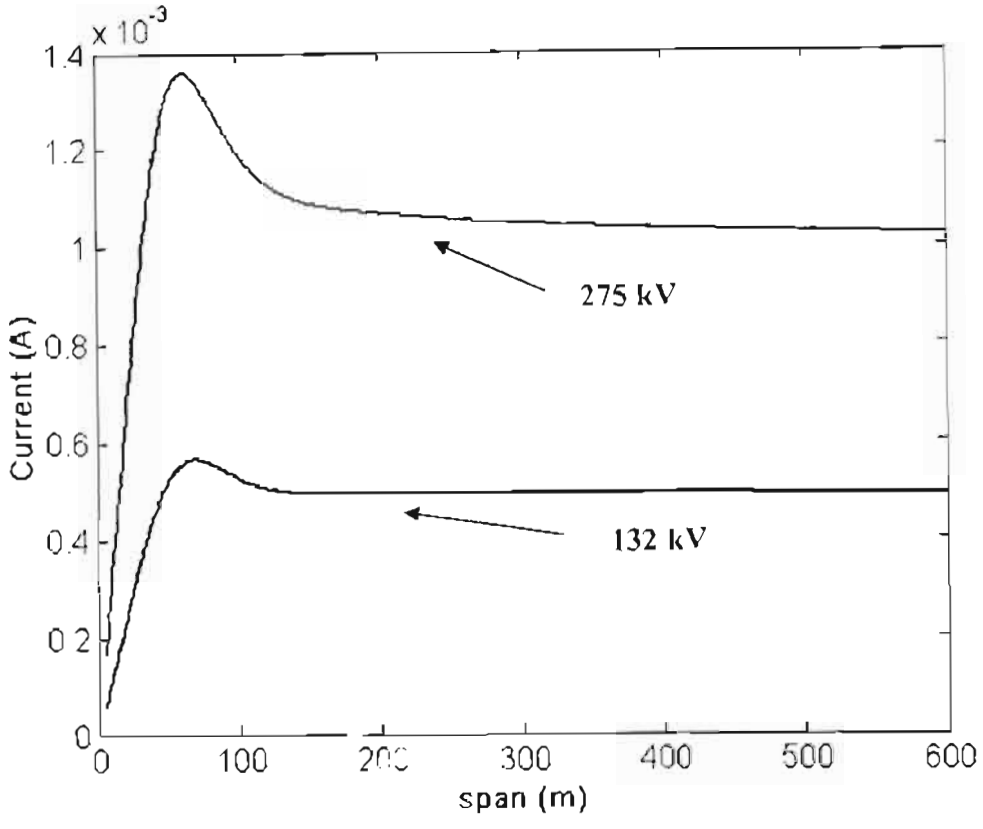

Figure 4.9: The effect of varying span length on leakage current for the 132kV and 275kV geometries

The currents displayed in Figure 4.9 correspond to the maximum induced current for the corresponding span length. As discussed earlier, these currents are found adjacent to the armour rod assembly on the tower. This result reveals that leakage current increases with span length until a critical span length, after which the current is roughly maintained for any further increase in span length. It was discovered that, at medium pollution, the critical span length for the 132 kV system was at 67 m, while the critical span length of the 275 kV system existed at 61 m.

It is common practice for power utilities to erect test spans to evaluate the feasibility of using ADSS fiber optic cables on their transmission lines. The result of this investigation suggests that these "test spans" should be of a similar length to those used in the field. At the very least, they should be of a similar length to a corresponding critical span length determined using predicted pollution levels. It was

found that the critical span length for the different system voltages increases with increasing pollution severity.

4.6 Effect of sag on leakage current

One of the most significant improvements of the currently employed algorithm over that which was postulated by Carter and Waldron (Carter and Waldron, 1992) is that this algorithm can take into account the effect of sag. In earlier models, the overhead conductors and the fiber optic cable were assumed to have the same sag, i.e. they were assumed to be in parallel. However, field research (Karady and Devarajan, 2001) suggests that the sag of the line conductors is typically greater than the sag of the ADSS fiber optic cable. The two factors that contribute to the differences in sag between the conductors and the ADSS are the differences in relative masses per unit length and the differences in the linear thermal coefficient of expansion of each.

It was decided to investigate the effect of sag on leakage currents induced using realistic sag parameters. In this investigation, the phase conductors were assumed to be suspended with a 2% sag whereas the sag of the ADSS fibre optic cable was 0.2%. The ADSS fibre optic cable is typically asymmetrically placed with respect to the three phase conductors on the tower window. Due to this asymmetrical placement, it was also decided to investigate the effect of phase sequence on the leakage current induced. The results of this investigation at medium pollution are displayed in Figure 4.10. This result was obtained on a 275 kV system and a span of 300 m was assumed.

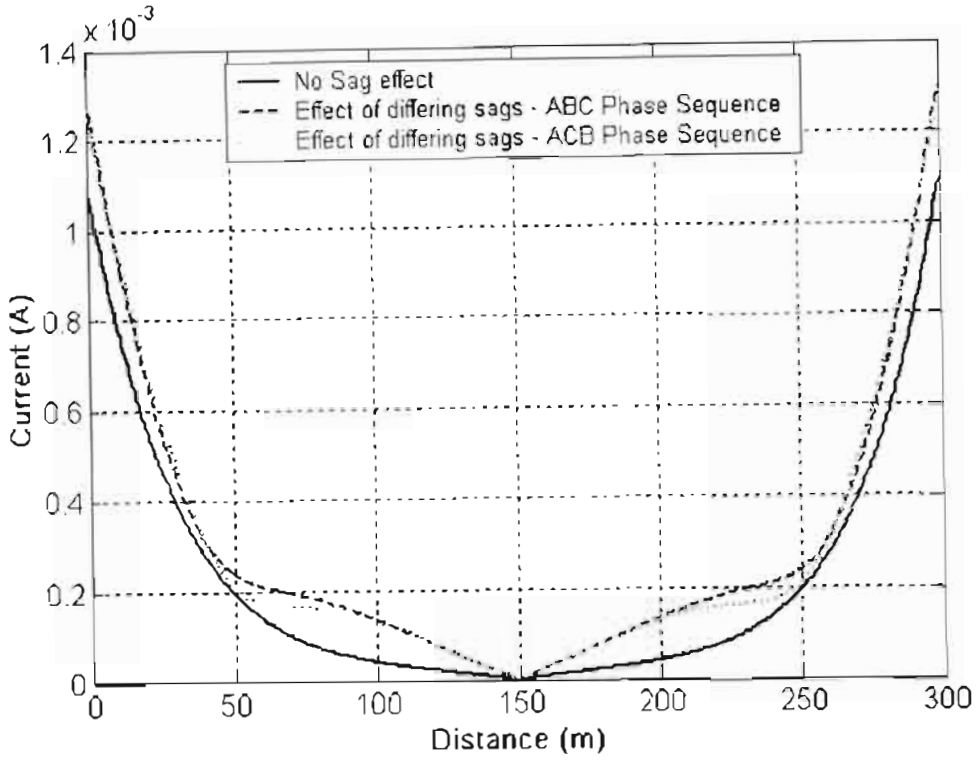

Figure 4.10: Effect of sag and phase sequence on current distribution

The result shows an increase in current induced along the entire span when the effect of sag is taken into account. This is, as expected for this tower configuration since the smaller sag of the fibre optic cable moves it effectively closer to the phase conductors. Changing the phase sequence of the transmission line was shown to not have a significant effect on the maximum current induced at the towers for this configuration but the current distribution did vary slightly. Phase sequence would obviously play a more significant role in double circuit transmission lines, which are common throughout the South African power grid.

4.7 The effect of uneven pollution deposition

In all prior investigations, it was assumed that the pollution level existed uniformly along the entire length of the fibre optic cable. It is rather unrealistic to assume that a constant pollution layer exists along the entire length of the cable, as pollution, whether windborne coastal pollution or industrial soot, is known to not settle uniformly. An investigation was thus carried out to observe the effect of uneven pollution deposition on the cable.

Two aspects of this phenomenon were investigated in this study. In the first instance, it was assumed that the entire fibre optic cable is lightly polluted, except the ends, which was assumed to be heavily polluted. This pollution profile could exist in grasslands where the ambient pollution conditions are not as harsh as those found along the coastline or in large industrial centres. Bird droppings could account for the high pollution layer formed near the tower. The current distribution for this pollution profile is compared to the current distribution for the uniform light pollution condition at 132 kV in the plot below. By increasing the pollution severity at the towers it is observed that the current magnitude at the tower is more than doubled.

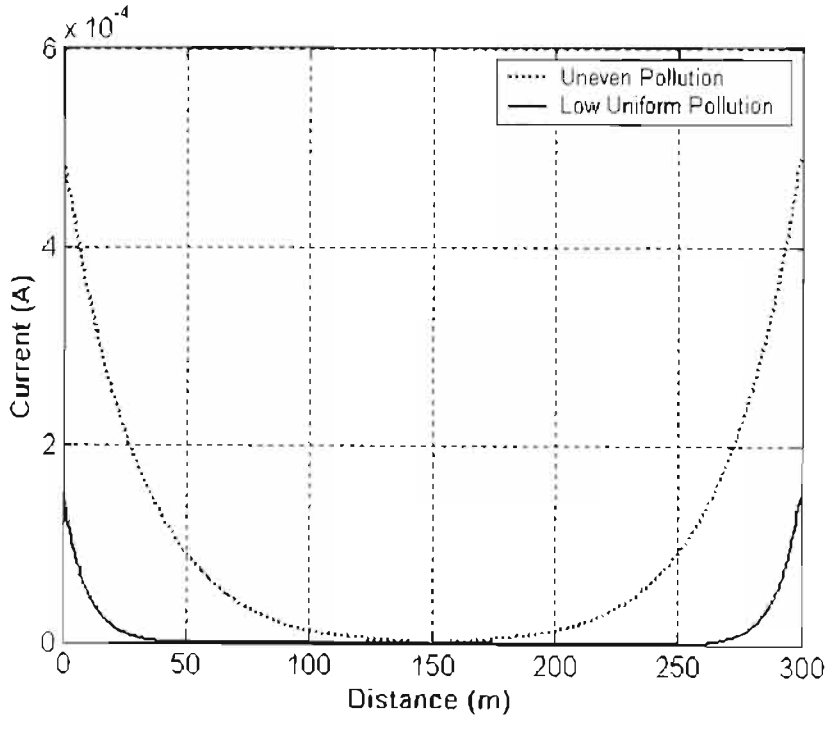

Figure 4.11: Current distribution illustrating the effect of heavy pollution close to the towers

The reciprocal pollution profile was then investigated. The entire cable was assumed to be heavily polluted, with the exception of either end, which was lightly polluted. This pollution profile may exist if cable washing at the towers was employed in a coastal or industrial region. This investigation was also conducted over a span of 300m at 132 kV. In this investigation, the current distribution for this pollution profile is compared to the current distribution for the high uniform pollution condition. Figure 4.12 illustrates the outcome of this investigation.

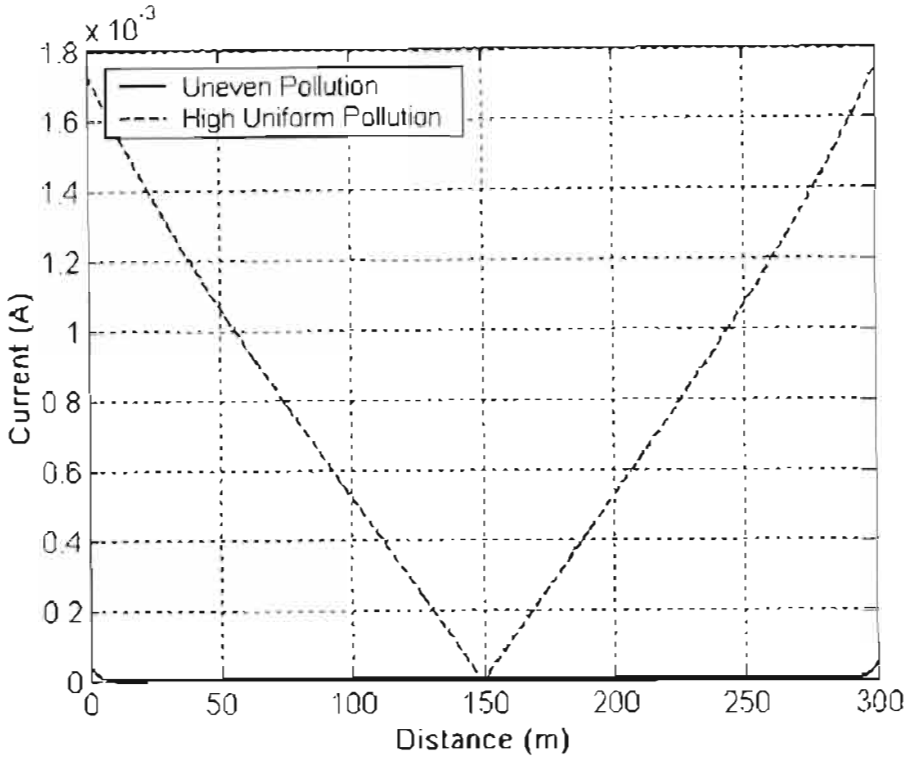

Figure 4.12: Current distribution illustrating the effect of light pollution close to the towers

The above result clearly indicates that it is the pollution severity closest to the tower that is most significant with regards to the leakage currents induced. This result could prove to have significant economic ramifications as it could considerably reduce the cost of possible fibre optic cable maintenance. Heavy pollution environments could require regular cable washing and this result suggests that only the first couple of metres of cable adjacent to the tower require cleaning. This would effectively lower both the cost and time taken for this maintenance procedure.

This chapter focuses on the results obtained using the algorithm developed in the preceding chapter. It began by outlining the simulation parameters and went on to observe the effect of pollution, system voltage, height above ground and span on the leakage current induced on the outer sheath of the fibre optic cable. It also illustrated the effect of uneven pollution deposition and sag of the ADSS cable on leakage current magnitudes.

CHAPTER FIVE

ATP SIMULATIONS

ATP (Alternative Transients Program) is the academic version of EMTP (Electro-magnetic transients program), which is used worldwide for the digital simulation of electromagnetic transients in power systems. Although it has extensive modelling capabilities, this program consists of many non-simulation supporting routines. An example of this is the "Line Constants Program", which is used to determine the line parameters of an overhead transmission line. The term "line parameters" is favourcd in industry today (as opposed to Line Constants) as they are functions of frequency and would thus vary with the synchronous frequency of the transmission network. One of the greatest advantages of the ATP program is that it avoids truncation errors that may accumulate from step to step and hence cause divergence from the true solution.

A 132 kV 3-phase transmission system was modelled in ATP, where the installed ADSS fibre optic cable was modelled as a "fourth phase conductor". This chapter will firstly review some of the ATP background theory, including theory regarding the "Line Constants Program", and then go through the development of the model used in this simulation. The simulation results are then presented.

5.1 ATP Theory

5.1.1 Solution method used by ATP

ATP may be used to solve any electrical network, comprised of resistances, inductances, capacitances, switches and most other electrical hardware. To facilitate understanding in the theory of the solution method used by ATP to solve an electrical network, a single-phase network will be considered. Figure 5.1.1 shows possible electrical connections to an assumed node connected to a much larger network.

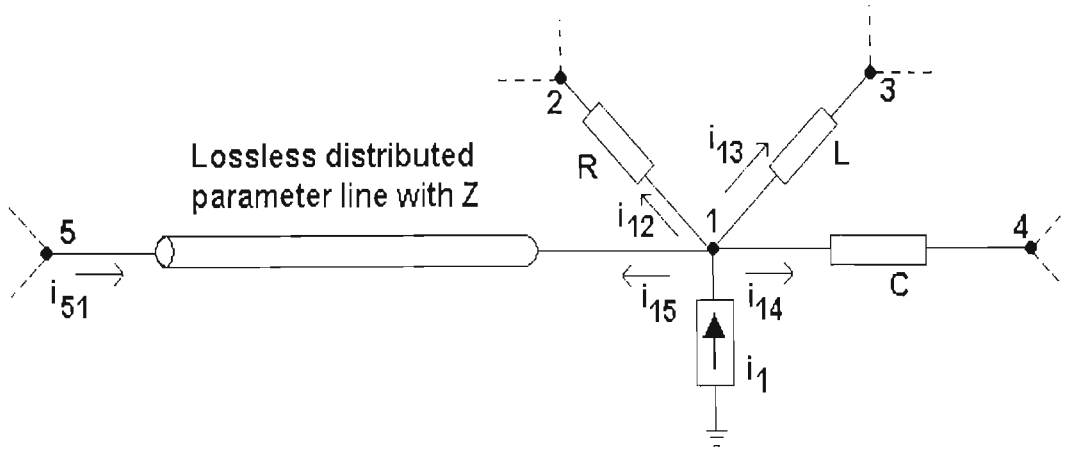

Figure 5.1.1: Diagram illustrating node 1 and connected network [Meyer, Liu, 1995]

Node voltages are used as state variables in the AC steady state solution of ATP. By Kirchoff's current law around node 1, it can easily be shown that,

$$I_{12} + I_{13} + I_{14} + I_{15} = I_1 ...(5.1)$$

In the equation above, I represents a complex phasor quantity. The branch equations are given below for resistance (equation 5.2), inductance (equation 5.3) and capacitance (equation 5.4).

$$I_{12} = \frac{1}{R}(V_1 - V_2) ...(5.2)$$

$$I_{13} = \frac{1}{j\omega L}(V_1 - V_3) ...(5.3)$$

$$I_{14} = j\omega C(V_1 - V_4) ...(5.4)$$

The exact steady state parameters for a line with distributed parameters is;

$$\begin{bmatrix} I_{15} \\ I_{51} \end{bmatrix} = \begin{bmatrix} Y_{series} + \frac{1}{2}Y_{shunt} & -Y_{series} \\ -Y_{series} & Y_{series} + \frac{1}{2}Y_{shunt} \end{bmatrix} \begin{bmatrix} V_1 \\ V_5 \end{bmatrix} ...(5.5)$$

where;

$$Y_{series} = 1/Z_{series}, \text{ with}$$
$$Z_{series} = l(R + j\omega L)\sinh(\gamma l)/\gamma l \quad \ldots(5.6)$$

$$\frac{1}{2}Y_{shunt} = \frac{l}{2}(G + j\omega C)\frac{\tanh(\frac{\gamma l}{2})}{\frac{\gamma l}{2}} \quad \ldots(5.7)$$

$$\gamma = \sqrt{(R + j\omega L)(G + j\omega C)} \quad \ldots(5.8)$$

γ represents the propagation constant in the above equations. If the line is assumed to be lossless and the value of ωl is small then the total current for node 1 is given by;

$$\left(\frac{1}{R} + \frac{1}{j\omega L} + j\omega C + Y_{series} + \frac{1}{2}Y_{shunt}\right)V_1 - \frac{1}{R}V_2 - \frac{1}{j\omega L}V_3 - j\omega C V_4 - Y_{series}V_5 = I_1 \ldots(5.9)$$

Using basic circuit theory it can therefore be assumed that any type of network with *n* nodes, can be represented by a system of *n* such equations;

$$[Y][V] = [I] \ldots(5.10)$$

where [Y] represents the symmetric nodal admittance matrix
[V] represents a vector of *n* node voltages, and
[I] represents a vector of *n* current sources

Equation 5.10 is further partioned into two sets of nodes; one set with known voltages and the other with unknown voltages. The unknown voltages are found by solving the resulting system of linear, algebraic equations.

5.1.2 Line constants program

This program is used to obtain the electrical parameters of an overhead transmission line. These values are required to accurately simulate the transmission network. To determine these parameters requires knowledge of the existing physical parameters. These include:

- (x, y) coordinate for each conductor and ground wire,
- Conductor phase designation (in a 3-phase system),
- Wire dimensions,
- Sag,
- Earth resistivity of the ground return path, and
- Bundle spacings (if applicable).

The voltage drop along a transmission line may be expressed in the form of partial differential equations, as shown below.

$$-\frac{\partial v}{\partial x} = Ri + L\frac{\partial i}{\partial t} \quad ...(5.11)$$

The resistance of a conductor (in ohms/km) is generally known or may be obtained from the manufacturer. The inductance of the line may be determined by theories developed by [Carson, 1926] or [Pollaczek, 1926]. These researchers derived formulae for calculating line constants on telephone circuits, but these may be used on power lines. Both the "Line Constants" and the "Cable Constants" program use Carson's formula. The equation for self impedance is given by;

$$Z_{ii} = (R_{i-\text{int}} + \Delta R_{ii}) + j\left(j\omega\frac{\mu_0}{2\Pi}\ln\frac{2h_i}{r_i} + X_{i-\text{int}} + \Delta X_{ii} \right) \quad ...(5.12)$$

and mutual impedance is;

$$Z_{ik} = Z_{ki} = \Delta R_{ik} + j\left(\omega\frac{\mu_0}{2\Pi}\ln\frac{D_{ik}}{d_{ik}} + \Delta X_{ik} \right) \quad ...(5.13)$$

where; μ_0 = permeability of free space

$R_{i\text{-}int}$ = ac resistance of conductor i in Ω/unit length,

h_i = average height above ground of conductor i,

D_{ik} = distance between conductor i and image conductor k,

D_{ik} = distance between conductors i and k,

r_i = radius of conductor i,

$X_{i\text{-}int}$ = internal reactance of conductor i,

$\omega = 2\Pi f$ with f = frequency in Hz,

$\Delta R, \Delta X$ = Carson's correction terms for earth return effects

The line constants program uses the method of Maxwell's potential coefficients to determine the capacitances of the transmission line. This method of capacitance calculation was explained previously in Section 3.3.2 of this study.

5.2 Model Description

The simulation of a transmission network using the ATP program may be broken down into the following steps;

- Construction of the overall system model,
- Obtaining the line parameters, and
- Simulation of the proposed model

5.2.1 System model

The physical parameters of the 132 kV transmission network that was simulated was identical to that simulated using MATLAB (Chapter 4). A two-dimensional diagram of the tower is shown in Figure 4.1 with the spatial positions of the conductors and fibre optic cable given in Table 4.1. The ADSS fibre optic cable was modelled as a fourth phase conductor in the ATP model. To simulate the effect of an insulated cable rather than a conductor, the DC resistance of the cable was set to 1×10^5 Ω/km and the skin ratio was set to 0.001. The skin ratio represents the ratio between the thickness of a tubular conductor to its outer diameter.

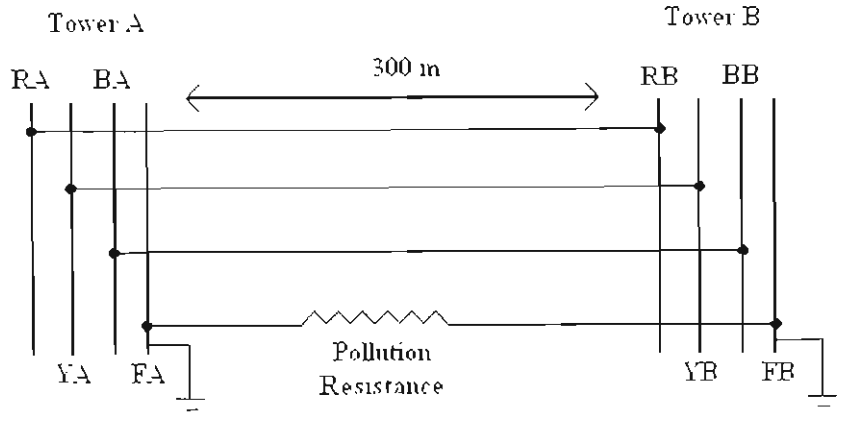

Figure 5.2.1: Schematic of ATP model

Figure 5.2.1 represents the three phases (R, Y and B) and fibre optic cable (F) attached to two towers, with a span length of 300 m between them. A resistor was used to represent the pollution on the surface of the fibre optic cable. The ADSS fibre optic cable is attached to armour rod assemblies on the transmission tower and are hence grounded. This was simulated by attaching switches to nodes FA and FB, forcing them to ground at the start of the simulation.

5.2.2 Line models and parameters

A transmission line may be modelled in different ways using the ATP program. Appropriateness of the model used is based on factors such as line length and frequency that is to be simulated. The following models are available in ATP;

- Pi model
- Constant distributed parameter model, and
- Frequency dependent models
  - Semlyn Set-up
  - J Marti Set-up, and
  - Taku Noda Set-up

The two models considered for this simulation were the Pi model and the distributed parameter model. The pi model is a discrete approximation to the constant distributed

parameter model. It is a highly reliable and accurate model for short lines with a fixed, low frequency. The constant distributed parameter model calculates the different time propagation of the decoupled mode components. In each extreme of the line, the values are converted from mode domain to phase domain using a transformation matrix. This model is also computationally efficient and has enough accuracy for general transient calculations of limited frequency range.

It has been reported [Hevia, 1999] that use of the constant distributed parameter model produces large errors for the ground mode currents. This model also requires greater calculation time for short lines as it requires that the time step be less than the propagation time. It was therefore decided to use the Pi model when simulating this network. The Pi model is represented below in Figure 5.2.2.

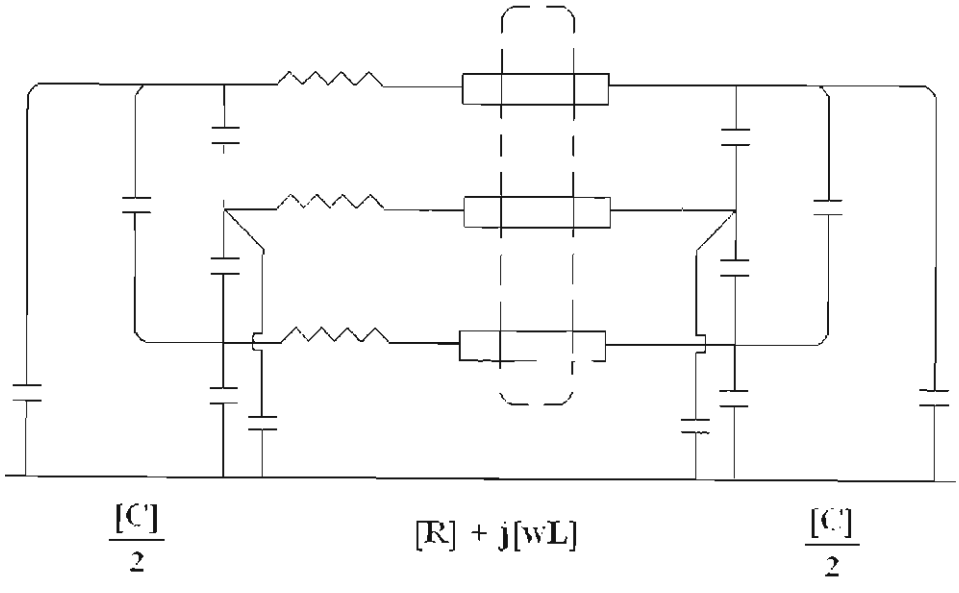

Figure 5.2.2: Diagrammatic representation of Pi model

5.3 Simulation Results

The network was first simulated at high pollution, i.e. the pollution resistance on the cable was assumed to be 1 x 10^5 Ω/m (see section 4.2). The parameters of the pi model that was used to simulate the network is determined using the "Line

Constants" program and the punch card is included in Appendix C. The output data from the line constants program was then used to simulate the developed model. This current waveform represents the leakage current that exists on the outer sheath of the ADSS fibre optic cable.

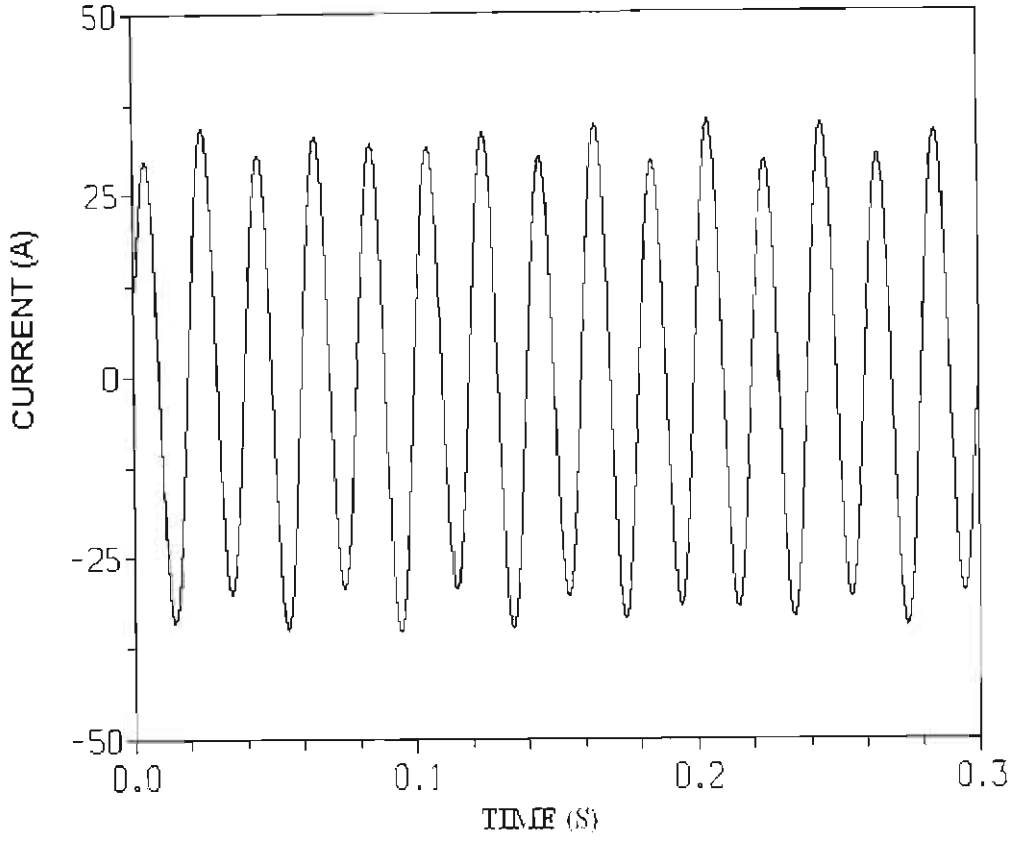

Figure 5.3.1: Leakage current waveform that exists on optical cable

It was discovered after an analysis of this current waveform, together with its corresponding voltage waveform, that the current lags the voltage by 90°. This implies that the current is largely inductive. The simulated leakage current was also very large and unrealistic.

It was believed that one of the contributing factors to this large current might be the strong effect of mutual inductance found in the ATP program. When the mutual inductance between the phase conductors and the fibre optic cable were made negligible (by altering the values of mutual inductance in the generated "pch" file), the simulation was found to yield results that were more favourable.

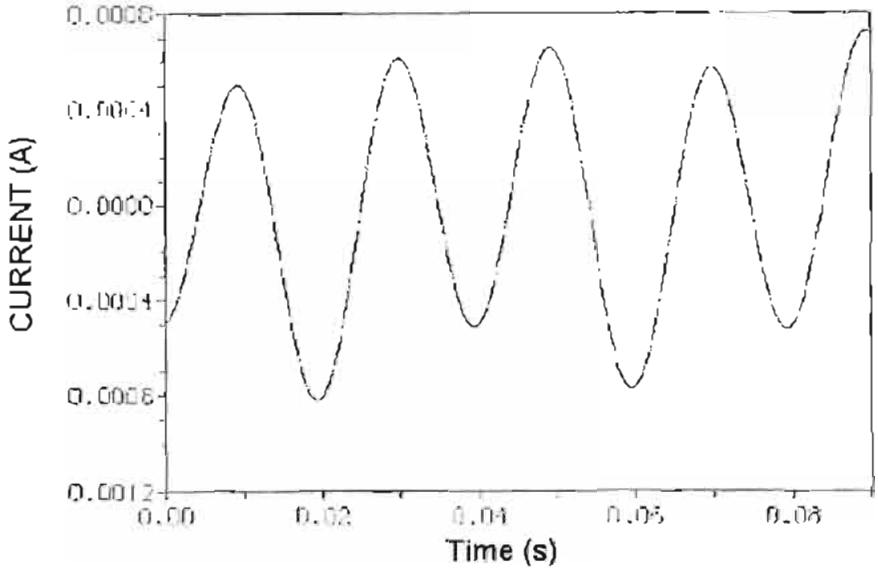

Figure 5.3.2: Leakage current waveform that exists after negating the effect of mutual inductance

This induced current was however, too small for the high pollution case. Another approach was therefore attempted. Sinusoidal voltage sources are once again applied to one end of each of the three phases but current sources are also added to each phase.

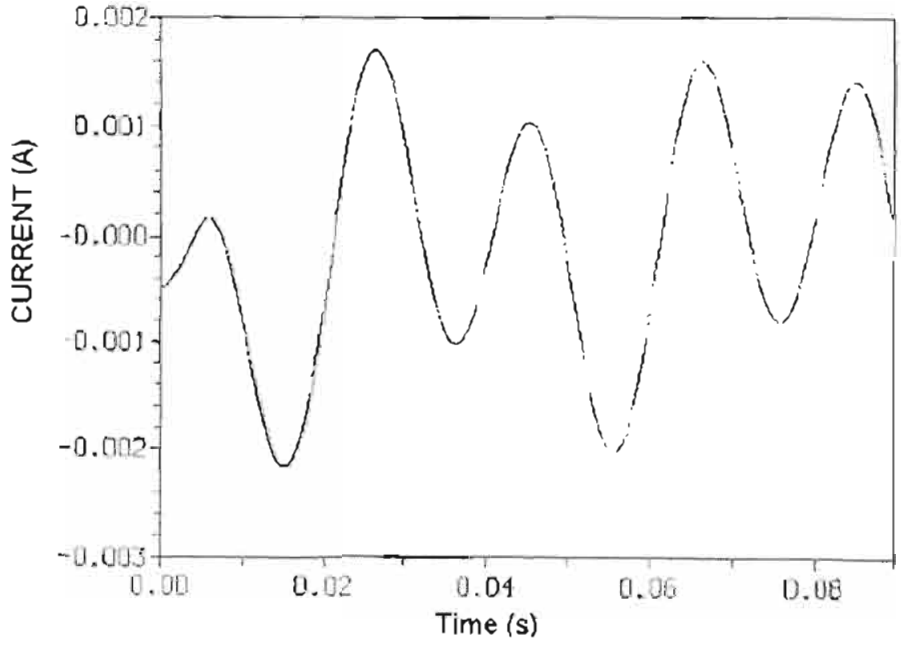

Figure 5.3.3: Leakage current waveform obtained using current source method

This current waveform does not appear purely sinusoidal, but it appears to simulate the condition well when compared to the numerical algorithm used in the previous chapter. The leakage current induced at high pollution, using the numerical algorithm, was found to be approximately 1.7 mA and this conforms well to the result obtained from ATP (peak to peak magnitude of approximately 2mA). Further comparisons between the two simulation methods employed are included in Chapter 8.

The current induced in the outer sheath of the fibre optic cable varied linearly with the pollution resistance and this was confirmed using this model. A major advantage of this new approach was that it did not require any manipulation of the pch output file. A single-phase adaptation of this model was used to predict the current induced on the fibre optic cable during laboratory experiments.

In closing, the main aspects covered in this chapter are reiterated.

- The underlying theory of ATP is discussed in;
  - the solution method used by ATP, and
  - the line constants program.
- The model that represents this network is developed and it was decided to model the transmission line using the pi-model.
- The results of the simulations are presented and it was found that the ATP simulation results conform closely to those obtained using the numerical algorithm method.

CHAPTER SIX

FEMLAB® SIMULATIONS

FEMLAB® is a newly developed software program that uses the computational power of MATLAB®, to model and solve scientific and engineering problems that are based on partial differential equations. It was used in this study to:

- Determine component parameters for laboratory work,
- Obtain the relationship between electric field strength and conductor height,
- Investigate the consequences of incorrect installation in the field,
- Investigate a possible leakage current mitigation method, and
- Calculate the mutual capacitance between the phase conductor and fibre optic cable

An overview of FEMLAB® is first given in this chapter and a detailed description of the simulations mentioned above would then be presented. It should be noted that FEMLAB® was not used to determine the magnitude of leakage currents induced on the fibre optic cable. It was used primarily as a tool to assist in the construction and design of the experimental set-up and also to qualitatively investigate certain aspects of this study.

6.1 FEMLAB® Overview

As mentioned above, FEMLAB® is a powerful modelling tool whose basic mathematical structure is a system of partial differential equations. These equations are solved using finite element modelling techniques. A useful advantage of the FEMLAB® package is its unique "multiphysics" feature that allows one to simultaneously model any combination of scientific phenomenon.

The first step in this modelling process is to create the geometry of the physical model that is to be simulated. This may be done in one of two ways, i.e. it may be drawn using the CAD tools found in FEMLAB® or imported from another CAD

package. The physical and scientific properties of all materials used in the model need to then be defined. When using the Electromagnetics module of FEMLAB®, this involves defining the electric and magnetic properties of all the materials used in the model.

A mesh is then generated so that finite element modelling techniques may be applied. Finite element modelling involves the descretization of a structure into elements or domains that are defined by nodes. These nodes describe the elements as they represent the geometric locations of the structure. Each element is approximated by:

$$\{\delta\} = [N]\{x\} \ldots (6.1)$$

Where {δ} – represents a vector of displacements within an element

[N] – represents the shape function for a selected element

{x} – represents the nodal variable

The shape function of an element can range from linear interpolation functions to higher order polynomial functions. The solution for each element becomes a function of unknown nodal values. These are solved when a general solution for all elements result in an algebraic set of simultaneous equations that are solved using a computer. The equation governing field simulation in the Electrostatics application modes (which was used in this study) is:

$$-\nabla.((\sigma + \varepsilon / T)\nabla V - (J^e + {}^{P}\!/_{T})) = {}^{\rho_0}\!/_{T} \ldots (6.2)$$

where: σ - conductivity

ε - permittivity

V – voltage

T – time constant

J^e – external current density

P – electric polarization

ρ_0 – space charge density

Another important aspect that needs to be considered in electrostatics is the continuity conditions that exist at interfaces between different media. For conducting media it is:

$$n_2.(J_1 - J_2) = 0 \ldots (6.3)$$

The boundary condition for non-conducting media is:

$$n_2.(D_1 - D_2) = \rho_s \ldots (6.4)$$

n_2 represents the outward normal from medium 2 in both equations (6.3) and (6.4). Once the problem has been solved, it may be visualised using one of the many visualisation tools that are available in FEMLAB®. These include streamlines, contours, isosurfaces, surfaces and vector field plots. Any function or parameter may also be visualised using animation. This is useful when trying to visualise a problem that is either time or frequency dependent.

6.2 Simulations and Investigations

6.2.1 Electric Field Strength vs. Insulator Length

This simulation was conducted to initially determine the length of insulator that should be used in the laboratory experiments that were conducted. In this experiment, a single-phase, high voltage supply is fed onto a conductor that is suspended between two grounded towers. The conductor is attached to the towers via a silicone rubber insulator. A suspended length of ADSS fibre optic cable is also attached to the towers. This cable is attached directly below the conductor and is grounded at the towers to simulate its installation in the field. An investigation was therefore conducted to ensure that flashover does not occur between the high voltage conductor and the grounded attachment of the fibre optic cable at the tower.

In this simulation, both the conductor and fibre optic cable are simulated as 3-dimensional, solid cylinders. For simplicity, the silicone rubber insulator was modelled as a solid cylinder with a greater radius than either cable. The effect of the insulator sheds were therefore not taken into account and provided an adequate safety factor. The physical parameters and heights used in this simulation model are illustrated in Figure 6.2.1.

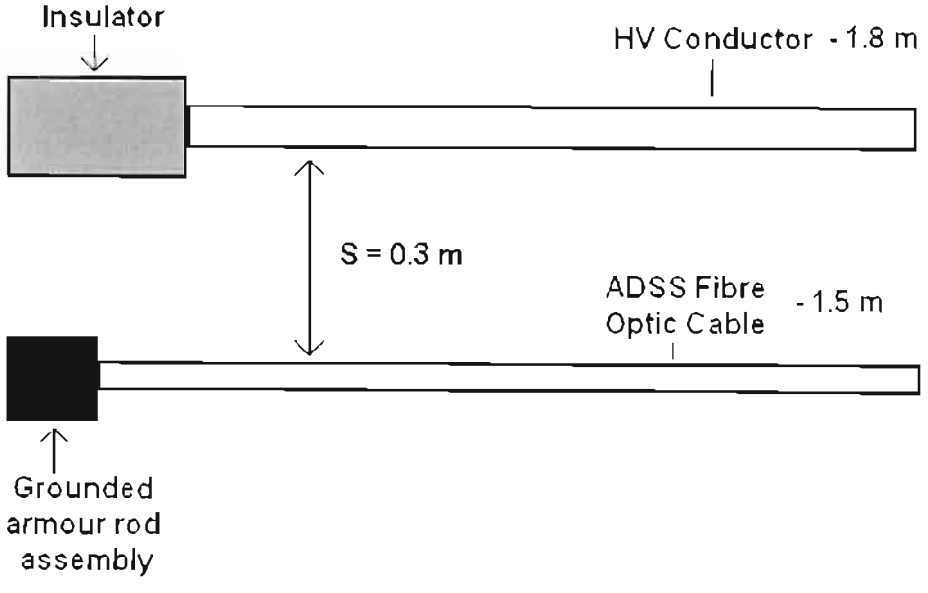

Figure 6.2.1: "Insulator length" simulation model

In this investigation, the length of the insulator was increased in increments of 5 cm (from a minimum of 0 cm to a maximum of 85 cm), and the corresponding electric field at the fibre optic cable attachment point was recorded using FEMLAB. These results were obtained assuming a 66 kV system voltage. Figure 6.2.2 represents the plot of electric field strength vs. insulator length obtained using Microsoft Excel.

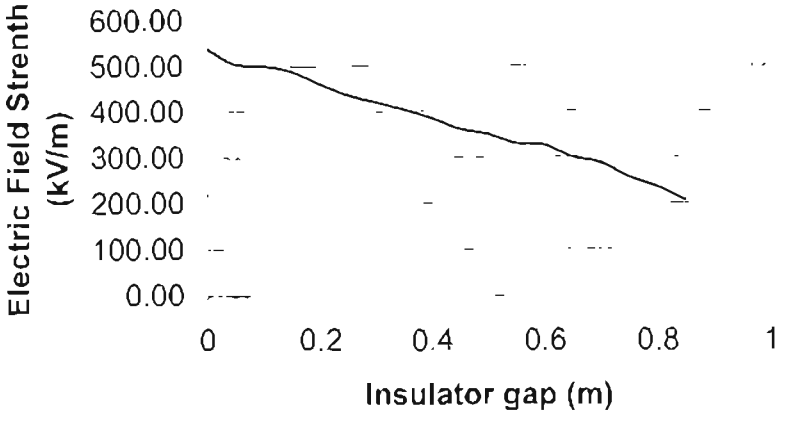

Figure 6.2.2: Plot of electric field strength vs. insulator length

The dielectric strength of air is approximately 3000 kV/m. This value is known to vary with the size and shape of the high voltage electrode and air pressure. However, it is obvious by the above result that the probability of a flashover between the high voltage conductor and the earthed attachment point of the fibre optic cable is very slim. This implies that the high voltage insulator to be used in this experiment should be determined by the maximum voltage that is expected to be seen on the line. This would prevent flashover between the high voltage conductor and the grounded tower to which it is attached.

6.2.2 Electric Field Strength vs. Conductor Height

The aim of this investigation was to observe the effect of varying conductor height on the electric field strength at the attachment point of the fibre optic cable. The conductor height was varied in increments of 10 cm between the heights of 1.6m and 2.3m, while the height of the fibre optic cable remained fixed at a height of 1.5m. As in the previous investigation, the conductor and fibre optic cable were represented by solid cylinders. The result of this investigation is illustrated in Figure 6.2.3 below.

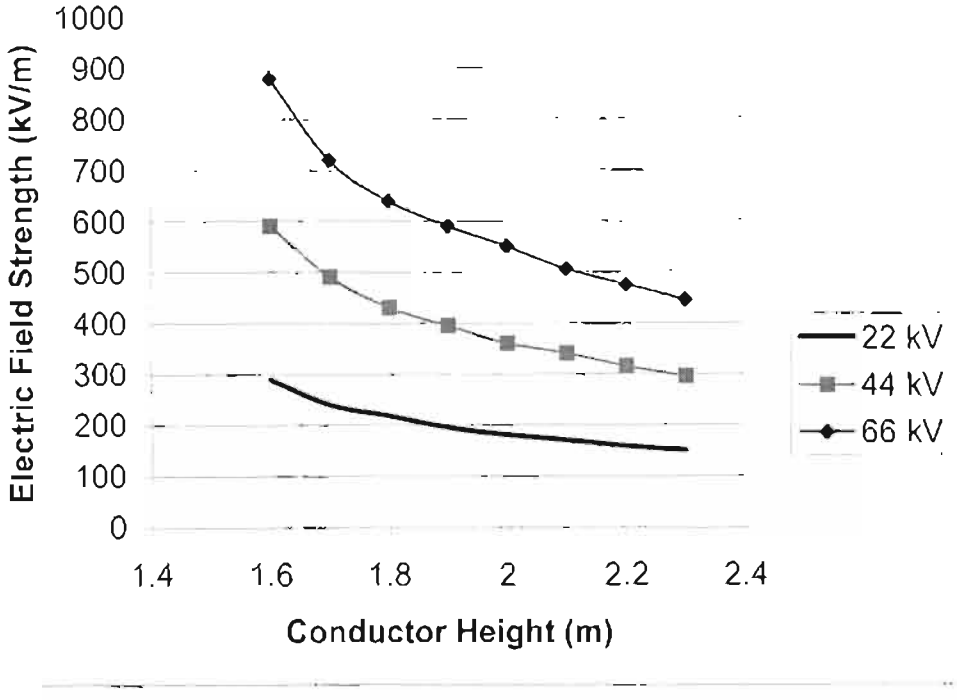

Figure 6.2.3: Plot of electric field strength vs. conductor height

This result confirms the expected result that the electric field strength would decrease as the distance between the phase conductor and fibre optic cable is increased. As the distance is increased, the phase to fibre optic cable capacitance is decreased correspondingly. This results in a decrease in induced voltage at the fibre optic cable attachment point. The strength of the electric field is also shown to increase with system voltage as expected.

6.2.3 Simulation of the effect of armour rod terminations

It has been reported [Karady et al, 1999d], that armour rod assemblies are seldom evenly terminated when installed on the transmission towers of a high voltage network. The effect of this was investigated [Karady et al, 1999d] using brass rods in the laboratory to simulate the effect of armour rods in the field (as described earlier in Section 2.4).

These brass rods surround the fibre optic cable and the cable is placed in an electric field similar to that generated by a transmission line. One rod is attached so that it

protrudes farther than the others so that the effect of uneven armour rod terminations may be investigated.

The geometry of this simulation is shown in Figure 6.2.4. As observed, the diameter of both the fibre optic cable and the conductor were exaggerated to facilitate the meshing process required by finite element analysis. This simulation was however unsuccessful. FEMLAB® was unable to mesh the small gaps that existed between the brass rods and the fibre optic cable using the computer hardware available (the software reported that there was not enough RAM available).

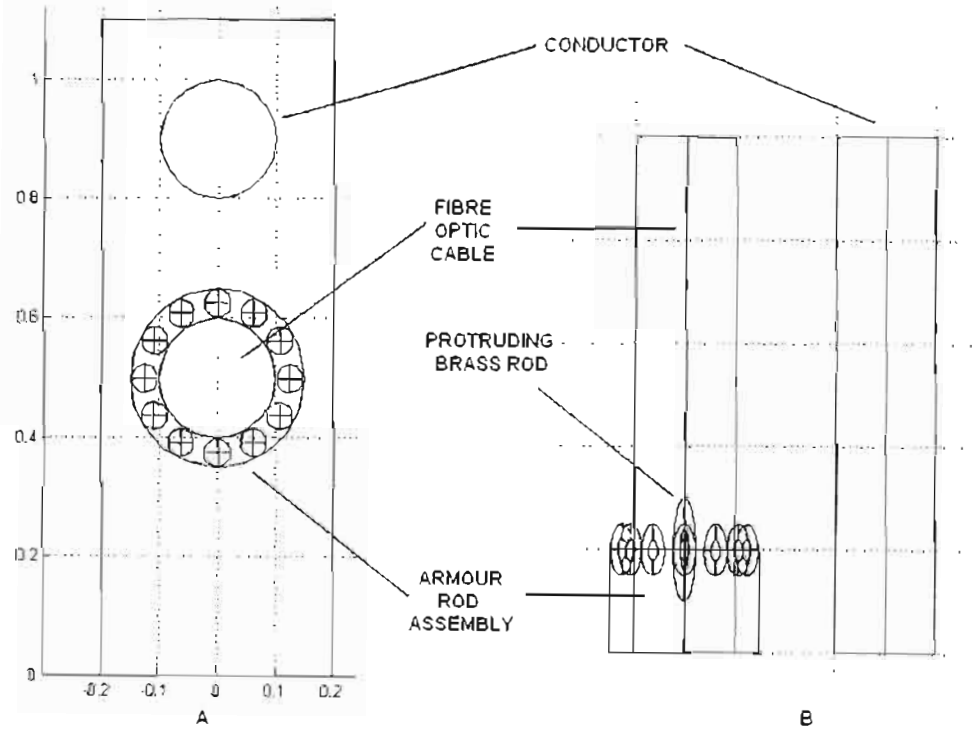

Figure 6.2.4(A): Cross section of geometry showing brass rod arrangement

Figure 6.2.4(B): View of geometry that highlights protruding brass rod

6.2.4 Simulation of a possible mitigation technique

To increase power flow in a transmission network, without structural modifications, requires increasing the amount of current that is flowing through the line. The limit to this increase is the conductor temperature, which when increased would cause the line to elongate and sag. American researchers, working in Russia, have devised a new inexpensive method to calculate this line sag using an installed length of a

grounded wire [Olsen, Edwards, 2002]. The current induced on this cable is measured and used to determine the sag of the phase conductors.

After reading this paper it was decided to simulate the effect that this grounded wire would have on the voltage induced on an ADSS fibre optic cable. A 132 kV transmission system was modelled at mid-span. The dimensions used in this simulation are identical to those used in both the MATLAB® and ATP simulations earlier, and are tabulated in Table 4.1. The system is firstly modelled without the grounded cable installed alongside the fibre optic cable. The result of this simulation is illustrated in Figure 6.2.5. This phasing (i.e. Maximum voltage on centre phase) was shown to yield the highest space potential at mid-span.

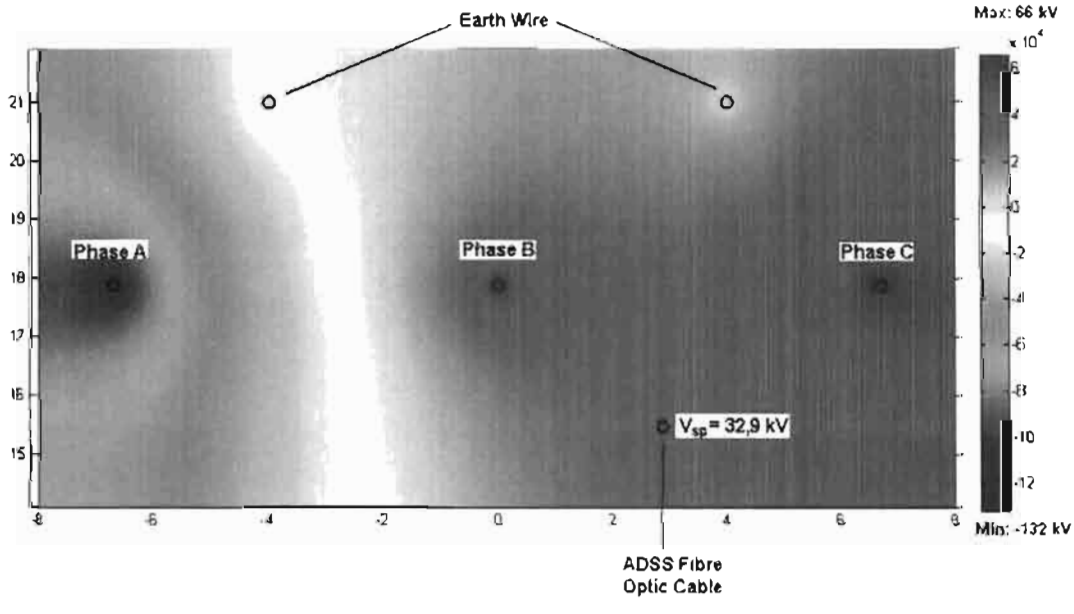

Figure 6.2.5: Space potential of simulated network at mid-span

In the corresponding simulation, the earthed cable was inserted alongside the fibre optic cable to observe the effect that it has on the induced space potential. As is illustrated by Figure 6.2.6, the mid-span space potential seen by the fibre optic cable decreased by a factor of 5.35 after the insertion of the grounded conductor. This is a very positive result and therefore requires further laboratory work to determine the feasibility of such a mitigation method for use in the field.

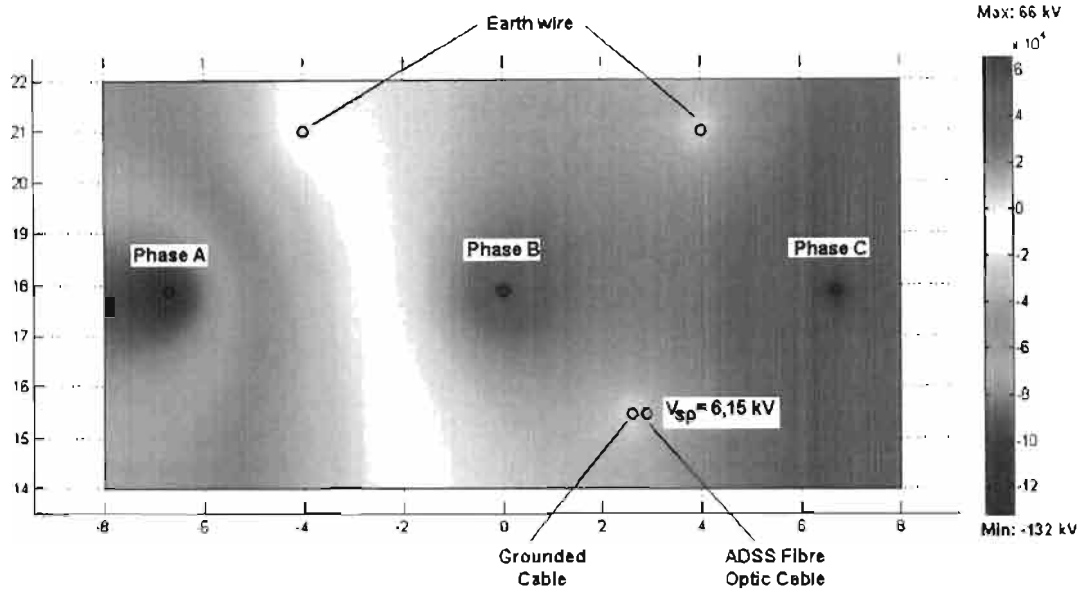

Figure 6.2.6: Space potential of simulated network after the insertion of grounded conductor alongside fibre optic cable

6.2.5 Requirement for proper shielding

It was decided to also use FEMLAB® to simulate the laboratory experiment and observe the effect of proper shielding on experimental results. Shielding is an important consideration for this experiment as it inhibits voltage coupling to the measurement circuit.

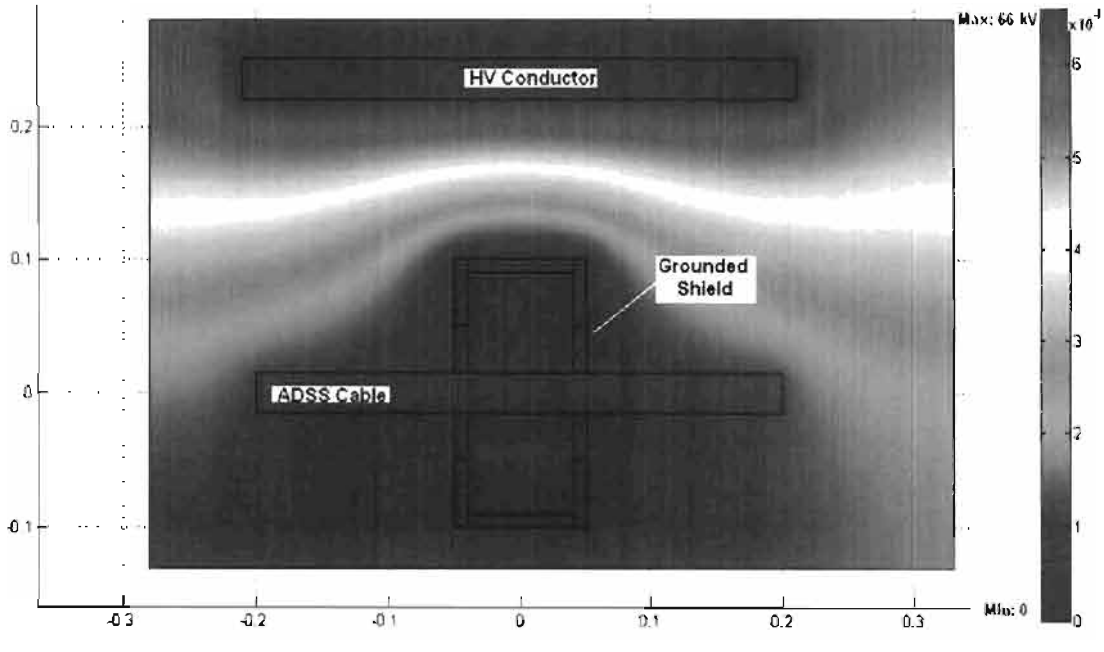

Figure 6.2.7: Effect of proper shielding

In this 2-dimensional simulation, both the conductor and fibre optic cable are represented as solid rectangles whilst the shield is represented as a grounded, hollow box. The fibre optic cable in left at a floating potential in this simulation. This result (Figure 6.2.7) confirms that a grounded shield would effectively protect the measurement circuit from any stray capacitances that could result in corrupted measurements.

6.2.6 Mutual Capacitance Calculation

Finally, FEMLAB® was used to assist in the "phase to fibre optic cable" capacitance calculation. As discussed in Section 3.3.2, the capacitance values required in the MATLAB® algorithm were determined using the method of Maxwell's potential coefficients. Using FEMLAB®, this capacitance calculation was also obtained using Finite Element techniques to obtain verification of the earlier employed method. The capacitance may be calculated based either on the definition of capacitance;

$$C = Q/V \quad \text{... (6.5)}$$

or using the total electric energy formula;

$$C = 2W_e/V^2 = \text{int}(E.D)/V^2 \quad \text{... (6.6)}$$

where "int" denotes the integral over the whole domain. When using Equation 6.5, "Q" may be found by integrating the surface charge over the conductor boundary. It is recommended that the energy method be employed to obtain more accurate answers but both methods were employed in this study so as to ascertain the level of accuracy involved.

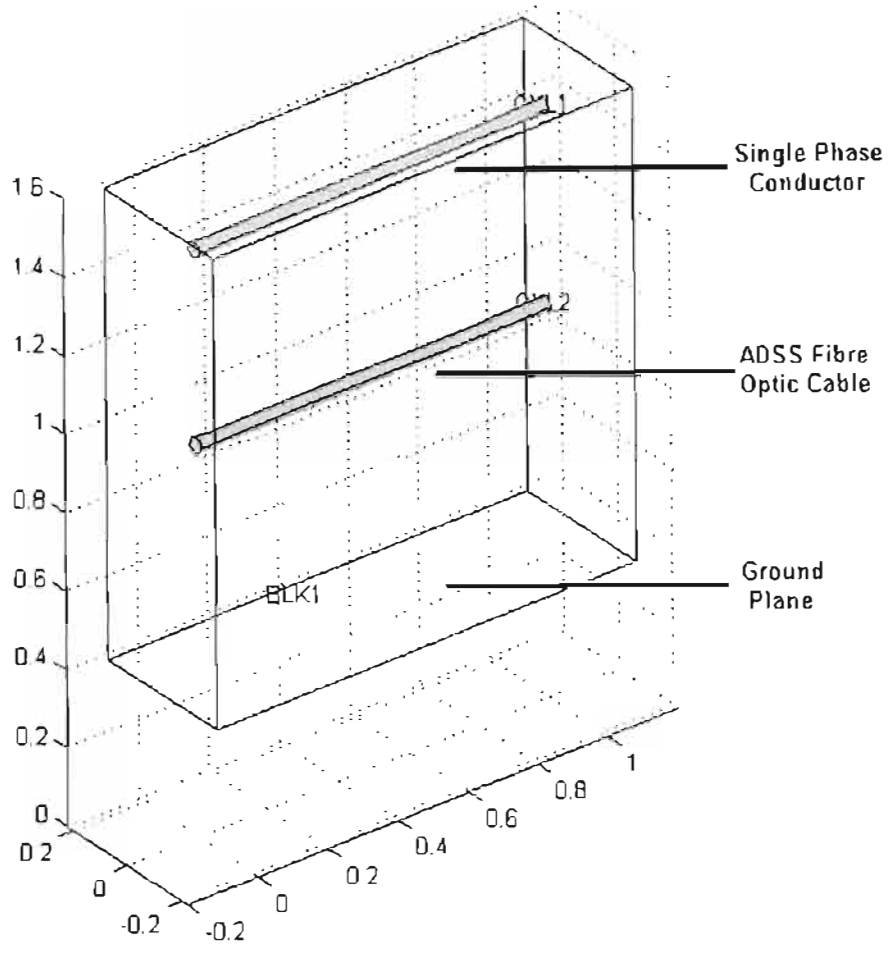

Figure 6.2.8: Model Geometry used in Capacitance Calculation

During this simulation, the radii of both the ADSS fibre optic cable and the conductor were increased to 10mm each. This was done so that the model could be properly "meshed", by FEMLAB®. The results of both methods are tabulated below in Table 6.1. The energy method is shown to provide the more accurate result. These results provide one with confidence in the capacitance calculation method employed earlier (Section 3.3.2), as they are all of the same order of magnitude. In the chapters that follow, simulated values of leakage current will be compared to values determined experimentally. These simulated values will use the "phase to fibre optic cable capacitance" determined by the method of Maxwell's Potential Coefficients. The values obtained by FEMLAB® were not used due to the simplifying assumptions

that were made in the model (i.e. increase in both the conductor and ADSS diameter).

Method Employed	Capacitance Value	Percentage Difference
Maxwell's Potential Coefficients	5.62 pF/m	-
FEMLAB® Charge Method (Eq. 6.5)	2.78 pF/m	51 %
FEMLAB® Energy Method (Eq. 6.6)	3.58 pF/m	36 %

Table 6.1: Comparison between different capacitance calculating methods

The primary aim of this chapter was to illustrate the use of the finite element modelling tool, FEMLAB®, in this study. It was shown how this program was used to set up the laboratory experiment and also how a possible dry-band arcing mitigation technique was investigated. Adequate shielding of the measurement circuit is pivotal when performing any high voltage experiment and the importance of this was shown in this chapter and two capacitance calculation methods (using FEMLAB®) were also investigated.

CHAPTER SEVEN

EXPERIMENTAL INVESTIGATION

Experimental investigations are essential if one is trying to obtain confidence in proposed system models or simulations. The design and construction of the experimental set-up is described in this chapter with particular attention being focused on the choice of measurement circuit used. A concise description and corresponding results of the many experiments that were conducted in this study is also included in this chapter. It should be noted, that an in-depth discussion of these results is included in Chapter 8.

7.1 Experimental Set-up

7.1.1 Physical Construction

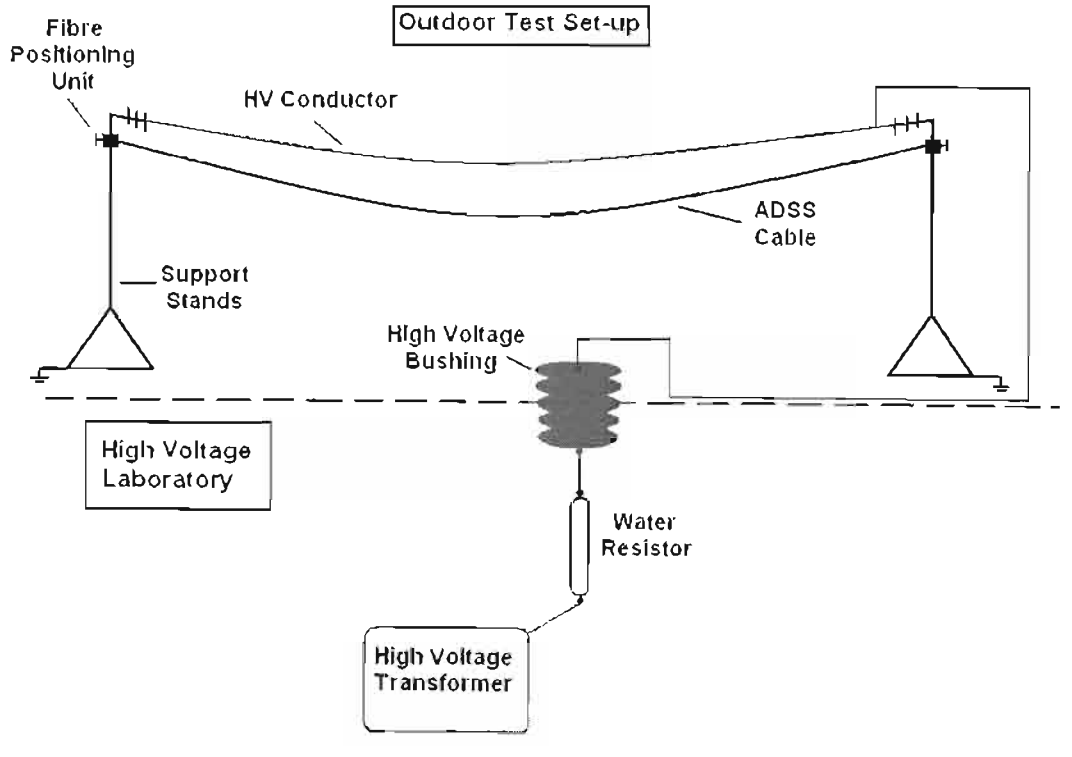

Figure 7.1.1: Physical arrangement of experiment

Figure 7.1.1 clearly illustrates the experimental set-up used during this study. These experiments were conducted outdoors, and this made it possible to obtain a much larger span length (It was shown in Chapter 4 that induced leakage currents increase with span length). The reduced span length and use of a single phase system would have resulted in leakage currents that were not of the same order of magnitude as those obtained in the field. The distance between the high voltage conductor and the fibre optic cable was therefore decreased to compensate for this and obtain larger leakage currents. The safety of this step was investigated using FEMLAB® in Chapter 6.

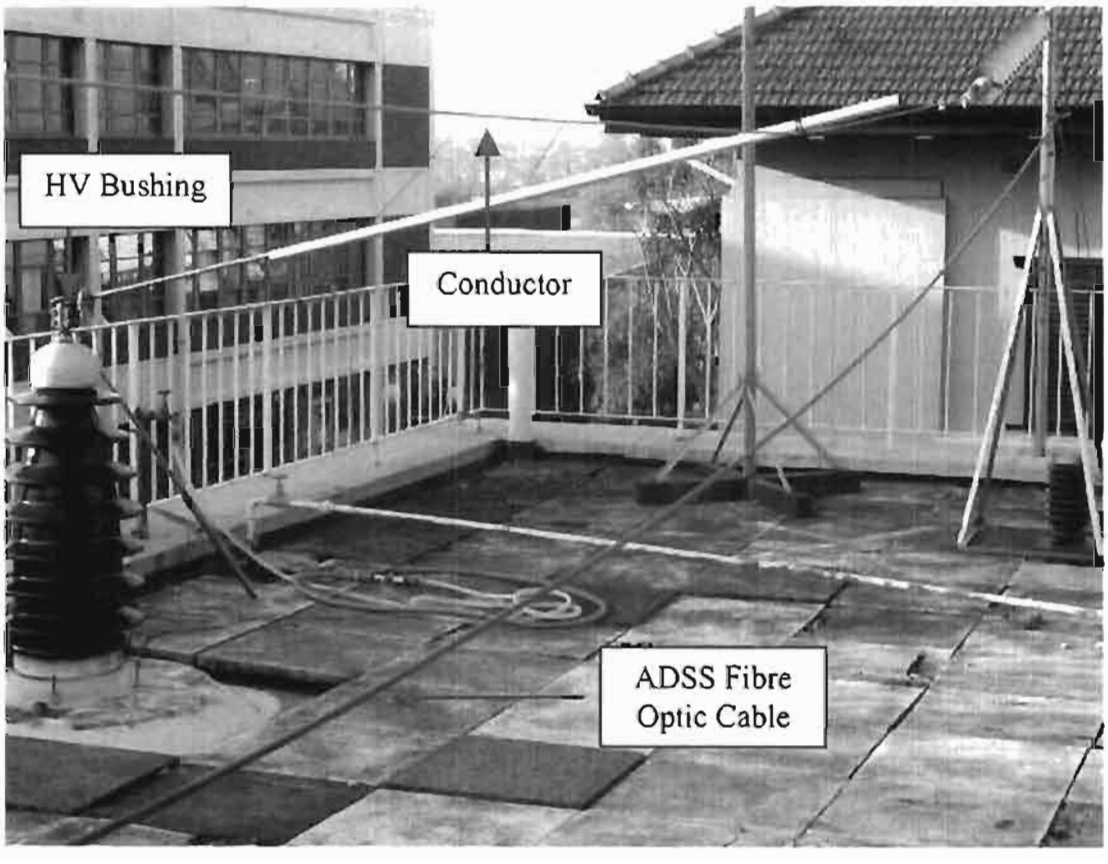

Figure 7.1.2: Picture of experimental set-up

The support towers were constructed using grade 316 stainless steel, as this material was known to possess superior weathering performance. The support towers were constructed such that the height of the ADSS fibre optic cable may be varied with respect to the energized conductor. The conductor may be positioned at a maximum height above ground of 3m. Furthermore, the distance between the fibre optic cable and the conductor may be varied from 0.2m to 0.8m in increments of 0.1m.

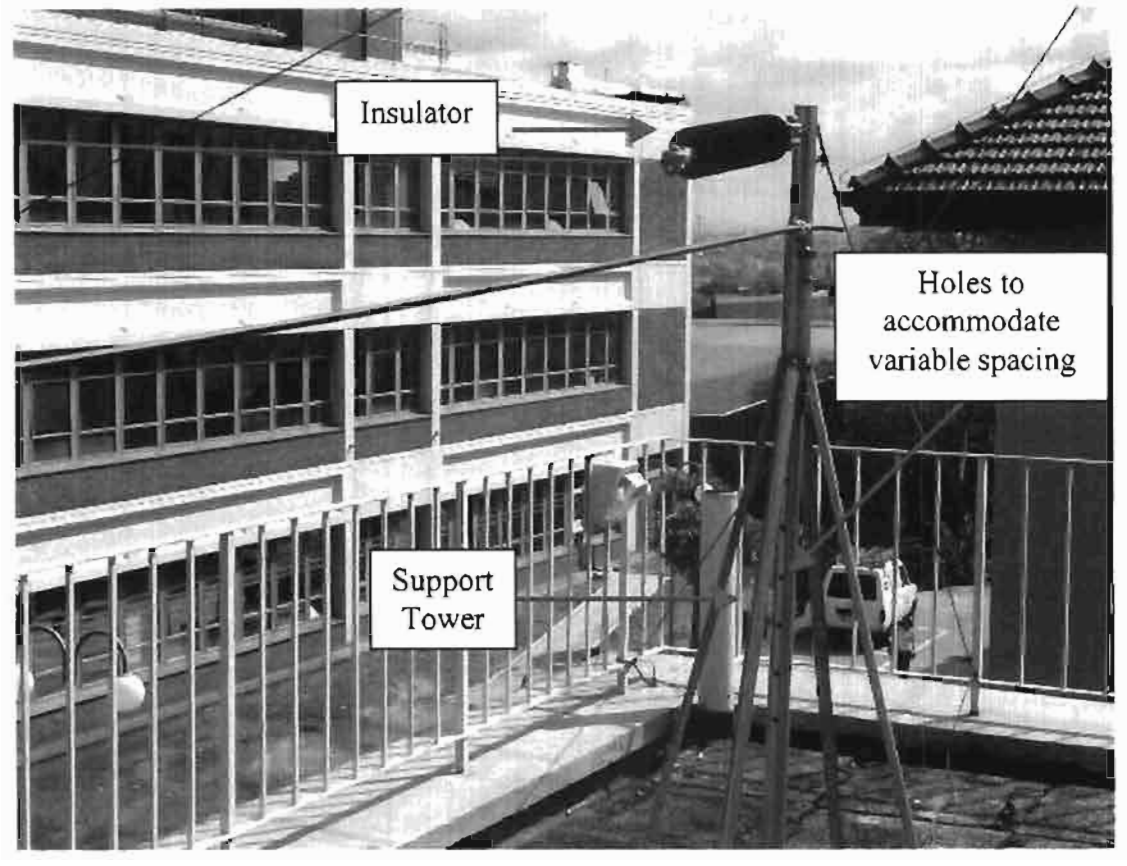

Figure 7.1.3: Picture of support tower

Varying degrees of pollution was simulated using a salt solution of varying conductivities. The salt solution was easily created by mixing rough salt with water and then stirring (agitating) to ensure a high degree of saturation. This solution was allowed to settle, before being measured using a conductivity meter. Use of this method allowed one to easily vary and control the application of pollution. The fibre was usually rubbed down with fine sandpaper before applying the pollution, and this was done to aid in wetting of the surface. The pollution was applied onto the surface of the fibre optic cable with a hand-held spray gun.

7.1.2 Measurement Circuit

The current is measured close to the support tower as it has been extensively reported that, in the field, the maximum leakage current occurs close to the grounded armour rod assembly on the tower (Karady et al, 2001a). A shunt resistor is used as a current sensor in this experiment and a motivation for this choice was outlined earlier in Section 2.3.3. (e). The current measurement system is illustrated in Figure 7.1.4.

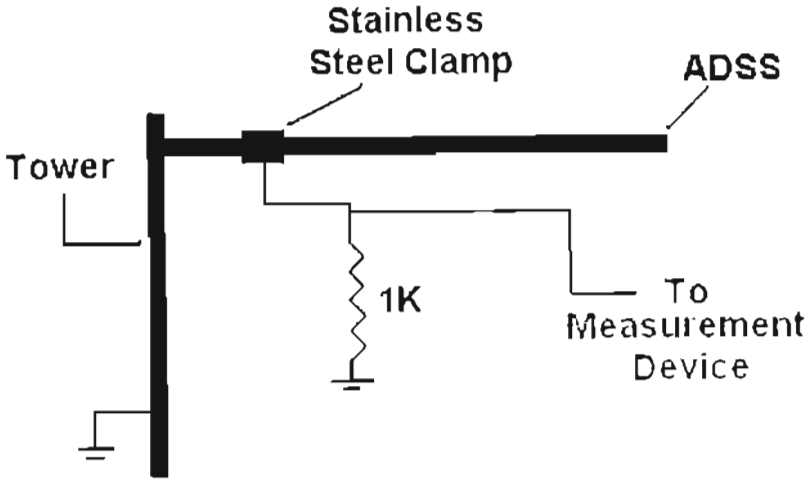

Figure 7.1.4: Diagram of Current Measurement System

FEMLAB® simulations conducted in Chapter 6 (6.2.5) also highlighted the need for proper shielding of this measurement circuit. The shielding is necessary to ensure that there is no capacitive coupling to the measurement circuit. For these experiments, shielding was achieved with the use of aluminium foil wrapped tightly around the measurement device.

7.2 Experimental Results

7.2.1 Effect of Voltage on Induced Leakage Current

It was assumed that the induced leakage current would increase with system voltage and this was confirmed using both the MATLAB® and ATP simulations. In the first series of experiments, the optical fibre was polluted using a salt solution whose conductivity measured 7.4 milliSiemens/cm. This represented a medium pollution case. In this experiment, the conductor was first energised to 40 kV and the voltage was then increased to a 100 kV at 20 kV intervals. At each voltage level, the corresponding induced current was noted. The voltage was then maintained at 100 kV until the induced current reduced significantly (indicative of "drying out" of pollution layer). Dry band activity was always noted (either audibly or visibly) prior to the above mentioned current reduction. This process was performed three times to ensure repeatability and the average value was used to plot Figure 7.2.1. Figure 7.2.1 compares these measured values against those obtained by the MATLAB®

simulation. The simulated values were found to conform reasonably well to those that were measured. Possible reasons for these differences will be discussed later, in Chapter 8.

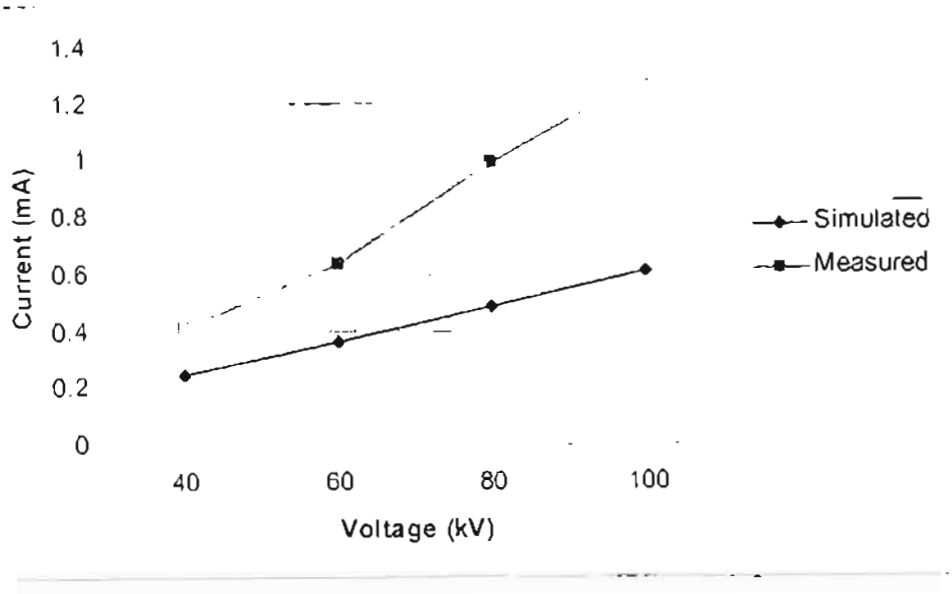

Figure 7.2.1: Comparison between Simulated and Measured Induced Current Magnitudes at Medium Pollution

7.2.2 Effect of Pollution Severity on Induced Leakage Current

The next set of experiments was conducted to test the effect of varying pollution on induced leakage current. For this experiment the conductor sag was 2.78% and the fibre optic sag was measured to be 17.65%. At the tower, the spacing between the conductor and the fibre optic cable was 10 cm. Three pollution levels were used to simulate the effect of heavy, medium and light pollution and are defined as shown:

Heavy Pollution	:	11.1 milliSiemens/cm (0.26 MΩ/m)
Medium Pollution	:	7.4 milliSiemens/cm (1.10 MΩ/m)
Light Pollution	:	0.34 milliSiemens/cm (5.25 MΩ/m)

A meggar was used to determine the pollution resistances in each of the above cases. The voltage was applied in a similar manner to the earlier experiment. The only exception being that the maximum voltage applied in this experiment was a 120 kV (light and heavy pollution cases only). When simulated, the effect of varying

pollution on this experimental set-up was found to be negligible. The medium pollution case was therefore plotted in Figure 7.2.2.

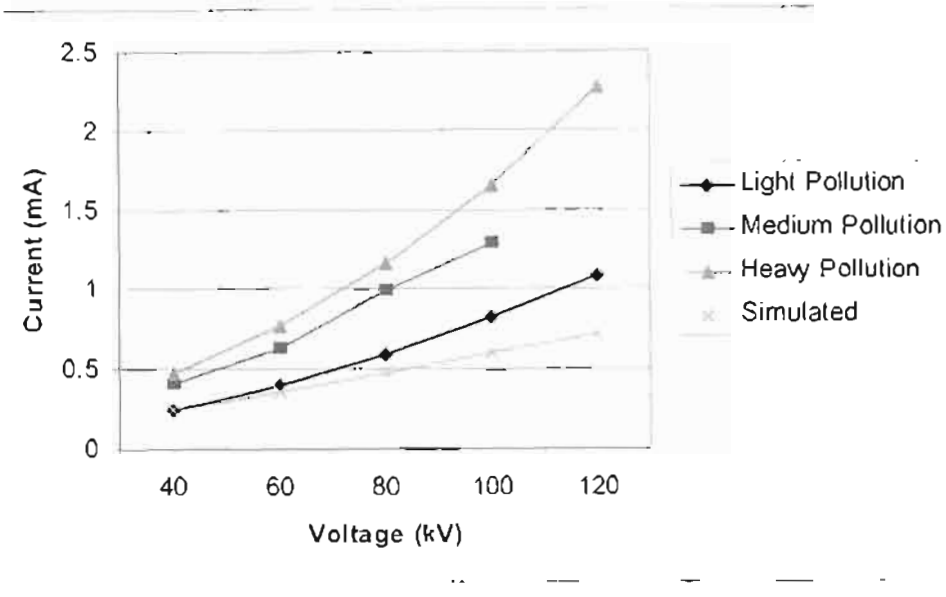

Figure 7.2.2: Effect of Pollution on Induced Current

7.2.3 The Effect of Spacing (between the Conductor and Fibre Optic Cable) on Induced Leakage Current

This experiment investigated the effect of varying the spacing between the fibre optic cable and the conductor. It follows from earlier simulations (Section 4.4), that the induced leakage current on the outer sheath of the fibre optic cable would decrease as the distance between the fibre optic cable and the conductor is increased [Khan, Hoch, 2002(b)].

The spacing between the fibre optic cable and the conductor was increased from 10 cm to 30 cm in this experiment. The sag for both the conductor and fibre optic cable were however unchanged and the conductivity of the salt solution used in this experiment was 25 mS/cm. When the results of this experiment are compared to an earlier experiment described above (10 cm spacing, conductivity: 11.1mS/cm) in Figure 7.2.3, the effect of spacing between the conductor and fibre optic cable becomes very apparent. The conductivity of 25mS/cm was chosen to illustrate that even when the pollution conductivity is doubled, the leakage current does not exceed the value obtained when the spacing was 10 cm.

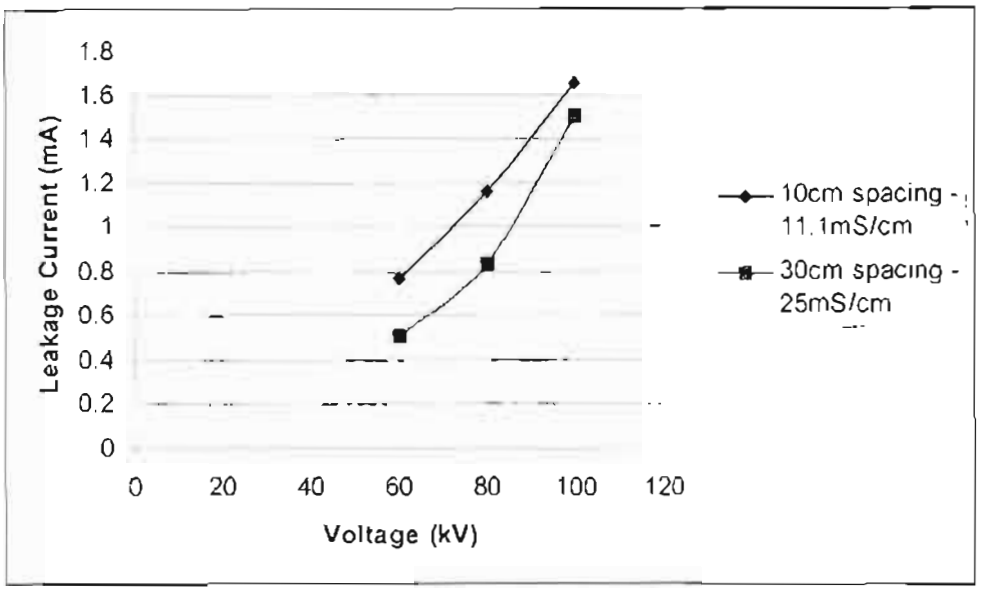

Figure 7.2.3: Effect of Spacing on Induced Current

7.2.4 The Effect of Sag on Induced Leakage Current

Earlier mathematical models [Carter and Waldron, 1992] assumed that the sag for both the conductor and fibre optic cable were the same. They therefore also assumed that the phase to fibre optic cable capacitance and fibre optic cable to ground capacitance were constant along the length of the span. This was an over-simplification as it is common practice for the sag of the fibre optic cable to be smaller than that of the phase conductors [Karady et al, 2001a]. An experiment was therefore set-up to investigate the effect of sag on the leakage currents induced.

The conductor height and sag was maintained for this experiment (Height = 1.8m; Sag = 2.78%). The support tension of the fibre optic cable was adjusted and the resulting mid-span height corresponded to a sag calculation of 43.18%. Three pollution levels were investigated (0.26 mS/cm; 14 mS/cm and 26 mS/cm) in a procedure similar to that conducted in Section 7.2.2 above i.e. the voltage is increased in 20 kV intervals from 60 kV to 100 kV. The experimental values are plotted together with those simulated using MATLAB® for the different pollution cases defined above (Figure 7.2.4 – Figure 7.2.6).

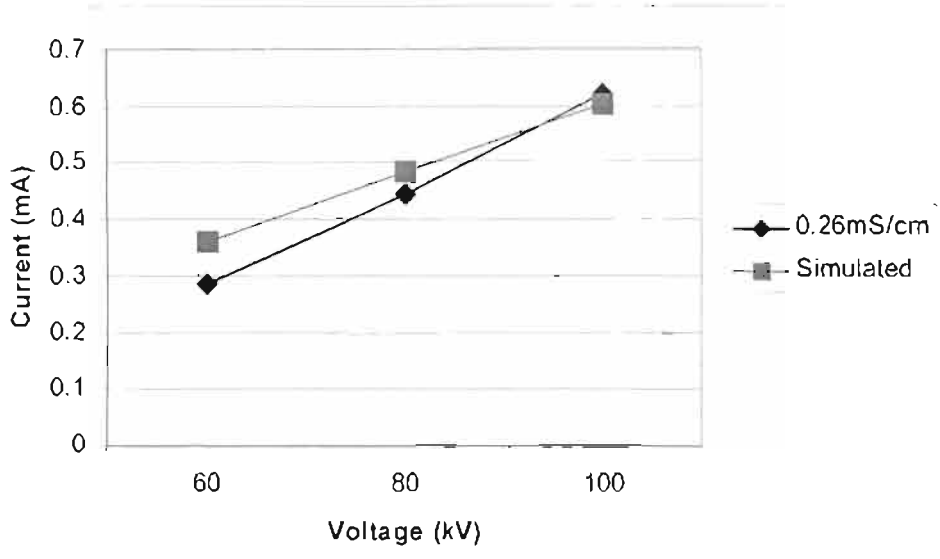

Figure 7.2.4: Effect of Sag on Induced Current

(Pollution = 0.26 mS/cm)

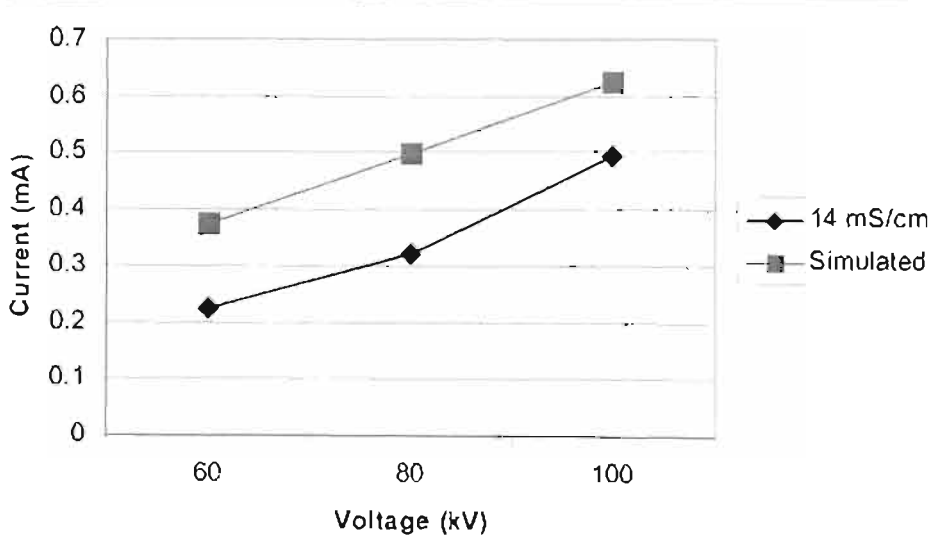

Figure 7.2.5: Effect of Sag on Induced Current

(Pollution = 14 mS/cm)

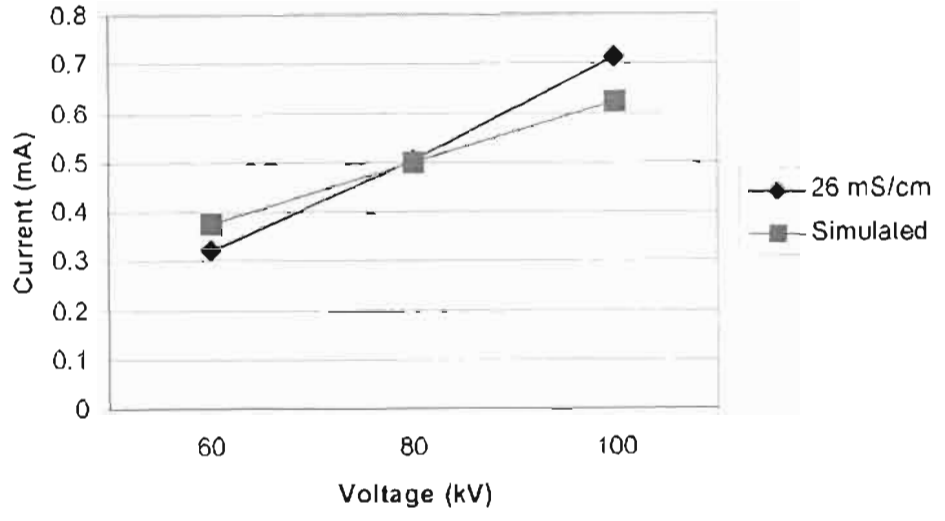

Figure 7.2.6: Effect of Sag on Induced Current

(Pollution = 26 mS/cm)

There appears to be improved correlation between the measured leakage currents and those simulated by MATLAB® for the low pollution (0.26 mS/cm) and high pollution (26 mS/cm) cases. Leakage current waveforms obtained during this experiment will be analysed in Chapter 8.

This chapter provided the reader with a concise description of the experimental set-up and described the aims and results of all investigations conducted. These results are to be reviewed and analysed in the subsequent chapter. All experiments conformed to expected trends (as discussed in earlier chapters). The experiments conducted were:

- The effect of voltage on induced leakage Current
- The effect of pollution on induced leakage current
- The effect of spacing (between Conductor and fibre optic cable) on induced leakage current, and
- The effect of sag on induced leakage current

CHAPTER EIGHT

ANALYSIS AND DISCUSSION OF RESULTS

The primary aim of this chapter is to analyse all obtained results (simulated and experimental). Possible reasons for non-correlation between the experimental and simulated results (where applicable) are also discussed and dry band formation is analysed using the leakage current waveforms obtained.

8.1 The Effect of Voltage on Induced Leakage Current

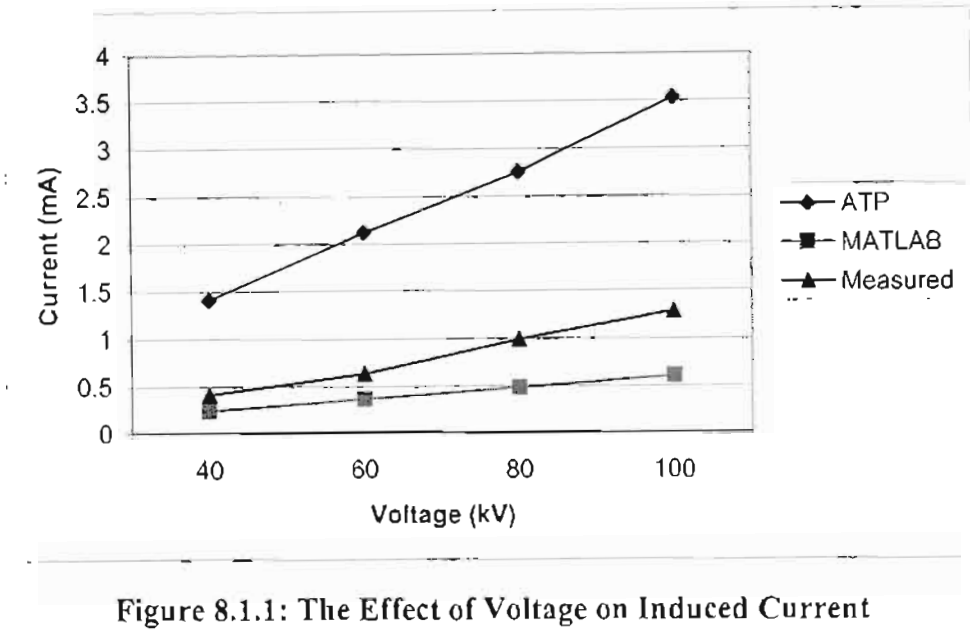

Figure 8.1.1: The Effect of Voltage on Induced Current (Comparative Plot between Simulations and Experiment)

Figure 8.1.1 compares the experimental data to that obtained by both the MATLAB® and the ATP simulations. Both simulations predicted values that were of the same order of magnitude and tracked the experimental trends reasonably accurately, with the MATLAB® simulation being the better of the two (Maximum variance = 53%).

A single-phase adaptation of the three-phase model developed earlier in Chapter 5 was used by ATP, to predict the maximum leakage currents induced on the cable, during the experiment. The maximum percentage difference between corresponding data points on the experimental trend and ATP trend on Figure 8.1.1 is 241% (at

40 kV). A pi model was used to simulate the transmission line in ATP and this could explain this large variance. A pi model is a discrete approximation of the constant distributed parameter model (see Figure 5.2.2). However, the model used in the MATLAB® simulation is a distributed model (see Figure 3.1). An ATP simulation was therefore attempted using the distributed parameter model. In the ATP simulation, the ADSS fibre optic cable is represented as a conductor with a very high resistance i.e. typical resistance of pollution layer. This ATP simulation was unsuccessful as the program assumes that the programmer has made an error and inputted an incorrect DC resistance value for a conductor. It therefore refuses to simulate. The ATP simulation was not used for any further comparative studies.

8.2 The Effect of Pollution Severity on Induced Leakage Current

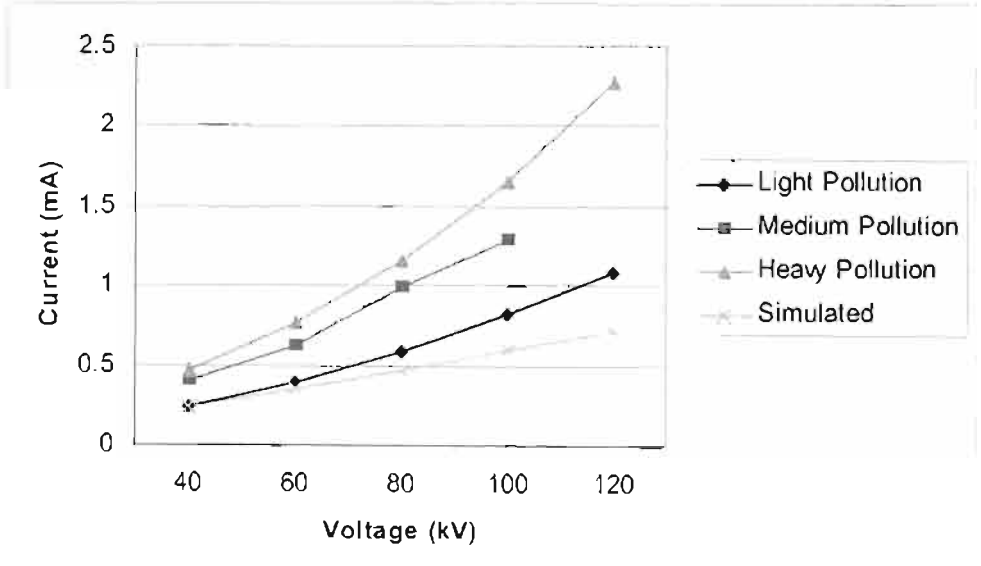

Figure 8.2.1: The Effect of Pollution Severity on Induced Current
[Figure 7.2.2 Recalled]

There appears to be negligible difference in leakage current magnitude, when the MATLAB® simulation is used to predict currents for the experiments conducted. Reasonable correlation is only obtained for the low pollution case with the error

obviously increasing with pollution severity. There are two possible reasons for this inconsistency.

Firstly, the method of phase-to-fibre capacitance calculation may need to be reviewed when simulating a small-scale experimental set-up. Capacitance is calculated using the method of Maxwell's Potential Co-efficients, which is commonly employed when parallel conductors are separated from each other and ground, by relatively large distances. This method assumes that a line charge is located at the centre of the conductor. Further work in this field must examine other methods of capacitance calculation e.g. using finite element analysis (Section 6.2.6).

Another possible reason for this discrepancy could be that the experimental span length is too small. The plot below illustrates the effect of increasing span length on the leakage currents induced for this laboratory experiment. This simulation was performed at a system voltage of a 100 kV and minimal sag.

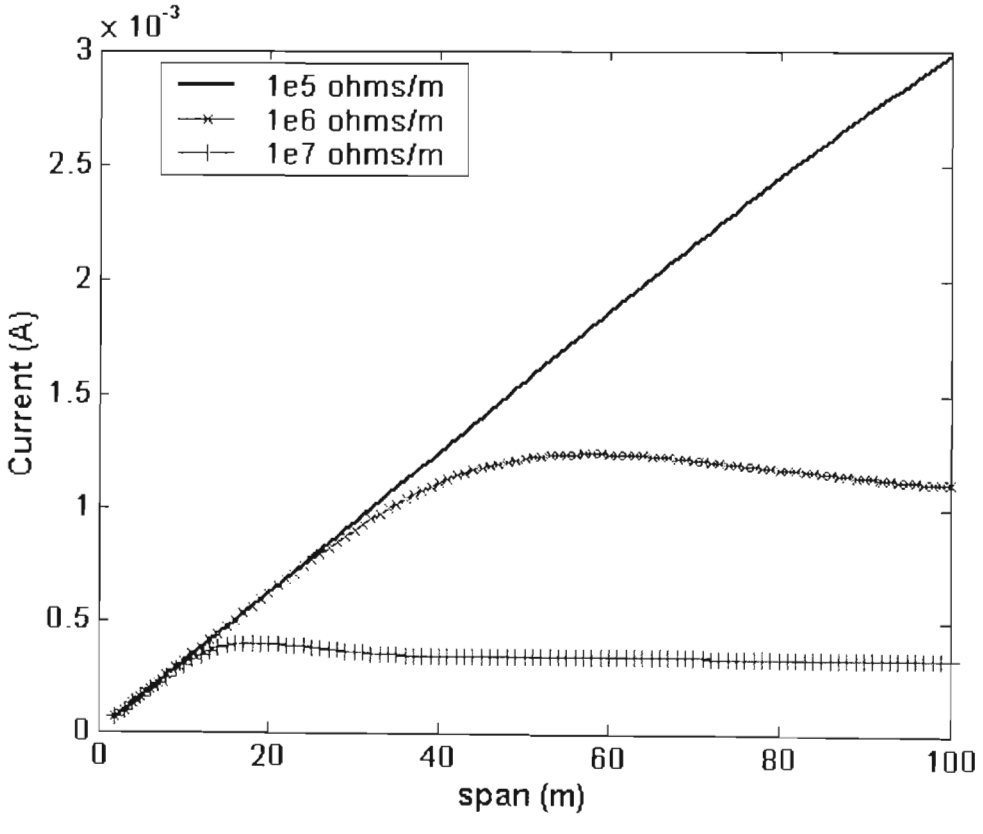

Figure 8.2.2: Effect of Increasing Span on Induced Leakage Current

As may be observed, the simulation predictions for all three pollution severities are almost identical for the first 12m. After 20m, an appreciable difference between the low and medium pollution case is observed and at 40m, the medium pollution case reaches it's "critical current". One may therefore interpolate that if an experimental investigation were conducted on a 60m long span, one would obtain better trend and value correlation. This too suggests that it may be the capacitance calculation for small spans and spacings that causes this irregularity.

8.3 The Effect of Sag on Induced Leakage Current

A remarkable degree of correlation was obtained between simulated and measured waveforms for this experiment (Figures 7.2.4 – 7.2.6) [N.B. Much greater spacing than previous experiments were correlation was poor]. Leakage current waveforms were obtained during the different stages of this experiment and it conceptually illustrates the phenomenon of dry band arcing well. In this experiment (Pollution resistance = 14 mS/cm) the system voltage was firstly increased from 60 kV to 80 kV and then to a 100 kV. The corresponding waveforms are shown below.

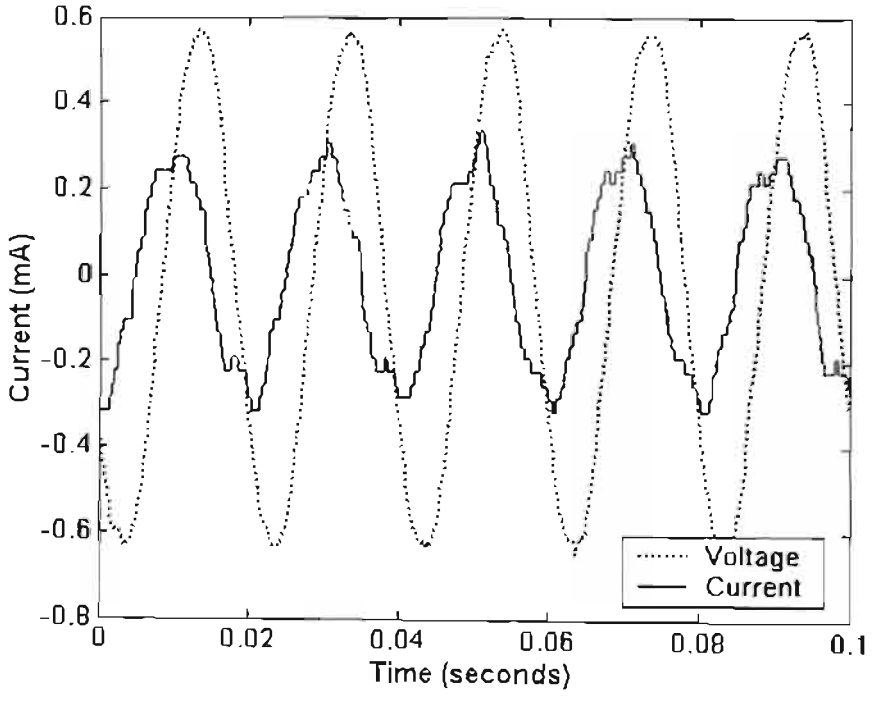

Figure 8.3.1: Leakage Current Waveform

Voltage = 60 kV; Pollution = 14 mS/cm

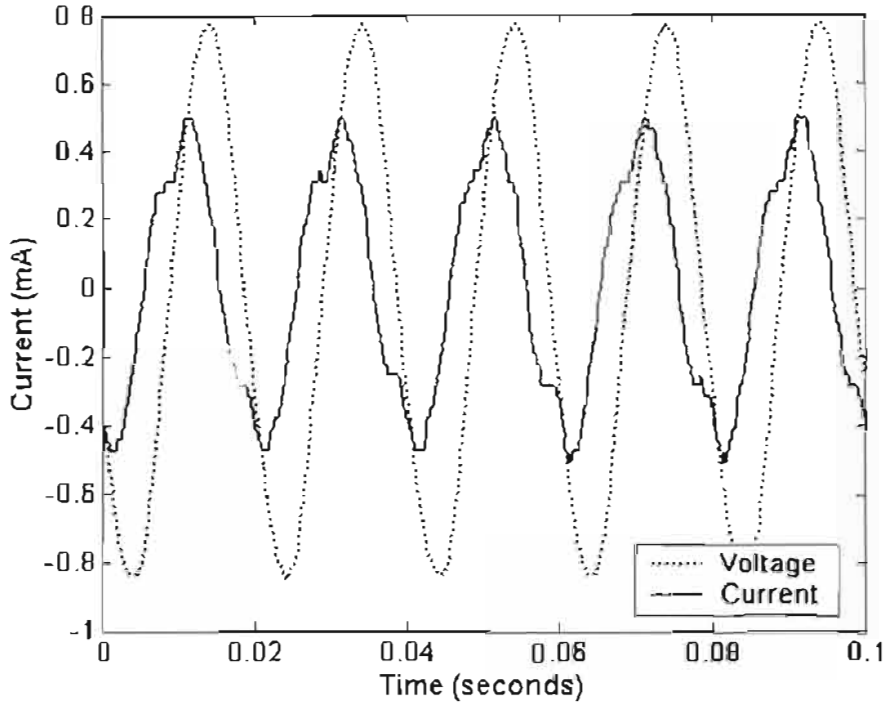

Figure 8.3.2: Leakage Current Waveform

Voltage = 80 kV; Pollution = 14 mS/cm

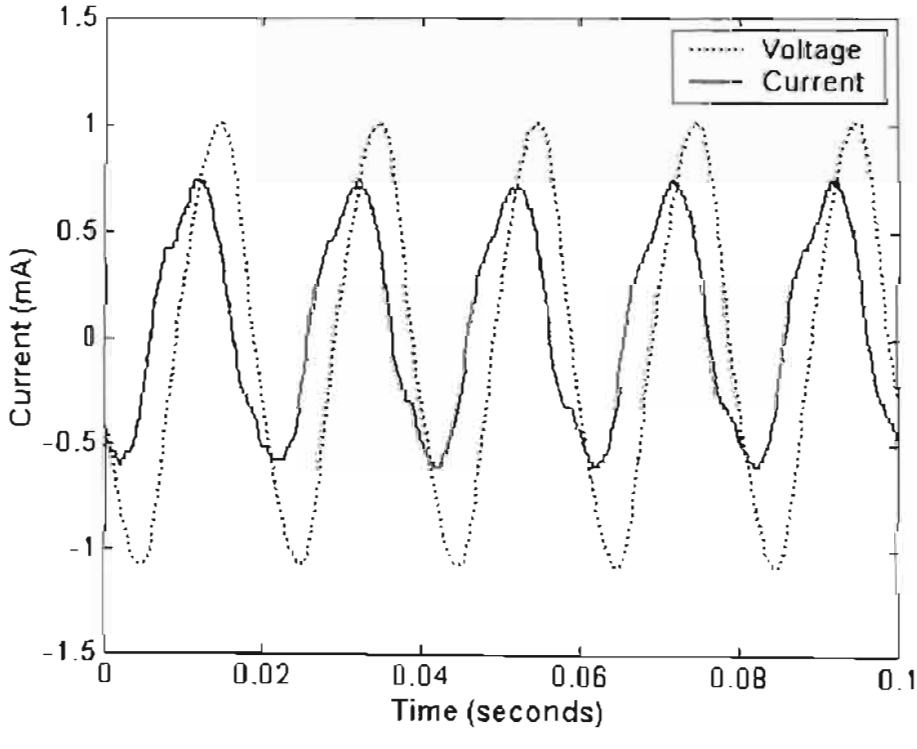

Figure 8.3.3: Leakage Current Waveform

Voltage = 100 kV; Pollution = 14 mS/cm

The leakage currents are observed to increase as the system voltage is increased. The system voltage waveform (dotted line) was scaled down, so that one may easily determine from these waveforms whether these leakage currents are resistive or capacitive etc. The leakage current (solid line) is observed to be lagging the voltage by approximately 90 degrees i.e. the current is capacitive.

The system voltage was then increased to 110 kV and maintained at this level until the formation of a dry band. It was noticed at this point that the current was at one stage sufficiently stable, but then increased by 1 – 2 mA. A visual inspection in subsequent runs revealed that this increase corresponded with an accumulation of pollutant (salt-water) on the underside of the fibre optic cable. This current is maintained until the layer dries out or there is arcing activity. The current then reduces considerably and becomes more resistive in nature as illustrated in Figure 8.3.4 below.

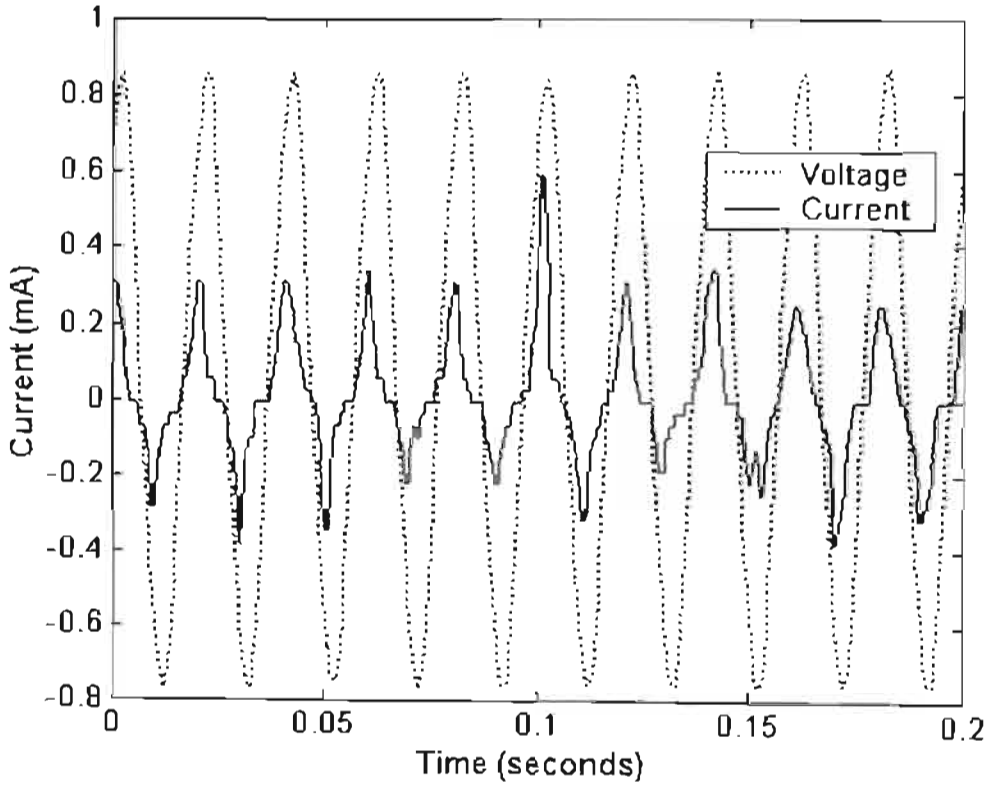

Figure 8.3.5: Leakage Current Waveform
Voltage = 110 kV; Pollution = 14 mS/cm
(After arcing activity)

Leakage current waveforms were also obtained from the same experiment at a higher pollution level (26mS/cm). It is observed to follow a similar trend to the waveforms above.

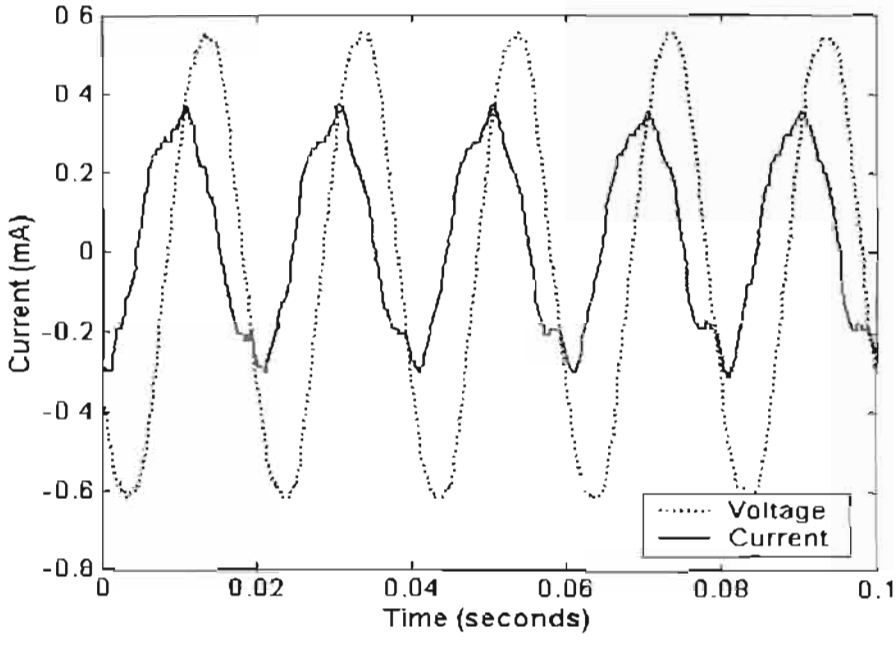

Figure 8.3.6: Leakage Current Waveform

Voltage = 60 kV; Pollution = 26 mS/cm

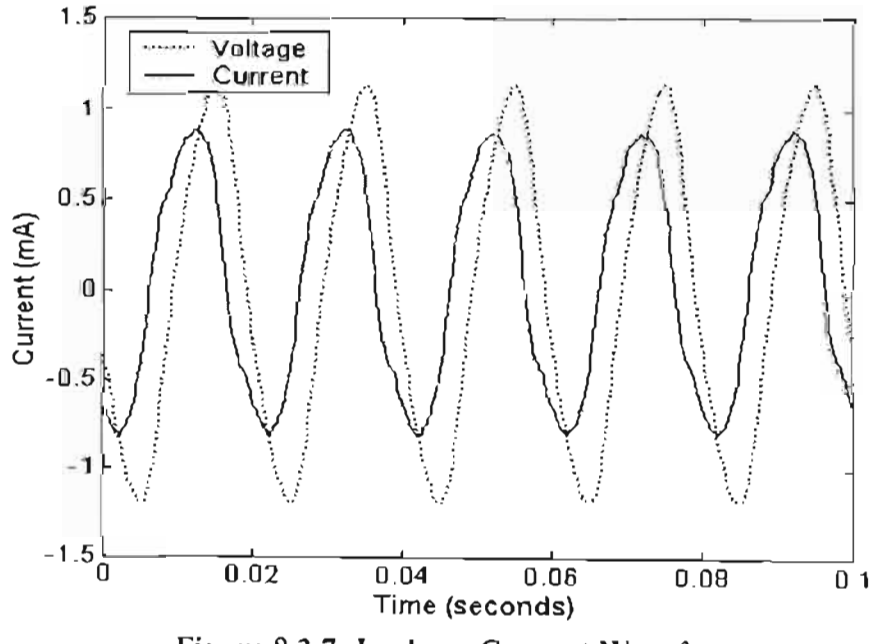

Figure 8.3.7: Leakage Current Waveform

Voltage = 110 kV; Pollution = 26 mS/cm

The voltage was once again maintained at 110 kV until the layer began to dry. The resultant arc activity was captured and is illustrated in the leakage current waveform below. The leakage current magnitude measured after this activity was, as above, much smaller than before the arcing activity

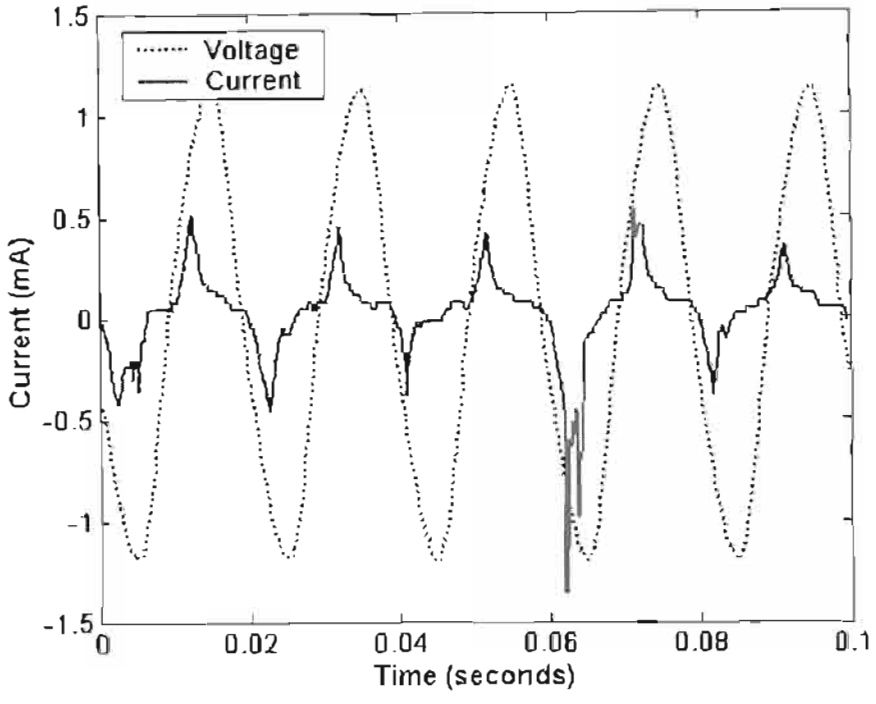

Figure 8.3.8: Leakage Current Waveform showing Dry – Band Arc
Voltage = 110 kV; Pollution = 26 mS/cm

This chapter served to primarily couple the different aspects of this study together. Results obtained from both simulation methods employed were now compared against those obtained by experiment. In the ATP simulation, results were generated for a single-phase system using the tower and line dimensions used in the experiment. In the second simulation technique employed (MATLAB®), the model developed by Karady et al needed to be modified such that it now represented a polluted fibre optic cable in a single-phase high voltage environment (Figure 3.6). The correlation between these different sets of data were analysed and discussed. The phenomenon of dry band formation is also explained using the current waveforms obtained during the experiments.

CHAPTER NINE

CONCLUSION

The following conclusions may be stated:

- Simulated results indicate that the installation of ADSS cable onto 132kV geometries as commonly used in South Africa may result in leakage currents in the range of 0.15mA (simulated at a low pollution level of 10MΩ/m) to 1.8mA (simulated at a low pollution level of 0.1MΩ/m).
- The induced leakage current depends primarily on the positioning of the fibre in the tower window, the phase spacing of the conductors, the sag of both the conductor and the fibre optic cable and the length of the span.
- Simulated results on the 275kV tower geometry indicate that great care needs to be taken when installing fibre optic cables at this system voltage. Careful consideration should be given to the point of attachment on the tower window. Simulated results indicate that leakage currents in the range of 0.2mA (10MΩ/m) to 3.9mA (0.1MΩ/m) may be induced for the 275kV installation.
- Simulations were performed to investigate the effect of span length on leakage currents induced. The recommendation of this investigation is that researchers should construct realistic spans (as found in the field) when "test spans" are erected to test the feasibility of ADSS cable installation. This would ensure that a more realistic indication of the leakage currents induced would be obtained.
- Simulations have indicated that it is the pollution severity closest to the tower that is most significant with regards to leakage currents induced. This result has significant economic ramifications as it could lower the cost of fibre optic cable maintenance in high pollution environments considerably.
- Comparisons between simulated and measured results for a simplified single phase span indicated differences of between 53% and 241% between simulated and measured data.

CHAPTER TEN

FUTURE WORK

10.1 Capacitance Calculation Methods

The method of Maxwell's potential coefficients, used to determine the phase to fibre optic cable capacitance is commonly employed when parallel conductors are separated from each other and the ground by relatively large distances. It follows, therefore, that other methods of calculating the phase to fibre optic cable capacitance should be investigated, to ensure better correlation between those results obtained experimentally and those simulated. It was shown in Chapter 6 how finite element analysis could be used to determine this capacitance. The induced leakage current predictions would benefit greatly from a more accurate determination of leakage current induced.

10.2 Increase Scale of Experiment

The effect of span length on induced leakage current was shown in Section 8.2. This highlights a shortcoming in the MATLAB® simulation that could also be related to the method of capacitance calculation. A potential area of investigation would be to increase the scale of the laboratory work, to ascertain whether this would result in better correlation between the simulated and measured values.

10.3 Thermal Analysis Experimentation

Dry-band arcing is a localised surface discharge phenomenon. The thermal component of this electrical activity is therefore important when both designing and choosing a fibre optic cable. The sheathing material of the fibre optic cables employed in the field should be investigated to determine their suitability to withstand a surface discharge. Suitability can be determined by analysing both, the materials phase transition temperatures and its decomposition behaviour. Although it would essentially be a material investigation, the results of this investigation would assist power utilities preparing to install a communications network significantly.

References

[Alston, Zoledziowski, 1963]; "Growth of Discharges on polluted Insulation", IEE Proceedings, Vol. 110, Nos. 7, July 1963, pp 1260 – 1266

[Bartlett et al, 1988]; Bartlett A.D., Carlton G., Carter C.N, Peacock A.J.: "The Design and Application of Optical cables into Overhead Lines up to 150 kV", IEE Conference on Overhead Line Design and Construction: Theory and Practice, November 1988, pp 211-219

[Bartlett et al, 1989]; Bartlett A.D., Carlton G., Carter C.N, Peacock A.J.: "Self Supporting, Metal Free, Optical Cable for Long Span, Power Line Use", IEE Conference Publications, Nos. 305, 1989, pp 252-258

[Barsch et al, 1997]; Barsch R., Lambrecht J., Pilling J., Weichold J., Haim K.D.:"The Behaviour of Medium Voltage Cable Terminations at Artificial Pollution", IEE Conference Publication, Nos. 438, June 1997, pp 3.14.1 - 3.14.5

[Besztercey et al, 2000]; Besztercey G., Karady G.G.: "An Artificial Contamination Method for Composite Insulators", IEEE Transactions on Power Delivery, Vol. 15, Nos.2, April 2000, pp 732 - 737

[Blaedel, Meloche, 1966]; Blaedel W.J., Meloche V.W.: "Elementary Quantitative Analysis: Theory and Practice", 2nd Edition, Harper & Row, 1966, pp 690 – 694

[Bologna, 2002]; Bologna F.: Personal Communication, 2002

[Brewer et al, 1992]; Brewer D.A., Dissado L.A., Parry M.J.: "Limitations on the Damage Mechanism in Dry Band Arcing on All Dielectric Self Supporting Cables", IEE Conference Publication, Nos. 363, 1992, pp 49 - 52

[Carson, 1926]; Carson J.R., "Wave propagation in overhead wires with ground return", Bell System Technical Journal, Vol. 5, 1926, pp 539 – 554

[Carlton et al, 1993]; Carlton G., Carter C.N., Peacock A.J., "Progress in the Long Term testing on All Dielectric Self Supporting Cable for Power System Use", IEE Conference Publications, Nos. 373, Part 3, 1993, pp 3.16.1 – 3.16.3

[Carter, Waldron, 1992]; Carter C.N., Waldron M.A., "Mathematical Model Of Dry Band Arcing on Self Supporting, All-Dielectric, Optical Cables Strung on Overhead Power Lines", IEE Proceedings – C, Vol. 139, Nos. 3, May 1992, pp 185 – 196

[Carter, 1993]; Carter C.N., "Arc Control Devices for Use on All Dielectric Self Supporting Optical Cables", IEE Proceedings – A, Vol. 140, Nos.5, September 1993, pp 357 – 361

[Danikas et al, 1998]; Danikas M.G., Karafyllidis I.: "Modelling of the Dry Band Problem on Outdoor Insulators: A New Perspective", IEEE International Conference on Conduction and Breakdown in Solid Dielectrics", June 22-25 1998, pp 410 - 413

[Devendranath et al, 1999]; Devendranath D., Nirgude P.M., Rao G.V., Shivakumara Aradhya Channakeshava R.S., Sudheer A.P., Mohan Rao N.S.: " Investigation on Rain Fog Pollution Test", IEE Conference Publication, Nos. 467, August 1999, pp 4.111.S25 – 4.114.S25

[Edwards et al, 1999]; Edwards K.S., Pedrow P.D., Olsen R.G.: "Portable ADSS Surface Contamination Meter", Conference on Electrical Insulation and Dielectric Phenomena, 1999, pp 158 – 161

[Edwards et al, 2003]; Edwards K.S., Pedrow P.D., Olsen R.G.: "Portable ADSS Surface Contamination Meter Calibrated in high Voltage Environment", IEEE Transactions on Power Delivery, Vol. 18, No. 3, July 2003, pp 888 – 894

[Eklund, Hartings, 1997]; Eklund A., Hartings R.: "Electric Field Measurements on Composite and Ceramic Insulators during Pollution Testing", IEE Conference Publication, Nos. 438, June 1997, pp 3.32.1 – 3.32.5

[Gonos et al, 2002]; Gonos I.F., Topalis F.V., Strathopolos I.A.: "Genetic Algorithm Approach to the Modelling of Polluted Insulators", IEE Proceedings – Generation, Transmission and Distribution, Vol. 149, Nos. 3, May 2002, pp 373 - 376

[Gorur et al, 1987]; Gorur R.S.,Cherney E.A., Hackam R.: "Performance of Polymeric Insulating Materials in Salt-Fog", IEEE Transactions on Power Delivery, Vol. PWRD-2, No. 2, April 1987, pp 486 – 492

[Hampton, 1964]; Hampton B.F.: "Flashover mechanism of polluted insulation", IEE Proceedings, 1964, 111, pp. 985-990

[Hevia, 1999]; Hevia O.P., Giminez W.F.: "Method to Determine the Parameters of the Electric ARC from Test Data", International Conference on Power System Transients, Conference Proceedings, pp 505, June 20-24 1999

[IEEE Std 4, 1995]; IEEE Standard Techniques for High Voltage Testing, IEEE Std 4, 1995

[Karady et al, 1995a]; Karady G.G., Shah M., Brown R.L.: "Flashover Mechanism of Silicone Rubber Insulators used for Outdoor Insulation – I", IEEE Transactions on Power Delivery, Vol. 10, Nos. 4, October 1995, pp 1965 – 1971

[Karady et al, 1995b]; Karady G.G., Shah M., Brown R.L.: "Flashover Mechanism of Silicone Rubber Insulators used for Outdoor Insulation – II", IEEE Transactions on Power Delivery, Vol. 10, Nos. 4, October 1995, pp 1972 – 1978

[**Karady et al, 1999a**]; Karady G.G., Torgerson M., Torgerson D., Wild J., Tuominen M.: " New Test Method for Evaluation of Corona-caused Aging of Fiber-optic Cables". IEEE Transmission and Distribution Conference, Vol. 2, pp. 734-738, April 11-16 1999.

[**Karady et al, 1999b**]; Karady G.G., Devarajan S., Tuominen M.W.: "Computer Simulation of Fiber-Optic Cable failures due to Dry-Band Arcing", Power Engineering Society Summer Meeting, July 1999, pp 890 - 894

[**Karady et al, 1999c**]; Karady G.G., Amarh F., Sundararajan R.: "Dynamic Modelling of AC Insulator Flashover Characteristic", IEE Conference Publication, Nos. 467, August 1999, pp 4.107.S25 – 4.110.S25

[**Karady et al, 1999d**]; Karady G.G., Devarajan S., Tuominen M.W.: "Novel technique to Predict Dry-Band Arcing failure of Fiber-Optic Cables Installed on High Voltage Lines", IEEE Power Tech '99, September 1999, Paper BPT99-160-30

[**Karady et al, 1999e**]; Karady G.G., Besztercey G., Tuominen M.W.: " Corona Caused Deterioration of ADSS Fiber Optic Cables on High Voltage Lines", IEEE Transactions on Power Delivery, Vol. 14, Nos. 4, October 1999, pp 1438 – 1445

[**Karady et al, 2000**]; Karady G.G., Srinivasen D., Reta-Hernandez M., Tuominen M., Torgerson D., Han B.: "A Mitigation Method for Dry Band Arcing Caused Deterioration of ADSS Fiber-Optic Cables", Power Engineering Society Winter Meeting, 2000 pp 2391 – 2396

[**Karady et al, 2001a**]; Karady G.G., Devarajan S.: "Algorithm to Predict Dry Band Arcing in Fiber Optic Cables", IEEE Transactions on Power Delivery, Vol.16, Nos. 2, April 2001, pp 286 – 291

[Karady et al, 2001b]; Karady G.G., Srinivasen D., Reta-Hernandez M., Tuominen M., Torgerson D., Huang Q.: "Sensor Design for Leakage Current measurement on ADSS Fiber-Optic Cable", Power Engineering Society Winter Meeting, 2001 pp 281 – 286

[Khan, Hoch, 2002(a)]; Khan M.F., Hoch D.A.: "Simulations of Leakage Currents found during Dry Band Arcing on Fibre Optic Cables", South African Universities Power Engineering Conference, 2002, pp 27 – 30

[Khan, Hoch, 2002(b)]; Khan M.F., Hoch D.A.: "Induced Currents on Optical Fibre Cables Installed in High Voltage Transmission Line Environments", IEEE Africon, 2002, pp 623 – 628

[Kim et al, 1990]; Kim S.H., Cherney E.A., Hackam R.: "The Loss and Recovery of Hydrophobicity of RTV Silicone Rubber Insulator Coatings", IEEE Transactions on Power Delivery, Vol.5, Nos. 3, July 1990, pp 1491 - 1500

[Lannes, Schneider, 1997]; Lannes W., Schneider H.: " Pollution Severity Performance Chart; Key to Just-in-Time Insulator Maintenance", IEEE Transactions on Power Delivery, Vol. 12, Nos. 4, October 1997, pp 1493 – 1499

[Liang et al, 1992]; Liang X.D., Li J., Xue J.Q., Warren L.: " The Change of surface Leakage Current of Composite Insulators in Salt Fog Test", IEE Conference Publication, Nos. 363, 1992, pp 41 – 44

[Looms, 1988]; Looms J.S.T.: "Insulators for High Voltages", Peregrinns, 1988, pp 118 – 167

[Murata, 1990]; Murata H.: "Application of Optical Communications for Power Distribution Companies", IEEE Region 10 Conference on Computer and Communication Systems, September 1990, Hong Kong, pp 788 – 792

[Meyer, Liu, 1995]; Meyer W.S., Liu T.H., "BPA EMTP Theory Book", July 1995

[Obenaus, 1958]; Obenaus F.; "Fremdschichtuberschlag und Kriechweglange", Deutsche Elektrotechnik, 1958, pp 153

[**Olsen, 1999a**]; Olsen R.G.: "An Improved Model for the Electromagnetic Compatibility of All-Dielectric Self-Supporting Fiber-Optic Cable and High-Voltage Power Lines", IEEE Transactions on Electromagnetic Compatibility, Vol. 41, No. 3, August 1999, pp 180 - 192

[Olsen, 1999b]; Olsen R.G.: "Laboratory Simulations of Dry Band Arcing on All Dielectric Self-Supporting Fiber Optic cable near High-Voltage Power Lines", IEEE International symposium on Electromagnetic Compatibility, Vol. 2, 1999, pp 993 - 997

[Peacock, Wheeler, 1992]; Peacock A.J., Wheeler J.C.G.: "Development of Aerial Fiber Optic Cables for Operation on 400 kV Power Lines", IEE Proceedings-A, Vol. 139, Nos. 6, November 1992, pp 304 – 314

[**Pollaczek, 1926**]; Pollaczek F., "On the field produced by an infinitely long wire carrying alternating current", Elektrische Nachrichtentechnik, Vol. 3, 1926, pp 339 – 359

[Rabek, 1980]; Rabek J.F., "Experimental Methods in Polymer Chemistry: Physical Principles and Applications", 1st Edition, John Wiley & Sons, 1980, pp 556 – 572

[Rowland, 1992]; Rowland S.M.: "Sheathing Materials for Dielectric, Aerial, Self Supporting Cables for Application on High Voltage Power Lines", IEE Conference Publications, Nos. 363, 1992, pp 53 –56

[Rowland, Easthope, 1993]; Rowland S.M., Easthope F.: "Electrical Ageing and testing of Dielectric Self Supporting Cables for Overhead Power Lines", IEE Proceedings – A, Vol.140, Nos. 5, September 1993, pp 351 – 356

[Rowland, Nichols, 1996]; Rowland S.M., Nichols I.V.: "Effects of Dry Band Arc Current on Aging of Self Supporting Dielectric Cables in High Fields", IEE Proceedings on Science, Measurement and Technology, Vol. 143, Nos. 1, January 1996, pp 10 – 14

[Tsanakas et al, 1999]; Tsanakas A.D., Papaefthimiou G.I., Agoris D.P.: "An Approach to the Affect of Rainfall on the Pollution Performance of Insulators in Island Networks", IEE Conference Publication, Nos. 467, August 1999, pp 4.297.P2 - 4.300.P2

[Vaughan, Swingler, 1992]; Vaughan A.S., Swingler S.G.: "Thermal Analysis of Polymeric Sheathing Materials for Fiber Optic Communication Cables", IEE Conference Publication, Nos. 363, December 1992, pp 57 – 60

[Wareing, 1997]; Wareing J.B.: "The Effects of Wind, Snow and Ice on Optical Fibre Systems on Overhead Line Conductors", IEE Conference Publication, Nos. 438, June 1997, pp 3.35.1- 3.35.5

[Xidong et al, 1999]; Xidong L., Shaowu W., Lengeng H., Qinghe S., Xueqi C.: " Artificial Pollution Test and Pollution Performance of Composite Insulators", IEE Conference Publication, Nos. 467, 1999, pp 4.337.P2 – 4.340.P2

Appendix A

Determination of Leakage Current as determined in (Carter and Waldron, 1992, 194)

A system was devised that accurately calculates the current and voltage at specific points on the cable. One needs a way of calculating how earth leakage currents flowing on the surface of the conductor modify the induced voltages. Thevinin's theorem may be used to replace the system of phase conductors by an equivalent conductor, at potential V_S relative to ground.

Consider an infinitesimal element of the cable, of length dx, whose capacitance's per unit length to line and ground are C_1 and C_2 respectively. If we assume that C_1, C_2 and R are independent of position, the problem can be treated quite simply. If the element has a potential relative to ground of V and carries a current I, then current continuity gives

$$dI = j\omega C_1 V_S dx - j\omega V(C_1 + C_2)dx \quad .....(B.1a)$$

And the resistive voltage drop along the cable gives

$$dV = -IRdx \quad ....(B.2b)$$

It is convenient at this point to define normalized parameters for voltage, current, position

$$v = V/V_0, \quad i = I/J_0 L$$

$$\lambda = x/L, \quad k^2 = J_0 RL^2/V_0 \quad .....(B.3)$$

and specific resistance, which simplify the algebra. Thus

Where L is the half span

$$V_0 = \frac{C_1 V_S}{(C_1 + C_2)} \quad .....(B.4)$$

Above is the cable potential when R tends to infinity, and

$$J_0 = j\omega C_1 V_S \quad .....(B.5)$$

Is the charging current when R tends to zero. This relates C_1 and C_2 to the calculated values of V_0 and J_0. Equations (B.4) and (B.5) now read

$$v = 1 - \frac{di}{d\lambda} \ldots (B.1b)$$

$$\frac{dv}{d\lambda} = -ik^2 \ldots (B.2b)$$

Now, taking into account these modifications, the equation reads

$$\frac{d^2 i}{d\lambda^2} = k^2 i \ldots\ldots (B.6)$$

Which has a solution

$$i = Ae^{k\lambda} + Be^{-k\lambda}$$

If we choose $\lambda = 0$ at mid-span, then the boundary condition $i = 0$ at $\lambda = 0$ yields $A = -B$ and $I = 2A \sinh k\lambda$

The cable is earthed at the support so that $v = 0$ at $\lambda = 1$. We can now obtain expressions for the normalized voltage and current as functions of position.

$$v(\lambda) = 1 - \frac{\cosh k\lambda}{\cosh k} \quad \text{and} \quad i(\lambda) = \frac{\sinh k\lambda}{k \cosh k} \ldots (B.7)$$

The normalized earth leakage current is therefore: -

$$i(1) = \frac{\tanh k}{k} \ldots (B.8)$$

The parameter **k** is complex, if we write:

$$k = (1 + j)\frac{L}{\delta}, \quad \text{where } \delta^2 = \frac{2}{\omega R(C_1 + C_2)} \ldots (B.9)$$

then equation (B.8) can be rewritten

$$i(1) = \frac{\delta}{2L}\left[\frac{\sinh\frac{2L}{\delta} + \sin\frac{2L}{\delta}}{\cosh\frac{2L}{\delta} + \cos\frac{2L}{\delta}} - j\frac{\sinh\frac{2L}{\delta} - \sin\frac{2L}{\delta}}{\cosh\frac{2L}{\delta} - \cos\frac{2L}{\delta}}\right] \ldots (B.10)$$

Where $L >> \delta$, as it will always be in the problem at hand, equation (B.10) reduces to

$$i(1) = \frac{\delta}{2L}(1 - j) \ldots (B.11)$$

This implies that the earth leakage current will have the magnitude,

$$I_1 = V_S \omega C_1 \delta \ldots (10.10)$$

The two ends of the span are thus independent of each other and of the span length. The magnitude of the earth leakage current is as though drawn from the line through a capacitor of value $C_1\delta$. δ is referred to as the active length and represents the length of cable adjacent to the support from which the majority of the earth leakage current is drawn.

Appendix B – MATLAB Code

```
% Program that allows the user to change the position of the fiber optic cable in a
% 275 kV tower system by manually entering the spatial position.
% span = 300m and Nsec = 500

% Constants
format short e
e = 8.854187817e-12;
w = 2*pi*50;
aa = -0.5+(sqrt(3)/2)*i;

% Transmission Tower and Line Dimensions
% Wire Co-ordinates
a = [-8.5 18.766];
B = [0 18.766];
C = [8.5 18.766];
F = [2.88 16.366];

dist = [a; B; C; F];

span = 300;
% 2 percent sag for cable
sag = 0.02;

% 2% sag for fiber optic cable
sag_fiber = 0.02;

%Wire Data
%Goat Wire
radius_l = ((25.97e-3)/2);
Vl_l = 275e3;

radius_c = (13e-3)/2;

%Resistance of layer as determined by pollution

R_layer = 1e7;

%Line to Neutral Voltage
Vl_n = (1.1*Vl_l)/ sqrt(3);


% Number of Sections
Nsec = 500;

%Initial height of cable
Y0_A = dist(1,2);
Y0_B = dist(2,2);
Y0_C = dist(3,2);
```

```
%Initial height of fiber
Yf = dist(4,2);

%Distance Calculations

A_A = Y0_A - (sag*span);
b_A = (2/span)*acosh(Y0_A/A_A);

A_B = Y0_B - (sag*span);
b_B = (2/span)*acosh(Y0_B/A_B);

A_C = Y0_C - (sag*span);
b_C = (2/span)*acosh(Y0_C/A_C);


height_cable_A = ones((Nsec+1),1);
height_cable_B = ones((Nsec+1),1);
height_cable_C = ones((Nsec+1),1);


for N = 0:(Nsec+1)
   Y = A_A*cosh(b_A*(span/2)*(((2*N)/(Nsec +1)) - 1));
   height_cable_A((N+1),1) = Y;
end

for N = 0:(Nsec+1)
   Y = A_B*cosh(b_B*(span/2)*(((2*N)/(Nsec +1)) - 1));
   height_cable_B((N+1),1) = Y;
end

for N = 0:(Nsec+1)
   Y = A_C*cosh(b_C*(span/2)*(((2*N)/(Nsec +1)) - 1));
   height_cable_C((N+1),1) = Y;
end

Af = Yf - (sag_fiber*span);
bf = (2/span)*acosh(Yf/Af);

height_fiber = ones((Nsec+1),1);

for N = 0:(Nsec+1)
   Y = Af*cosh(bf*(span/2)*(((2*N)/(Nsec +1)) - 1));
   height_fiber((N+1),1) = Y;
end

N = 0:(Nsec+1);

%Determining the distances between the conductors and the cable
% The first matrix L measures the actual distance between the conductors

L = ones(4,4);
```

```
for n = 1:4
   for m = 1:4
      if n == m
         L(n,m) = 0;
      else
         L(n,m) =(((dist(m,1) -dist(n,1))^2 + (dist(m,2) -dist(n,2))^2))^0.5;
      end
   end
end

% The second matrix measures the distances between the mirrored images

Lm = ones(4,4);

for n = 1:4
   for m = 1:4
      if n == m
         Lm(n,m) = 2*dist(n,2);
      else
         Lm(n,m) =(((dist(m,1) - dist(n,1))^2 + (dist(m,2) + dist(n,2))^2))^0.5;
      end
   end
end

Ctot = ones((Nsec+1),4);

for x =1:(Nsec + 2)

%The Potential matrix can now be determined

P = ones(4,4);
for n = 1:4
   for m = 1:3
      if n == m ==1
         P(n,m) = ((1/(2*pi*e))*log(2*height_cable_A(x)/radius_l));
      elseif n == m == 2
         P(n,m) = ((1/(2*pi*e))*log(2*height_cable_B(x)/radius_l));
      elseif n == m == 3
         P(n,m) = ((1/(2*pi*e))*log(2*height_cable_C(x)/radius_l));
      else
         P(n,m) = ((1/(2*pi*e))*log(Lm(n,m)/L(n,m)));
      end
  end
end

for n = 1:4
   if n == 4
         P(n,4) = ((1/(2*pi*e))*log(2*height_fiber(x)/radius_c));
      else
         P(n,4) = ((1/(2*pi*e))*log(Lm(n,4)/L(n,4)));
      end
  end
```

```
%Now to work out the Capacitance Matrix

C = inv(P);
Ctemp = C(:,4)';
Ctot(x,:) = Ctemp;
end

%Space Potential

Vtot = ones((Nsec+1),1);

for y = 1:(Nsec + 2)

Vp = ones(4,1);
Vp = [0 Vl_n (aa^2)*Vl_n aa*Vl_n]';
temp1 = 0;

for g = 1:3
   temp1 = (Vp(g,1)*Ctot(1,g)) + temp1;
end

temp2 = -1*temp1/Ctot(y,4);

Vtot(y) = abs(temp2);
end


% Section Capacitances in Analysis
Ca = ones((Nsec +1),1);
Cb = ones((Nsec +1),1);
Cc = ones((Nsec +1),1);
Cg = ones((Nsec +1),1);

for s = 1:(Nsec+2)
   Ca(s) = (span/(Nsec+1))*abs(Ctot(s,1));
   Cb(s) = (span/(Nsec+1))*abs(Ctot(s,2));
   Cc(s) = (span/(Nsec+1))*abs(Ctot(s,3));

   temp3 = 0;

   for t = 1:4
      temp3 = temp3 + Ctot(s,t);
   end
   Cg(s) = (span/(Nsec+1))*temp3;
end


%Thevenin Equivalent

%Equivalent Capacitance and Admittance
Cth = ones((Nsec+1),1);
Yth = ones((Nsec+1),1);
```

```
for q = 1:(Nsec+2)
   Cth(q) = Ca(q) + Cb(q) +Cc(q);
   Yth(q) = i*w*Cth(q);
end

% Open Circuit Voltage

Vth = ones((Nsec+1),1);

% It should be noted that the equation below is valid for ABC phase only

for r = 1:(Nsec +2)
   Vth(r) = Vl_n*((Ca(r) + (aa^2)*Cb(r) + aa*Cc(r))/Cth(r));
end

%Ground Admittance

Yg = ones((Nsec+1),1);
for r = 1:(Nsec +2)
   Yg(r) = i*w*Cg(r);
end

%Section Resistance

Rc = ones((Nsec+2),1);
Rc = Rc*(span/(Nsec+1))*R_layer;

Yr = ones((Nsec+2),1);
Yr = Yr*((Nsec+1)/(span*R_layer));

% Node Point Equations
%Forward Elimination

Ith = ones((Nsec+1),1);
Y = ones((Nsec+1),1);

for n = 2:(Nsec+1)
   Ith(n) = Vth(n)*Yth(n);
   Y(n) = Yr(n-1) + Yr(n) + Yth(n) + Yg(n);
end
Y(1) = Yth(1) + Yg(1);
Y(Nsec+2) = Yth(Nsec+2) + Yg(Nsec+2);

Ith(1) = Vth(1)*Yth(1);
Ith(Nsec+2) = Vth(Nsec+2)*Yth(Nsec+2);

Ynew = ones((Nsec +2),1);
Inew = ones((Nsec +2),1);

Ynew(1) = Y(1);
Ynew(Nsec+2) = Y(Nsec+2);
```

```
Ynew(2) = Y(2);
Inew(2) = Ith(2);
Inew(1) = 0;
Inew(Nsec+2) = 0;
for n = 3:(Nsec+1)
   Ynew(n) = Y(n) - (Yr(n-1)^2)/Ynew(n-1);
   Inew(n) = Ith(n) + Inew(n-1)*(Yr(n-1)/Ynew(n-1));
end

% Node Voltages (Backward Substitution)

V = ones((Nsec +2),1);
V(Nsec) = Inew(Nsec)/Ynew(Nsec);
V(1) = 0;
V(Nsec+2) = 0;


for n = (Nsec+1):-1:2
   V(n) = (Inew(n) + (Yr(n)*V(n+1)))/Ynew(n);
end

Vabs_l=abs(V);
j = 0:Nsec+1;

%Section Currents

I = ones((Nsec +2),1);

for q = 1:(Nsec+1)
   I(q) = (V(q+1) -V(q))*Yr(q);
end

I(Nsec+2) = I(1);
Iabs_l = abs(I);

%Resistance of layer as determined by pollution - medium

R_layer = 1e6;

%Section Resistance

Rc = ones((Nsec+2),1);
Rc = Rc*(span/(Nsec+1))*R_layer;

Yr = ones((Nsec+2),1);
Yr = Yr*((Nsec+1)/(span*R_layer));

% Node Point Equations
%Forward Elimination

Ith = ones((Nsec+1),1);
Y = ones((Nsec+1),1);
```

```
for n = 2:(Nsec+1)
   Ith(n) = Vth(n)*Yth(n);
   Y(n) = Yr(n-1) + Yr(n) + Yth(n) + Yg(n);
end
Y(1) = Yth(1) + Yg(1);
Y(Nsec+2) = Yth(Nsec+2) + Yg(Nsec+2);

Ith(1) = Vth(1)*Yth(1);
Ith(Nsec+2) = Vth(Nsec+2)*Yth(Nsec+2);

Ynew = ones((Nsec +2),1);
Inew = ones((Nsec +2),1);

Ynew(1) = Y(1);
Ynew(Nsec+2) = Y(Nsec+2);

Ynew(2) = Y(2);
Inew(2) = Ith(2);
Inew(1) = 0;
Inew(Nsec+2) = 0;
for n = 3:(Nsec+1)
   Ynew(n) = Y(n) - (Yr(n-1)^2)/Ynew(n-1);
   Inew(n) = Ith(n) + Inew(n-1)*(Yr(n-1)/Ynew(n-1));
end

% Node Voltages (Backward Substitution)

V = ones((Nsec +2),1);
V(Nsec) = Inew(Nsec)/Ynew(Nsec);
V(1) = 0;
V(Nsec+2) = 0;


for n = (Nsec+1):-1:2
   V(n) = (Inew(n) + (Yr(n)*V(n+1)))/Ynew(n);
end

Vabs_m=abs(V);
j = 0:Nsec+1;

%Section Currents

I = ones((Nsec +2),1);

for q = 1:(Nsec+1)
   I(q) = (V(q+1) -V(q))*Yr(q);
end

I(Nsec+2) = I(1);
Iabs_m = abs(I);
```

```
%Resistance of layer as determined by pollution - high

R_layer = 1e5;

%Section Resistance

Rc = ones((Nsec+2),1);
Rc = Rc*(span/(Nsec+1))*R_layer;

Yr = ones((Nsec+2),1);
Yr = Yr*((Nsec+1)/(span*R_layer));

% Node Point Equations
%Forward Elimination

Ith = ones((Nsec+1),1);
Y = ones((Nsec+1),1);

for n = 2:(Nsec+1)
   Ith(n) = Vth(n)*Yth(n);
   Y(n) = Yr(n-1) + Yr(n) + Yth(n) + Yg(n);
end
Y(1) = Yth(1) + Yg(1);
Y(Nsec+2) = Yth(Nsec+2) + Yg(Nsec+2);

Ith(1) = Vth(1)*Yth(1);
Ith(Nsec+2) = Vth(Nsec+2)*Yth(Nsec+2);

Ynew = ones((Nsec +2),1);
Inew = ones((Nsec +2),1);

Ynew(1) = Y(1);
Ynew(Nsec+2) = Y(Nsec+2);

Ynew(2) = Y(2);
Inew(2) = Ith(2);
Inew(1) = 0;
Inew(Nsec+2) = 0;
for n = 3:(Nsec+1)
   Ynew(n) = Y(n) - (Yr(n-1)^2)/Ynew(n-1);
   Inew(n) = Ith(n) + Inew(n-1)*(Yr(n-1)/Ynew(n-1));
end

% Node Voltages (Backward Substitution)

V = ones((Nsec +2),1);
V(Nsec) = Inew(Nsec)/Ynew(Nsec);
V(1) = 0;
V(Nsec+2) = 0;
```

```
for n = (Nsec+1):-1:2
   V(n) = (Inew(n) + (Yr(n)*V(n+1)))/Ynew(n);
end

Vabs_h=abs(V);
j = 0:Nsec+1;
figure,plot(j*(span/(Nsec+1)),Vabs_h,'m:',j*(span/(Nsec+1)),Vabs_m,'r--
',j*(span/(Nsec+1)),Vabs_l,'b-')
grid
xlabel('Distance')
ylabel('Voltage')
title('Voltage Distribution along Fiber Optic Cable')
legend('High Pollution','Medium Pollution','Low Pollution')

%Section Currents

I = ones((Nsec +2),1);

for q = 1:(Nsec+1)
   I(q) = (V(q+1) -V(q))*Yr(q);
end

I(Nsec+2) = I(1);
Iabs_h = abs(I);
figure,plot(j*(span/(Nsec+1)),Iabs_h,'m:',j*(span/(Nsec+1)),Iabs_m,'r--
',j*(span/(Nsec+1)),Iabs_l,'b-')
%axis([0 span 0 0.001])
grid
xlabel('Distance')
ylabel('Current')
%title('Current Distribution along Fiber Optic Cable')
legend('High Pollution','Medium Pollution','Low Pollution')
```

Appendix C – ATP Code

C.1 File used to obtain Line Constants

```
C SIM_PI.dat
C A Pi model is used to determine the line constants
BEGIN NEW DATA CASE
$OPEN, UNIT=7 FILE=A:\SIM_pi.PCH FORM=FORMATTED
LINE CONSTANTS
METRIC
BRANCH RA   RB   YA   YB   BA   BB   FA   FB
C Data for conductors of transmission line
 1 .428    .05 4        2.597  -6.72  17.875  12.025
 2 .428    .05 4        2.597   0.0   17.875  12.025
 3 .428    .05 4        2.597   6.72  17.875  12.025
 4 .001   1.E10 4        1.300   2.88   15.5    9.65
 0 .5      .4 4        1.325   -4.2   21.7   15.85
 0 .5      .4 4        1.325    4.2   21.7   15.85
BLANK card ending conductor cards
C We now request the modal parameter matrices
 1000.0     5.E5       1              0.2945     1      44
$PUNCH
BLANK card ending frequency cards
BLANK card ending line constants
BEGIN NEW DATA CASE
BLANK card ending session
```

C.2 File used to generate plot file

```
C SIM4
C PI ANALYSIS WITH A PARALLEL COMMS CCT
BEGIN NEW DATA CASE
$OPEN, UNIT=4 FILE=A:Sim4.PL4 FORM=UNFORMATTED
  5.E-7  30.E-2    50.0    50.0
    10                                    1
C Modal parameters of transmission line
$INCLUDE c:\ATP\SIM_pi.pch
00FA    FB              1.E0                                  3
BLANK card ending branch cards
 FA             -1.0                                  3
 FB             -1.0                                  3
BLANK card ending switch cards
14RA    0   132.E3     50.0    180.0       1
14YA    0   132.E3     50.0    240.0       0
14BA    0   132.E3     50.0    120.0       0
BLANK card ending source cards
 YA   YB   RA   RB   BA   BB   FA   FB
BLANK card ending output variable requests
BLANK card ending plot cards
BEGIN NEW DATA CASE
BLANK card ending session
```

Experiment values for Masters Appendix D

First experiment set-up
Span = 11m
Sag_ Conductor = 2,78% Sag_Fiber = 17,65%
Measurement Resistor = 987

	Dry Run 11/5	Megar	1,2Gigaohm/0.1m	12 Gigaohm/m		
	V_applied (kV)	V_meas (V)		I_meas(mA)		
	40	0.003	987	0.003		
	60	0.006	987	0.006		
	80	0.008	987	0.008		
	100	0.012	987	0.012		
	120	0.018	987	0.018		
	0,31 Megaohm/m					
	V_applied (kV)	**V_meas (V)**		**I_meas(mA)**	**Ave I**	**Simulated**
First run	40	0.609	987	0.617	0.64286	
	60	0.911	987	0.923	0.94022	
	80	1.472	987	1.491	1.50811	
	100	2.163	987	2.191	2.19453	
Second	40	0.660	987	0.669		
Run	60	0.945	987	0.957		
	80	1.505	987	1.525		
	100	2.169	987	2.198		
	0.2 Megaohm/m					
	40	0.595	987	0.603		
	60	0.870	987	0.881		
	80	1.362	987	1.380		
	100	2.031	987	2.058		
	1,1 Megaohm/m	**7,4 milliSiemens/cm**		Medium Pollution		
	V_applied (kV)	**V_meas (V)**		**I_meas(mA)**	**Ave I**	**Simulated**
	40	0.437	987	0.443	0.41439	0.242
First	60	0.668	987	0.677	0.63627	0.362
Run	80	1.101	987	1.116	0.99054	0.483
	100	1.359	987	1.377	1.28504	0.604
	40	0.407	987	0.412		
Second	60	0.622	987	0.630		
Run	80	0.945	987	0.957		
	100	1.213	987	1.229		
	40	0.383	987	0.388		
Third	60	0.594	987	0.602		
Run	80	0.887	987	0.899		
	100	1.233	987	1.249		

	5.25 Megaohm/m	0.34 milliSiemens/cm		Light Pollution		
	V_applied (kV)	V_meas (V)		I_meas(mA)	Ave I	Simulated
	40	0.277	987	0.281	0.24856	0.241
First	60	0.433	987	0.439	0.39885	0.36
Run	80	0.656	987	0.665	0.59473	0.481
	100	0.900	987	0.912	0.82134	0.601
	120	1.224	987	1.240	1.0797	0.721
	40	0.210	987	0.213		
Second	60	0.343	987	0.348		
Run	80	0.514	987	0.521		
	100	0.701	987	0.710		
	120	0.938	987	0.950		
	40	0.249	987	0.252		
Third	60	0.405	987	0.410		
Run	80	0.591	987	0.599		
	100	0.831	987	0.842		
	120	1.035	987	1.049		

	0.26 Megaohm/m	11.1 milliSiemens/cm		Heavy Pollution		
	V_applied (kV)	V_meas (V)		I_meas(mA)	Ave I	Simulated
	40	0.476	987	0.482	0.48075	0.242
First	60	0.774	987	0.784	0.77102	0.363
Run	80	1.174	987	1.189	1.16261	0.483
	100	1.668	987	1.690	1.65299	0.604
	120	2.306	987	2.336	2.2619	0.725
	40	0.473	987	0.479		
Second	60	0.748	987	0.758		
Run	80	1.121	987	1.136		
	100	1.595	987	1.616		
	120	2.159	987	2.187		

Varied the spacing on the experimental set-up
Sag_conductor = **2.780**
Sag_fiber = **19.460**

982 ohm measuring resistor

	135 MicroSiemens/cm					
	V_applied (kV)	V_meas (V)		I_meas(mA)	Ave I	Simulated
First	60	0.557	982	0.567	0.55295	0.347
Run	80	0.881	982	0.897	0.85794	0.462
	100	1.264	982	1.287	1.21589	0.578
Second	60	0.529	982	0.539		
Run	80	0.804	982	0.819		
	100	1.124	982	1.145		

	25 milliSiemens/cm					
	V_applied (kV)	V_meas (V)		I_meas(mA)	Ave I	Simulated
First	60	0.679	982	0.691	0.51392	0.367
Run	80	1.075	982	1.095	0.83842	0.49
	100	1.605	982	1.634	1.50238	0.612

Second Run	60	0.433	0.532	0.441		
	80	0.708	0.833	0.721		
	100	1.317	1.203	1.341		
Third Run	60	0.402	982	0.409		
	80	0.687	982	0.700		
	100	1.504	982	1.532		

46.4 millSiemens/cm

	V_applied (kV)	V_meas (V)		I_meas(mA)	Ave I	Simulated
First Run	60	0.483	982	0.492	0.47692	0.367
	80	0.798	982	0.813	0.78208	0.49
	100	1.772	982	1.804	1.84114	0.612
	110	1.840	982	1.874	2.07094	
Second Run	60	0.455	982	0.463		
	80	0.747	982	0.761		
	100	1.856	982	1.890		
	110	2.147	982	2.186		
Third Run	60	0.467	982	0.476		
	80	0.759	982	0.773		
	100	1.796	982	1.829		
	110	2.114	982	2.153		

Adjusted the sag on this experiment for the fibre

Sag_conductor = 2.780

Sag_fiber = 43.180

0.26 milliSiemens/cm

	V_applied (kV)	V_meas (V)		I_meas(mA)	Ave I	Simulated
First Run	60	0.292	982	0.297	0.2836	0.361
	80	0.456	982	0.464	0.44399	0.482
	100	0.626	982	0.637	0.62118	0.602
Second Run	60	0.265	982	0.270		
	80	0.416	982	0.424		
	100	0.594	982	0.605		

26 milliSiemens/cm

	V_applied (kV)	V_meas (V)		I_meas(mA)	Ave I	Simulated
First Run	60	0.349	982	0.355	0.32281	0.374
	80	0.526	982	0.536	0.50339	0.498
	100	0.727	982	0.740	0.71317	0.623
Second Run	60	0.253	982	0.258		
	80	0.389	982	0.396		
	100	0.582	982	0.593		
Third Run	60	0.349	982	0.355		
	80	0.568	982	0.578		
	100	0.792	982	0.807		

	14 milliSiemens/cm					
	V_applied (kV)	V_meas (V)		I_meas(mA)	Ave I	Simulated
First	60	0.200	982	0.204	0.22454	0.374
Run	80	0.311	982	0.317	0.32026	0.498
	100	0.447	982	0.455	0.4944	0.623
Second	60	0.241	982	0.245		
Run	80	0.318	982	0.324		
	100	0.524	982	0.534		